

Dissertation zur Erlangung des Doktorgrades
der Fakultät für Chemie und Pharmazie
der Ludwig-Maximilians-Universität München

**How the mammalian endoplasmic reticulum handles
aggregation-prone β -sheet proteins**

Lisa Vincenz-Donnelly geb. Vincenz

aus

Velbert, Deutschland

2016

Erklärung

Diese Dissertation wurde im Sinne von § 7 der Promotionsordnung vom 28. November 2011 von Herrn Prof. Dr. Franz-Ulrich Hartl betreut.

Eidesstattliche Versicherung

Diese Dissertation wurde eigenständig und ohne unerlaubte Hilfe erarbeitet.

München, am 06.12.2016

Lisa Vincenz-Donnelly

Dissertation eingereicht am: 23.03.2016

1. Gutachter: Prof. Dr. Franz-Ulrich Hartl
2. Gutachter: PD Dr. Dietmar E. Martin

Mündliche Prüfung am: 06.12.2016

Contents

Erklärung.....	2
Contents.....	3
Summary	6
Introduction	8
Protein folding and molecular chaperones	8
Proteostasis	12
The endoplasmic reticulum	13
Protein translocation into the ER.....	14
The special folding environment of the ER.....	15
ER protein folding factors	17
The calnexin/calreticulin system.....	18
The BiP chaperone system.....	19
The GRP94 chaperone	22
Degradation of ER proteins	23
Cellular stress responses	27
The cytosolic stress response	27
The unfolded protein response.....	27
Protein aggregation toxicity.....	33
Conformational diseases caused by mutant ER proteins	34
Mutations in ERQC factors can cause diseases	38
ER stress responses in disease	38
ER quality control in aging	39
Aims of the study	41
Aim of part 1.....	41
Aim of part 2.....	44
Materials and Methods	46
Materials	46
Chemicals.....	46
Antibodies	50
Enzymes.....	51
Bacterial strains.....	52

Mammalian cell lines	52
Buffers.....	52
Polyacrylamide Bis-Tris gels	53
Media	53
Kits.....	54
Other materials and Instruments	54
Plasmids	57
siRNAs.....	58
Softwares.....	58
Methods	59
Production of chemically competent E. coli	59
Plasmid preparation	59
PCR amplification and purification of PCR products.....	60
DNA Restriction Digestion and Ligation.....	60
Cloning of expression plasmids	60
Cell culture and transfections.....	61
Immunofluorescence imaging.....	61
Immunoblotting.....	62
Solubility analysis	63
Cell viability assay	64
Analysis of secreted proteins	64
Cycloheximide chase	65
SILAC labelling	65
Sample preparation for SILAC-MS analysis	65
Sample preparation for label-free MS analysis.....	66
LC-MS/MS	67
Analysis of MS data.....	67
Fluorescence-activated cell sorting (FACS)	68
siRNA knockdowns	68
Luciferase assays.....	68
Deglycosylation	69
Analysis of Q97 inclusions by fluorescence microscopy	69
Results	70
Part 1 - How the ER handles aggregation-prone β -sheet proteins.....	70

Targeting an aggregation-prone β -protein to the ER	70
ER- β proteins are retained in the ER	73
Targeting β -protein to the ER reduces toxicity and aggregation propensity	76
ER- β 17 is also retained in a detergent-soluble state in stably expressing cell lines	82
Analysis of the ER- β 23 interactome	84
ER- β 23 interacts with a distinct set of ER chaperones and ERAD factors	86
ER- β 23 accumulates at levels exceeding those of interacting chaperones	90
ER- β 23 inhibits UPR induction	91
ER- β 23 is not glycosylated	93
ER- β 23 inhibits ERAD	93
NRS ^{G392E} interacts productively with SEL1L	96
Part 2: Small molecule enhancers of proteostasis	98
Fluphenazine and gefitinib reduce HttQ97-induced UPS impairment	98
Fluphenazine induces the heat shock response	100
Droperidol also induced the HSR and improved proteostasis	100
Erlotinib also reduces HttQ97-induced UPS impairment	102
Gefitinib reduces the size of Q97 aggregates	103
Discussion	105
Acknowledgements	111
References	112
Appendices	134
Supplementary table 1. Amino acid sequences of model proteins	134
Supplementary table 2. List of ER- β 23 interactors	136
Supplementary table 3. Compartmental enrichment of ER- β 23 interactors	142
Supplementary table 4. Abundances of ER- β 23 interactors in IP eluates	143
Supplementary table 5. Cellular abundance values of ER chaperones and ERAD factors	149
Supplementary table 6. SILAC H/L ratios of UPR transcriptional targets in total proteome	150
Abbreviations	153

Summary

Misfolded proteins are prone to engage in aberrant intermolecular interactions that can lead to formation of large aggregate structures. Aggregation causes loss-of-function toxicity because the aggregating protein fails to reach its native fold and function. In addition, protein aggregates may exert gain-of-toxicity, which is due to the sheer presence of aggregate conformations that sequester important cellular factors and disturb cell morphology. Protein aggregation is associated with a large number of human diseases.

The endoplasmic reticulum (ER) is a membrane-bound cellular organelle and the site of synthesis of one third of the eukaryotic proteome including secretory proteins and proteins destined for the endomembrane system. After co-translational translocation into the ER, nascent proteins are assisted to fold by molecular chaperones and are subject to post-translational modifications. Secretory proteins are retained in the ER lumen until they are correctly folded and are then delivered to the Golgi apparatus for further modifications. If a protein fails to fold properly after repeated folding cycles, it is instead targeted for degradation via the ER-associated degradation pathway (ERAD).

The aim of the study presented in this thesis was to determine how the human ER quality control (ERQC) machinery deals with aggregation-prone proteins. This is of great interest because protein aggregates are differentially regulated by distinct cellular environments and many of the proteins that aggregate in diseases are in fact synthesised in the ER. To this end, we utilised *de novo* designed amyloidogenic β -proteins as generic models for protein aggregation. Due to their lack of evolved biological function, these model proteins allow the exclusive study of gain-of-function toxicity and enable us to dissect the effect of the ER environment on amyloidogenic proteins.

We determined that ER-targeted versions of the model β -sheet proteins are significantly less toxic and more soluble than their non-targeted counterparts, which form

toxic insoluble aggregates in the cytosol and nucleus. We found that the ER-targeted β -protein ER- β 23 is recognised by ERQC machinery and efficiently retained in the ER lumen in a soluble polymeric state. Strikingly, ER- β 23 interacted with factors of the ERAD pathway, even though it was not efficiently degraded. Instead, ER- β 23 inhibited the degradation of other ERAD substrates by sequestering low-abundant ERAD factors. The presented results demonstrate a marked capacity of the ER to prevent the secretion of potentially toxic aggregation-prone proteins and to limit the formation of insoluble aggregates in the ER lumen. In addition, the data reveal a mechanism by which amyloidogenic proteins may disturb ER proteostasis.

Another aim of this study was to analyse the effects of small molecule proteostasis modulators. We found that the anti-dopaminergic drugs fluphenazine and droperidol as well as the epidermal growth factor receptor (EGFR) inhibitors gefitinib and erlotinib improved proteostasis in the presence of protein aggregates. In case of the former, this effect was most likely achieved via induction of the cytosol stress response.

In summary, the work presented in this thesis provides novel insights into how aggregation-prone proteins behave in the environment of the ER and also demonstrates the potential of using small molecule modulators to improve cellular proteostasis in a disease context.

Introduction

Protein folding and molecular chaperones

Virtually all processes within cells depend on the proper functioning of proteins. Proteins are synthesised within cells as polypeptide chains that need to be correctly folded into three dimensional structures to give rise to fully functional proteins (Dobson et al., 1998; Bartlett and Radford, 2009). The conformation at which a protein is functional is referred to as the native state of a protein. The native state represents a thermodynamically stable state at the minimum of the protein's accessible free energy (Anfinsen et al., 1961; Anfinsen, 1973). The information that specifies a protein's native conformation is given by its primary structure, namely, the amino acid sequence of the polypeptide chain (Anfinsen, 1973). Early studies of protein folding showed that some proteins are able to fold spontaneously *in vitro* and suggested mechanisms of protein folding that involved the formation of secondary structures in a hierarchical process driven by various interactions between amino acid side chains as well as the hydrophobic effect, which favours burial of hydrophobic amino acid residues in the inside of the protein and exposure of hydrophilic residues to the aqueous environment (Dill et al., 1995; Daggett and Fersht, 2003). However, under physiological conditions the process is not as straightforward because in the crowded environment of the cell protein folding faces several challenges. One challenge is that long polypeptide chains may not have space to move freely to find their native folds due to molecular crowding of highly concentrated biomolecules, in particular other proteins (Ellis, 2001). Furthermore, the process of translation is relatively slow (about 15-74 seconds per 300 amino acids) and the polypeptide chain cannot fold into its native conformation before it is fully synthesised and released from the ribosome (Etchells and Hartl, 2004; Lu and Deutsch, 2005). This means that during translation the nascent chain can only fold partially and exposes hydrophobic patches that would in the folded state be buried in the core of the protein. Unfolded hydrophobic

patches are prone to interact aberrantly, potentially leading to toxic misfolding and aggregation.

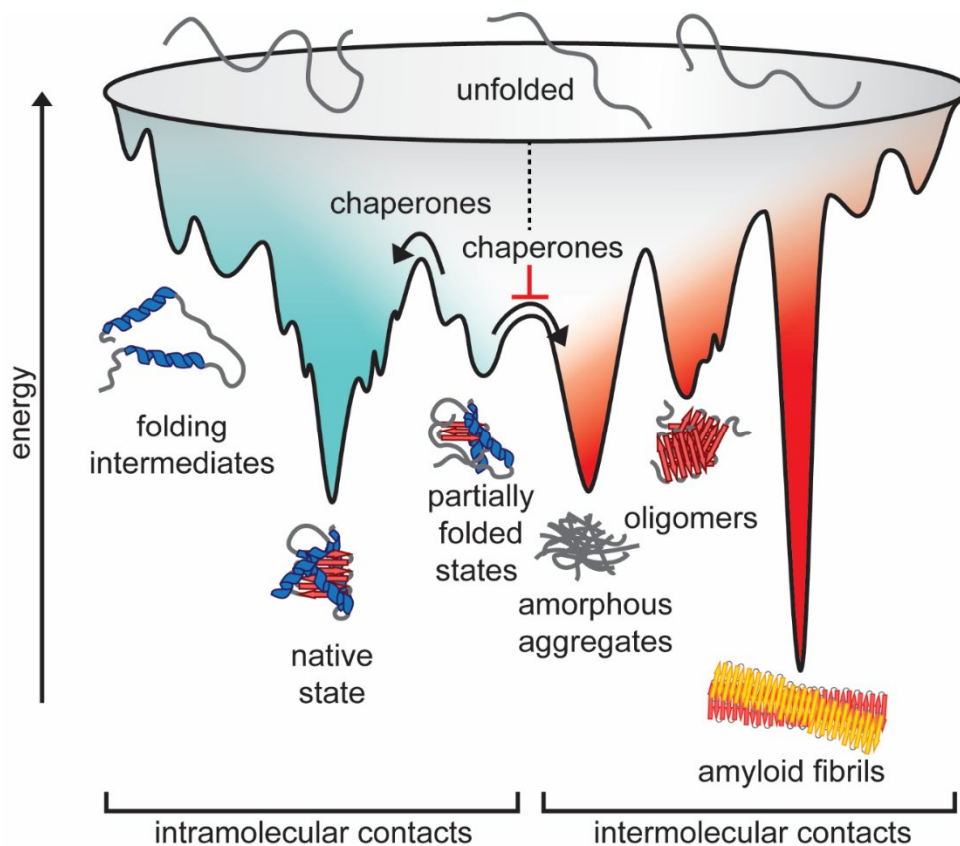


Figure 1. The protein folding funnel. The funnel illustrates the energy landscape of a protein during folding and aggregation. Many intermediate conformations 'funnel' to the native state via intramolecular interactions (cyan surface). Non-native conformations can lead to formation of amorphous aggregates or amyloid fibrils that are based on aberrant intermolecular interactions (red surface) but also via folding intermediates or partially folded states (moving from cyan to red surfaces). Destabilisation of the native conformation and aggregate formation is prevented by chaperones. Figure adapted and modified from (Kim et al., 2013) and (Jahn and Radford, 2005).

Taken together, both kinetic and thermodynamic factors determine the folding process of a protein. To explain the connection between kinetic and thermodynamic control of protein folding the model of the “folding funnel” was introduced. The folding funnel depicts the complex energy landscape that a polypeptide chain must navigate during folding (Figure 1) (Bryngelson et al., 1995; Dill and Chan, 1997; Clark, 2004; Hartl and Hayer-Hartl, 2009; Kim

et al., 2013), and illustrates the different potential energy states of a protein in various conformations. The vertical axis represents the internal free energy, which is dependent on the properties of a given polypeptide chain and on external conditions such as temperature or solvents. A protein's native conformation represents an energy minimum. The number of potential conformations is represented by the lateral area of the funnel. There is not just one single folding pathway but multiple paths that may lead from the unfolded chain to the native conformation. As folding progresses, the polypeptide chain's conformational options are more and more narrowed towards the native state. However, most cellular proteins form folding intermediates that are prone to collapse into more compact and stable non-native conformations (Brockwell and Radford, 2007). The intramolecular interactions that such non-native conformations are based on need to be reversed in order for correct folding to proceed, which increases the activation energy required to reach the stable native state. Thus, the path from the high energy state of an unfolded polypeptide chain to its native low energy conformation via folding intermediates contains kinetic traps of local energy minima that make the folding funnel rugged (Jahn and Radford, 2005; Hartl and Hayer-Hartl, 2009) (Figure 1). The propensity of a protein to get caught in such traps is largely dependent on the chemical properties of its amino acid side chains, the length of the polypeptide chain, its concentration and the stability of its native state (Netzer and Hartl, 1997; Chiti and Dobson, 2006; Ciryam et al., 2013). In addition to aberrant intramolecular interactions, non-native conformations are also prone to engage in aberrant intermolecular interactions. This is due to the fact that unfolded proteins or folding intermediates characteristically expose hydrophobic and unstructured regions that would in the native conformation be buried in the core of the structure. Such aberrant intermolecular interactions cause two problems: First, they represent further kinetic energy traps that slow down the folding process. Second, they can lead to aggregate conformations such as amyloid fibrils that may be even more thermodynamically stable than the native state (Figure 1).

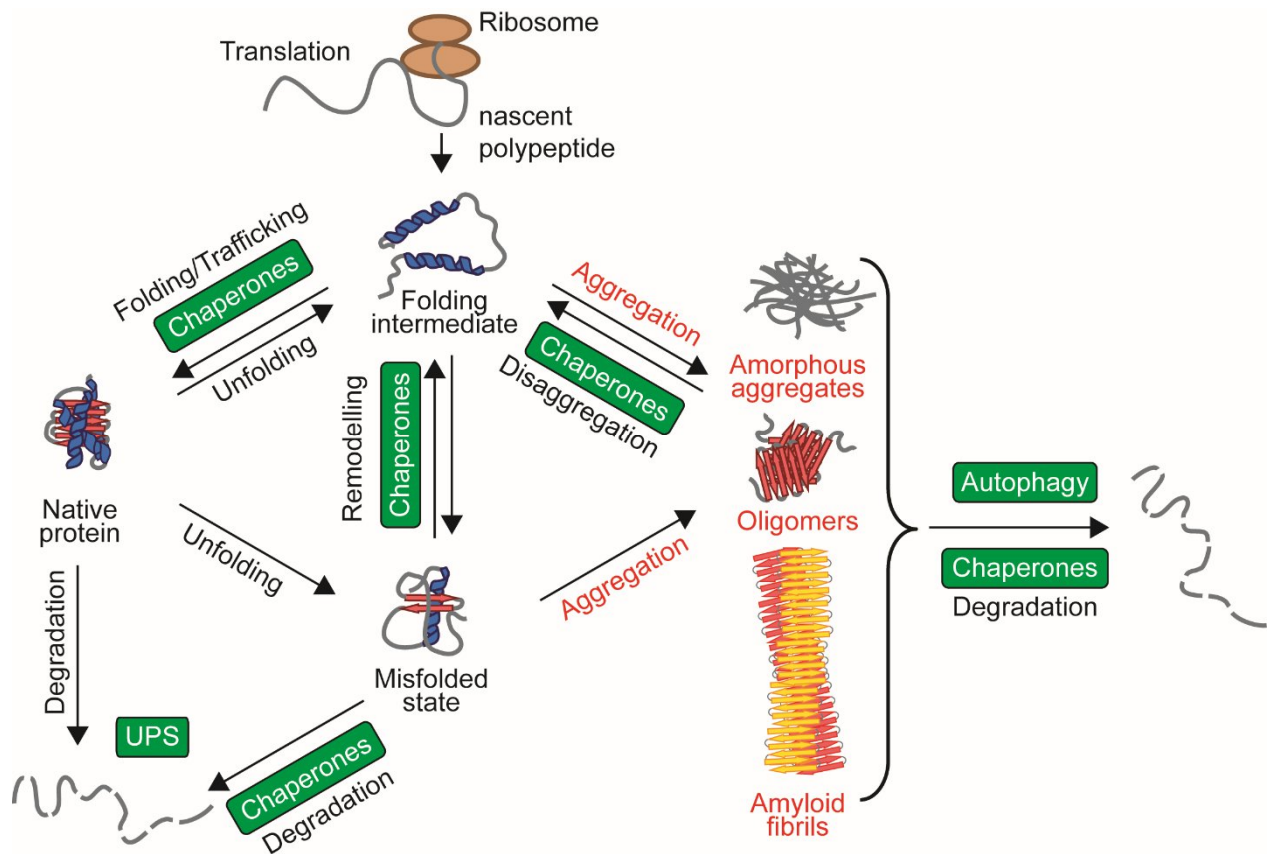


Figure 2. The different functions of molecular chaperones. Chaperones fold newly synthesised proteins, remodel misfolded species, dissolve aggregates and target proteins for degradation via the ubiquitin proteasome system (UPS) or autophagy. Figure adapted and modified from (Kim et al., 2013) and (Eichner and Radford, 2011).

To overcome the challenge of kinetic traps, protein folding in the cell is assisted by molecular chaperones (Hartl, 1996) (Figure 1 and 2). Molecular chaperones are proteins that bind to a broad range of protein substrates and assist their correct folding without being part of the final structure. Chaperones not only facilitate *do novo* folding, but also refolding, prevent protein aggregation, actively dissociate protein aggregates and are also involved in protein degradation (Figure 2). Mammalian chaperones can be largely classified into five families of so called heat shock proteins (HSPs): the ATP-independent small HSPs (sHSPs) that are also referred to as holdases and which are almost exclusively stress-induced, and the ATP-dependent families HSP60, HSP70, HSP90 and HSP100 that are also referred to as

foldases and consist of both cognate and stress-inducible members (Richter et al., 2010; Vabulas et al., 2010; Kim et al., 2013).

Proteostasis

Since cells depend on a balance of correctly folded and functioning proteins - a state referred to as protein homeostasis or proteostasis - they must tightly regulate the conformations, concentrations, interactions and subcellular localisations of all proteins that make up the proteome (Balch et al., 2008; Powers et al., 2009; Hipp et al., 2014). For this purpose, cells have evolved a network of protein quality control pathways that control transcription, translation, protein folding, trafficking, processing, assembly, localisation and degradation and are collectively referred to as the proteostasis network (PN) (Douglas and Dillin, 2010) (Figure 2).

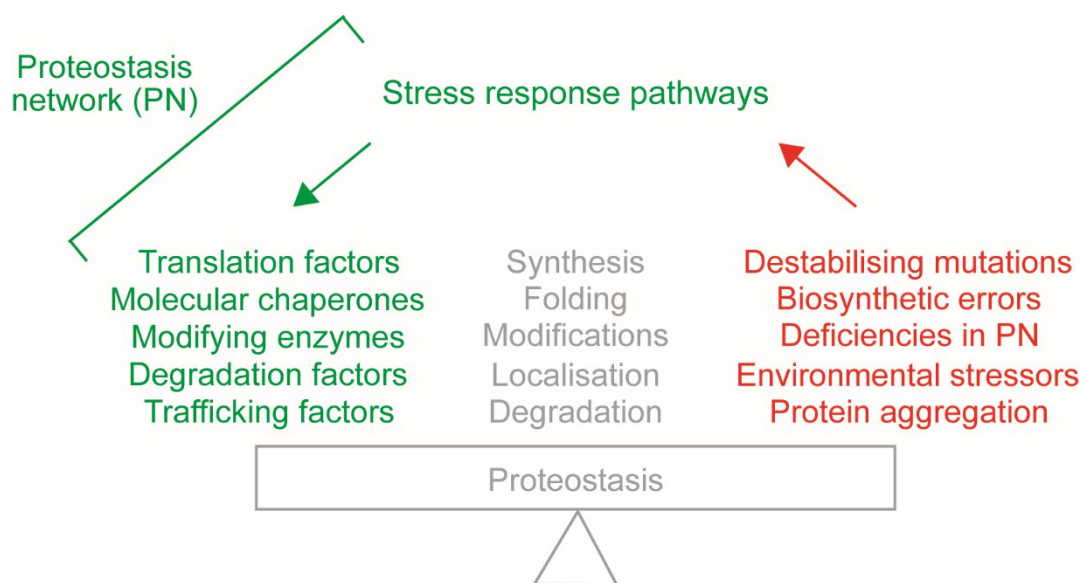


Figure 3. The proteostasis network. Proteostasis is the healthy cellular balance of correctly folded and functioning proteins at controlled concentrations and localisations that is maintained by the proteostasis network (PN) and can be disturbed by multiple factors.

Proteostasis can be disturbed by destabilising mutations, errors in protein biosynthesis, deficiencies of PN components or by environmental stressors (Figure 3). These disturbances

can lead to protein misfolding and aggregation which in turn aggravates proteostasis imbalance because protein aggregates can interfere with folding, processing, trafficking and degradation of other proteins. Impairments in proteostasis induce cellular stress responses, which represent a feedback mechanism that up-regulates protein quality control factors of the PN (Figure 3). The PN maintains proteostasis under basal conditions and also under conditions of intrinsic or environmental stress and is essential to prevent the build-up of potentially toxic and aggregation-prone misfolded protein species that can jeopardize cell fitness and survival (Douglas and Dillin, 2010).

The endoplasmic reticulum

One third of the eukaryotic proteome is synthesised at a specialised cellular organelle: the endoplasmic reticulum (ER) (Ghaemmaghami et al., 2003). The ER forms an interconnected network of membrane-bound flat vesicular structures called cisternae that span the cell and are continuous with the outer nuclear membrane (Figure 4) (Alberts et al., 2014). The main functions of the ER are calcium storage and lipid and protein biosynthesis. Lipid biosynthesis takes place in the smooth ER, which in most cells comprises only a small fraction of the organelle, whereas the part of the ER where protein synthesis takes place is referred to as the rough ER because its surfaces are covered with ribosomes. Proteins that are processed in the ER include those destined for the endomembrane system that consists of the ER, the Golgi, endosomes, lysosomes and the plasma membrane as well as secretory proteins that are transported in membrane-bound vesicles from the ER via the Golgi to the plasma membrane for secretion into the extracellular space (Figure 4).

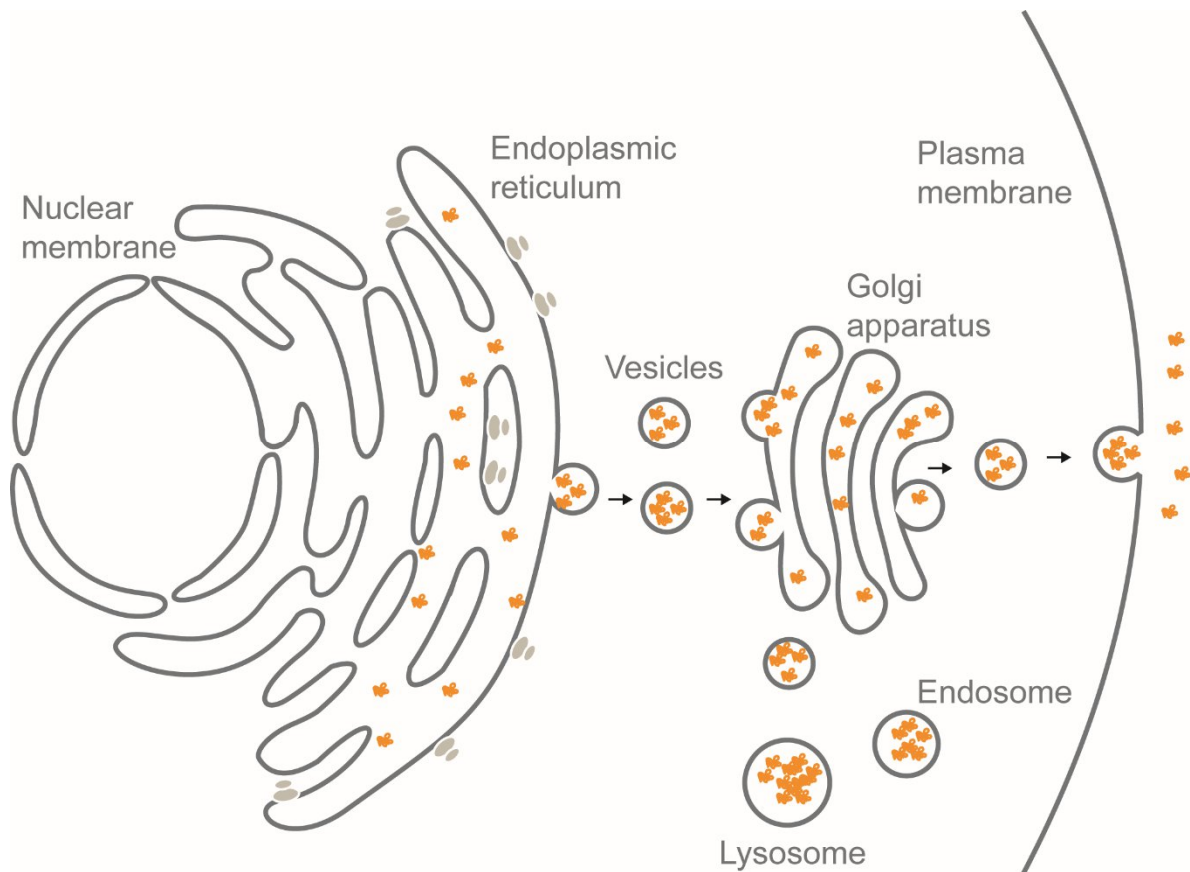


Figure 4. The endomembrane system. Secretory proteins are translated at the endoplasmic reticulum (ER). After folding in the ER lumen they are transported in vesicles to the Golgi apparatus for further modifications and sorting before transport to the plasma membrane and secretion.

Protein translocation into the ER

Protein translocation into the mammalian ER usually occurs co-translationally, although there are also examples of proteins such as tail-anchored (TA) proteins that are post-translationally inserted into the ER after completion of translation in the cytosol (Araki and Nagata, 2011).

Translation of ER-destined proteins always starts in the cytosol. Once the N-terminal signal peptide of an ER-destined nascent chain emerges from the ribosome, it is recognised by the signal-recognition particle (SRP) (Figure 5) (Araki and Nagata, 2011). SRP interacts with the SRP receptor (SR) at the ER membrane and thus causes relocation of the ribosome-nascent chain complex (RNC) to the Sec61 translocon complex (Figure 5). Translation then

proceeds through the Sec61 translocon (Johnson and Van Waes, 1999; Saraogi and Shan, 2011).

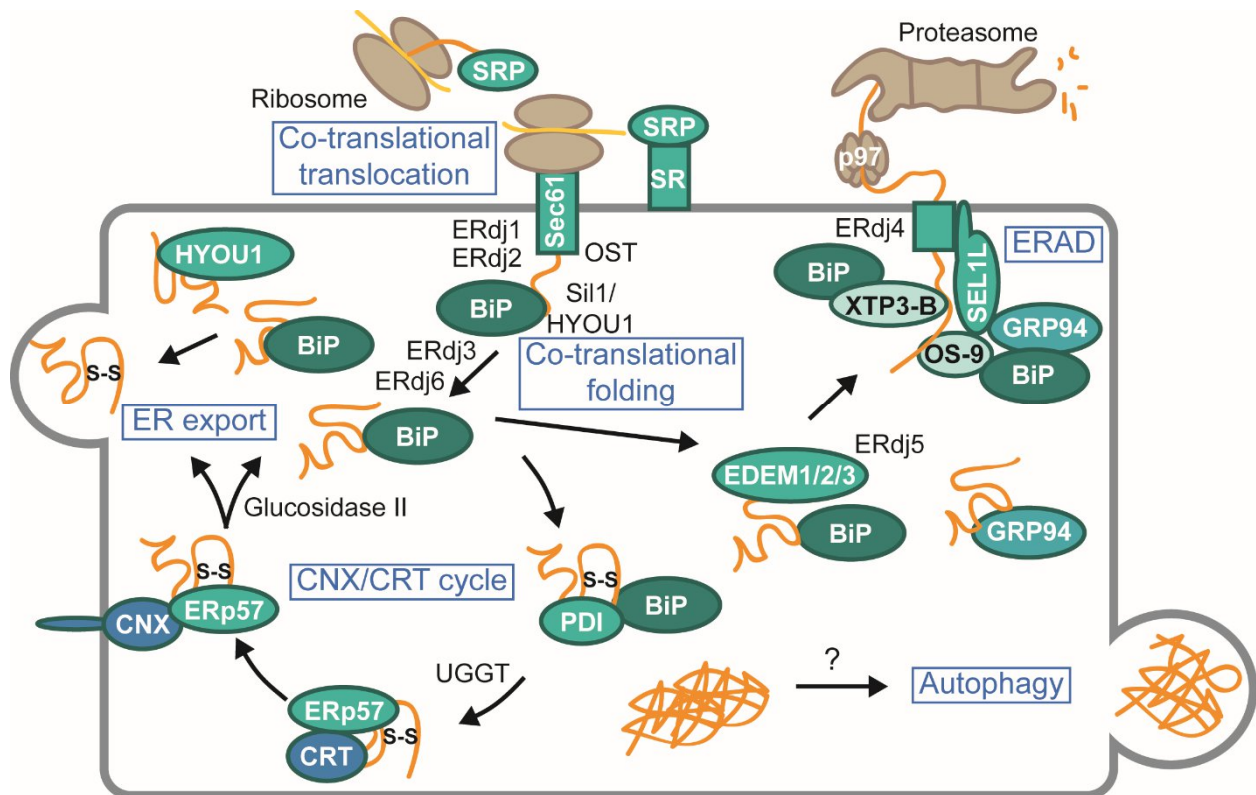


Figure 5. The ER quality control machinery. Most ER-destined proteins are co-translationally translocated into the ER, where they are acted on by molecular chaperones and modifying enzymes. Correctly folded secretory proteins are exported from the ER in transport vesicles. Terminally misfolded ER proteins are targeted for ER-associated degradation or in some cases autophagy.

The special folding environment of the ER

Proteins that enter the ER are exposed to a protein folding environment that is different from that of the cytosol in several aspects (Table 1). First, the ER proteostasis network, often referred to as the ER protein quality control (ERQC) system, consists of a set of molecular chaperones, protein-modifying enzymes and degradation factors that are distinct from those of the cytosolic protein quality control machinery. Second, in the ER, proteins are subject to distinct post-translational modifications that include N-glycosylation, acetylation, lipidation,

membrane insertion and disulphide bond formation. The latter is facilitated by a highly oxidising environment (30 times higher than in the cytosol (Hwang et al., 1992)). These various post-translational modifications render ER-targeted proteins more vulnerable to errors during maturation; however, once a protein is correctly folded these modifications make it in fact more thermodynamically stable than cytosolic proteins (Buchberger et al., 2010).

Parameter	ER	Cytosol
Redox state	Oxidising	Reducing
Calcium	0-1 mM	<1 μ M
Energy generating system	No	Yes
N-glycosylation machinery	Yes	No
HSP70 family	BiP/GRP78	HSP70/HSP72, HSC70
Large HSP70s NEF family	HYOU1/GRP170	HSP110
Sil1-like NEF family	Sil1/BAP	HspBP1, Bag-1
HSP40 co-chaperone family	ERdj1-5	DnaJA1-2,4, DnaJB1,2,4-6
HSP90 family	GRP94	HSP90
Major stress response	Unfolded protein response	Heat shock response

Table 1. Differences in the folding environment of the ER and the cytosol. Modified and extended from (Marzec et al., 2012).

Another factor that distinguishes the folding environment of the ER is its unique ion composition, which is mainly due to the fact that the ER is the main cellular Ca^{2+} storage site. Fluctuations in calcium levels are buffered by Ca^{2+} -binding ER chaperones (Van et al., 1989). Furthermore, ER chaperones and protein-modifying enzymes heavily depend on ATP as a source of energy. However, ATP is not synthesised in the ER and must be imported from the cytosol by a so far unknown mechanism that may depend on Ca^{2+} release (Zuehlke and Johnson, 2010; Vishnu et al., 2014). Another biomolecule that is not readily available in the ER and requires active transport is acetyl-CoA that is important for ER proteostasis, as a

donor for protein acetylation. The activity of many ER-resident enzymes and chaperones, as well as many secretory and membrane proteins depends on N^ε-lysine acetylation (acetylation of the ε amino group of lysine residues) by the acetyl-CoA:lysine acetyltransferases 1 and 2 (ATase 1 and ATase 2) (Ko and Puglielli, 2009). N^ε-lysine acetylation is a reversible post-translational modification that is different from N^α-acetylation (N-terminal acetylation) and O-acetylation (Pehar and Puglielli, 2013). Acetyl-CoA, which serves as an acetyl group donor for this modification, cannot cross lipid bilayers because it is highly charged and needs to be actively imported by the acetyl-CoA transporter 1 (AT-1) (Jonas et al., 2010).

ER protein folding factors

Notably, the Golgi apparatus contains protein modifying enzymes but no molecular chaperones (Ellgaard and Helenius, 2003). Thus, protein folding must be completed before proteins exit the ER and the ERQC machinery must prevent exit of incompletely folded proteins as they may pose a threat to the cell. Thus, proteins are retained by the ERQC machinery until either folding is completed or the protein is targeted for degradation in the case of terminally misfolded proteins (Figure 5). Due to this mechanism of retention until folding is completed, secretory proteins with increased conformational stability are more efficiently secreted (Kowalski et al., 1998).

The ER contains distinct members of some of the main chaperone families. Namely, the HSP90 family member GRP94, the HSP70 family member binding immunoglobulin protein (BiP) (also referred to as glucose-regulated protein 78 (GRP78)), and distinct sets of HSP40 family co-chaperones and nucleotide exchange factors (NEFs) (Figure 5). In addition, the ER contains the lectin chaperones calnexin (CNX) and calreticulin (CRT), peptidyl-prolyl isomerases, thiol-disulphide oxidoreductases and protein disulphide isomerases (PDIs) that facilitate protein folding. Notably, the ER does not contain members of the HSP100 and HSP60 families (Ellgaard and Helenius, 2003; Rodriguez-Lopez et al., 2014). Incompletely

folded proteins are recognised by ERQC factors via exposed hydrophobic regions, unpaired cysteine residues or specific glycosylation signatures.

The calnexin/calreticulin system

One of the most important protein folding systems in the ER is the CNX/CRT system, which is unique to this organelle (Figure 5). The CNX/CRT cycle integrates protein folding and N-glycosylation that affects most secretory proteins and is thus the major quality control system for such proteins (Hebert et al., 2005). Both CNX and CRT bind N-linked glycans (Hammond et al., 1994; Hebert et al., 1995). The type I membrane protein CNX and the soluble ER-luminal protein CRT share about 39% sequence identity and contain Ca^{2+} -binding sites (Smith and Koch, 1989; Wada et al., 1991). Both proteins also bind ATP but do not have any known ATPase activity (Ou et al., 1995; Saito et al., 1999).

The glycosylation cycle begins already co-translationally when oligosaccharyltransferase (OST) adds the oligosaccharide $\text{Glc}_3\text{Man}_9\text{GlcNAc}_2$ to asparagine residues within the consensus sequence Asn-Xxx-Ser/Thr of emerging polypeptide chains (Shibatani et al., 2005; Ruiz-Canada et al., 2009). The outermost glucose of this oligosaccharide is then removed by glucosidases I and II to allow for polypeptide chains to be recognised by CNX and CRT (Grinna and Robbins, 1979). CNX and CRT assist correct protein folding by preventing protein aggregation as well as premature ER exit. Furthermore, they recruit other chaperones and modifying enzymes including the protein disulphide isomerase (PDI) ERp57 (Figure 5) (Williams, 2006; Rutkevich and Williams, 2011). Only after removal of the innermost glucose residue by glucosidase II, is a polypeptide released from CNX and CRT. Unfolded or incorrectly folded polypeptides are subsequently re-glycosylated by UDP-glucose/glycoprotein glucosyl transferase (UGGT) and returned into the CNX/CRT cycle (Solda et al., 2007; D'alessio et al., 2010). This process is repeated until

finally, correctly folded proteins are released from the cycle and transported to their final destination (Hebert et al., 2005).

In addition to binding oligosaccharides, CNX and CRT also recognise proteins via their polypeptide-binding sites (Ware et al., 1995; Ihara et al., 1999). Numerous studies have demonstrated that both CNX and CRT recognise normally glycosylated clients even in glycosylation-deficient cells and also bind unfolded non-glycosylated proteins (Rajagopalan et al., 1994; Basu and Srivastava, 1999; Saito et al., 1999; Spee et al., 1999; Danilczyk and Williams, 2001; Swanton et al., 2003). These results clearly suggest the possibility of a glycan-independent recognition mechanism. However, the existence of this additional client-binding mechanism is still under debate (Williams, 2006).

The BiP chaperone system

BiP is a member of the highly conserved HSP70 family that can be found in all organisms (Gupta and Golding, 1993). There are eight different HSP70 family members in human cells. HSP70s can be found in the cytosol, the ER, mitochondria and in the nucleus (Kampinga et al., 2009). BiP is one of the most abundant chaperones in the ER (Araki and Nagata, 2011), where it is co-translationally targeted via an N-terminal signal sequence and retained via a C-terminal KDEL retention signal (Behnke et al., 2015). Proper morphology and functioning of the ER depends on BiP activity (Hendershot et al., 1995; Paton et al., 2006). The BiP folding cycle is thought to be the most important quality control system for non-glycosylated proteins as well as for proteins that are glycosylated relatively late in their folding cycle (Molinari and Helenius, 2000). BiP's activities include facilitating client protein folding, prevention of aggregation as well as delivering proteins for ER-associated degradation (ERAD) (Figure 5) (Brodsky et al., 1999; Hendershot, 2004; Christianson et al., 2008; Hosokawa et al., 2008; Olzmann et al., 2013). BiP is present in cells in an active state, which is thought to be unmodified and monomeric, and in an inactive state that is AMP-ribosylated,

phosphorylated and oligomeric (Carlsson and Lazarides, 1983; Welch et al., 1983; Freiden et al., 1992; Behnke et al., 2015). It is thought that BiP is present mostly in its inactive state forming an oligomeric pool, which can be readily activated when required, for example during conditions of stress. Unfolded protein substrates as well as elevated ATP levels cause dissociation of BiP oligomers into the active monomeric form (Carlino et al., 1992; Freiden et al., 1992; Blond-Elguindi et al., 1993; Behnke et al., 2015).

All HSP70 family members contain an N-terminal ATPase domain, also called the nucleotide binding domain (NBD), and a peptide-binding domain (PBD). The PBD contains an extended hydrophobic stretch that interacts with hydrophobic regions of client proteins (Bertelsen et al., 2009). In the ATP-dependent client binding and release cycle that is the common activity cycle of all HSP70s, the NBD regulates the conformation of the PBD (Gaut and Hendershot, 1993; Hendershot et al., 1996; Kampinga and Craig, 2010). In the ATP-bound state, HSP70s rapidly bind and release client proteins. ATP hydrolysis then locks client binding tightly. However, due to the very weak intrinsic Mg^{2+} -dependent ATPase activity of HSP70s (Kassenbrock and Kelly, 1989; Mayer et al., 2003), their activity cycle requires the HSP40 J-domain-containing co-chaperone family (HSP40/DNAJ) that stimulate the ATPase activity to stabilise the client interactions after delivery of client proteins to HSP70 (Laufen et al., 1999). HSP40s are structurally very diverse and the large number of different HSP40s is thought to determine both substrate specificity and differential functions of HSP70s. ER-localised Hsp40 family members control the various functions of BiP by regulating client binding and release rates (Kampinga and Craig, 2010; Behnke et al., 2015). Seven members of the HSP40 family, ERdj1-7, have been identified as BiP co-chaperones (Araki and Nagata, 2011). The transmembrane proteins ERdj1 and ERdj2 are homologues of the yeast translocation protein Sec63 and are thus thought to recruit BiP to the translocon, where it assists folding of newly synthesised polypeptides (Lyman and Schekman, 1997; Muller et al.,

2010; Araki and Nagata, 2011). The HSP40 member ERdj3 assists in *de novo* protein folding and also acts in a complex with BiP, GRP94, GRP170 and other folding factors to assist folding of immunoglobulin G (Meunier et al., 2002; Otero et al., 2010). During conditions of ER stress, ERdj3 is secreted and binds misfolded proteins to prevent their toxic aggregation in the extracellular space (Genereux et al., 2015). ERdj4 and ERdj5 interact with the ERAD components p97 and EDEM, respectively, and target misfolded proteins for degradation (Dong et al., 2008; Ushioda et al., 2008). ERdj6 (also referred to as p58^{IPK}) is involved in *de novo* protein folding (Gale et al., 1998; Yan et al., 2002).

Once a substrate is correctly folded, BiP needs to return from its ADP- to its ATP-bound state to release its client and complete the chaperone cycle. For this release step, the activity of nucleotide exchange factors (NEFs) is required. NEFs swap ADP for ATP, which loosens the HSP70-client interaction and thus NEFs control substrate release (Dragovic et al., 2006). BiP especially relies on NEFs because nucleotide exchange is thought to be the rate-limiting step of the chaperone cycle in the folding environment of the ER. This is due to the fact that the high Ca^{2+} concentration increases the affinity of BiP for ADP by almost 1000-fold (Lamb et al., 2006; Behnke et al., 2015). The ER-localised NEFs that are responsible for BiP regulation are the hypoxia up-regulated protein 1 (HYOU1/ GRP170/ ORP-150) and BiP-associated protein (BAP/ Sil1) (Lin et al., 1993; Chung et al., 2002; Meunier et al., 2002; Kampinga and Craig, 2010; Behnke et al., 2015). HYOU1 is conserved in eukaryotes and is, like the cytosolic NEF HSP110, a member of the family of the so-called large HSP70s that have a similar domain organisation as the HSP70 family (Chen et al., 1996; Craven et al., 1997; Easton et al., 2000). HYOU1 bears a similar NBD as BiP but with higher ATP affinity (Dierks et al., 1996). However, unlike BiP, HYOU1 is highly glycosylated and the two proteins vary greatly in their SBDs. HYOU1 also facilitates protein folding directly via interactions with unfolded proteins through a mechanism that is distinct from the

chaperone activity of HSP70s (Behnke and Hendershot, 2014). HYOU1 lacks a highly conserved arginine residue that is present not only in all HSP70s but also in the cytosolic large HSP70s and is required for interactions with HSP40s. Thus, HYOU1 must be regulated by a distinct mechanism (Behnke et al., 2015). HYOU1 is retained in the ER via a C-terminal KDEL retention signal (Ikeda et al., 1997). Notably, the cytosolic NEF HSP110 has been suggested to act as a disaggregase (Rampelt et al., 2012; Mattoo et al., 2013) but it is hitherto unknown whether HYOU1 has a similar activity. The second ER-localised NEF, Sill, shares some identity with the cytosolic NEF HSPBP1, consisting of four armadillo motifs that fold around the ATPase domain of BiP (Behnke et al., 2015). The interaction with BiP is thought to be responsible for ER retention since Sill does not contain a retention signal (Howes et al., 2012). HYOU1 and Sill do not interact with one another and regulate BiP in a mutually exclusive manner (Behnke et al., 2015). Taken together, the chaperone cycle of BiP is controlled by the relative concentrations of both HSP40s and NEFs.

The GRP94 chaperone

The ER chaperone 94 kDa glucose regulated protein (GRP94/endoplasmic reticulum chaperone 1/HSP90B1) is part of the highly conserved HSP90 chaperone family that also includes the cytosolic HSP90A and mitochondrial TNFR-associated protein (TRAP) (Taipale et al., 2010). GRP94, which is retained in the ER by a C-terminal retention signal, is found in all multicellular animals and plants but not in yeast or other unicellular organisms (Marzec et al., 2012). Unlike other major ER chaperones, GRP94 is very selective. To date, less than twenty substrates that rely on GRP94 for folding and/or assembly have been identified. These mainly include secretory and membrane proteins. GRP94 is essential for animal and plant development. However, it is not required for global protein trafficking and secretion and is also not essential for mammalian cells grown in cell culture, most likely because of its selectivity for a small number of substrates (Marzec et al., 2012). GRP94 is active mostly as a dimer in a conformational cycle

that is common to HSP90 family members and requires its ATPase activity (Stefanovic and Hegde, 2007; Taipale et al., 2010; Marzec et al., 2012). ATP binding via the N-terminal domain (NTD) results in a closed conformation of HSP90s. Subsequent hydrolysis of ATP to ADP and ADP dissociation restores the open conformation. Due to the similar affinity of GRP94 for ATP and ADP (Soldano et al., 2003; Immormino et al., 2004), which is uncommon amongst HSP90 chaperones, GRP94 has a unique mechanism of regulation.

GRP94 is subject to N-glycosylation, acetylation and phosphorylation and is a potent Ca^{2+} carrier. Ca^{2+} binding induces a conformational change and thus regulates GRP94 activity (Van et al., 1989; Marzec et al., 2012). The cytosolic HSP90 is regulated by different co-chaperones (Zuehlke and Johnson, 2010). In comparison, GRP94 also interacts with other ER proteins that may act as co-chaperones, including protein canopy homolog 3 (CNPY3), which is required for proper folding of toll-like receptor (TLR) (Liu et al., 2010), ATPase ASNA1, which is required for delivery of TA proteins, and the protein OS-9, which targets misfolded proteins for ERAD (Kao et al., 2007; Stefanovic and Hegde, 2007; Christianson et al., 2008; Liu et al., 2010). Thus, in addition to its role in protein folding, GRP94 is also involved in directing misfolded proteins to the ERAD machinery (Figure 5).

Degradation of ER proteins

ER proteins that are terminally misfolded and thus cannot reach their native state, are prevented from exiting the ER by retention in chaperone cycles and are targeted for ER-associated degradation (ERAD) (Figure 5) (reviewed in (Olzmann et al., 2013)). Terminal misfolding can occur due to destabilising mutations, erroneous protein synthesis or deficiencies in the ER proteostasis network. ER-localised proteins must be relocated into the cytosol before they can be degraded by the proteasome. Thus, after recognition of an ERAD substrate, the substrate is retro-translocated (dislocated) through the dislocon in the ER

membrane. In the cytosol, the substrate is then subject to ubiquitination followed by proteasomal degradation.

Most ERAD substrates are recognised via their specific glycosylation signature, which is generated by mannosidases that trim mannose residues from misfolded glycans. This glycan is then further processed by the activity of EDEM1, EDEM3, ERMan1, and Man1C1, stimulating progressive removal of terminal mannose residues. The resulting demannosylated and deglycosylated substrates cannot re-enter the CNX/CRT cycle and are thus irreversibly targeted for degradation (Gonzalez et al., 1999; Tremblay and Herscovics, 1999; Olivari et al., 2006; Hosokawa et al., 2007; Hosokawa et al., 2009; Lederkremer, 2009; Aebi et al., 2010; Hosokawa et al., 2010). The substrate recognition factors OS-9 and XTP3-B then bind substrates via their mannose-6-phosphate receptor homology (MRH) domains (Bernasconi et al., 2008; Christianson et al., 2008; Hosokawa et al., 2008). Even though OS-9 and XTP3-B share little sequence homology except for the MRH domain, they have some redundant activity and only simultaneous knock-down of both genes affects the stability of model substrates (Bernasconi et al., 2010). OS-9 and XTP3-B are also involved in ERAD of non-glycosylated substrates (Sekijima et al., 2005; Okuda-Shimizu and Hendershot, 2007; Bernasconi et al., 2008; Christianson et al., 2008; Hosokawa et al., 2008). However, while the mechanisms of glycosylated substrate recognition have been studied extensively, the underlying molecular mechanisms of non-glycosylated substrate recognition are not as well understood. Both OS-9 and XTP3-B may recognise misfolded regions within a substrate in addition to the glycosylation signature (Hosokawa et al., 2009). Alternatively, OS-9 and XTP3-B may bind non-glycosylated substrates indirectly via an interaction with GRP94 and with BiP (Christianson et al., 2008; Hosokawa et al., 2008). BiP is also thought to be involved in ERAD via its co-chaperone ERdj5, which interacts with EDEM1 (Ushioda et al., 2008).

Another suggested mechanism for degradation of non-glycosylated substrates involves targeting via post-translational glycosylation (Sato et al., 2012).

Following substrate recognition, EDEM1, EDEM3, OS-9 and XTP3-B bind the adaptor protein SEL1L that links substrate recognition complexes to the dislocon factor Hrd1 (Bernasconi et al., 2008; Christianson et al., 2008; Hosokawa et al., 2008; Cormier et al., 2009; Carvalho et al., 2010; Saeed et al., 2011; Hosokawa and Wada, 2016). SEL1L is a transmembrane protein and interacts with the integral membrane proteins AUP1, Derlin-1, Derlin-2, Herp, UBXD8 and VIMP. The cytosolic VCP/p97 complex is recruited to this complex to facilitate substrate dislocation into the cytosol (Mueller et al., 2006; Christianson et al., 2008; Hosokawa et al., 2008; Mueller et al., 2008; Iida et al., 2011; Klemm et al., 2011; Christianson et al., 2012). In addition to SEL1L, the intramembrane proteins Erlin-1 and Erlin-2 are also substrate adaptors that connect substrates to the E3 ubiquitin ligases gp78, Hrd1 and Trc8 (Christianson et al., 2012; Olzmann et al., 2013). E3 ubiquitin ligases bind substrates and catalyse transfer of ubiquitin from E2 ligases to target substrates for proteasomal degradation (Berndsen and Wolberger, 2014).

It remains to be fully elucidated which factors make up the dislocon through which ERAD substrates are retro-translocated into the cytosol but Derlins 1-3, Hrd1, Sec61 and the signal peptidase (SP) have been proposed to be involved (Plemper et al., 1997; Lilley and Ploegh, 2004; Ye et al., 2004; Loureiro et al., 2006; Scott and Schekman, 2008; Carvalho et al., 2010). Notably, retro-translocation does not require substrates to be completely unfolded, unlike translocation of proteins into the ER through the Sec61 translocon, as it has been reported that substrates with tightly folded and ligand-stabilised domains, proteins with glycosylated residues and even whole virus particles can be retro-translocated (Fiebiger et al., 2002; Tirosh et al., 2003; Blom et al., 2004; Lilley et al., 2006; Geiger et al., 2011). The mechanism of retro-translocation must be fundamentally different from that of classic protein

channels such as the Sec61 complex because substrates that are even larger than the Sec61 pore complex itself can be retro-translocated through the dislocon. Despite the finding that partially folded proteins can be retro-translocated, it is thought that a reduction of disulphide bonds is required (Olzmann et al., 2013).

Once a substrate emerges from the dislocon complex, it is recognised by the cytoplasmic homohexameric ATPase p97/VCP that drives further retro-translocation. In the cytosol, substrates are processed by deglycosylating enzymes, ubiquitin-binding proteins and deubiquitinating enzymes. The polytopic RING domain ligases gp78 and Hrd1 are among the major E3 ubiquitin ligases that are thought to be involved in ERAD (Bays et al., 2001; Fang et al., 2001; Nadav et al., 2003; Kikkert et al., 2004). In addition, the more specialised ligases Kf-1/RNF103, Nixin, RFP2/TRIM13, RNF5/Rma-1, RNF170 and TEB4/MARCH6 have also been implicated as playing a role in ERAD (Hassink et al., 2005; Younger et al., 2006; Lerner et al., 2007; Maruyama et al., 2008; Stagg et al., 2009; Altier et al., 2011; Lu et al., 2011; Neutzner et al., 2011). These ligases may work in parallel depending on substrate specificity, simultaneously on different residues of the same substrates, cooperatively or sequentially (Olzmann et al., 2013). ERAD substrates are then subject to degradation by the 26S proteasome, whose substrates also include cytosolic proteins that are also targeted for degradation cooperatively by molecular chaperones and E3 ubiquitin ligases (Kim et al., 2013).

The second major cellular degradation pathway is lysosomal degradation via the autophagy pathway. This involves double-membrane-bounded structures, so-called autophagosomes, which enclose substrates to deliver them to the lysosome. Autophagosomes are thought to also pinch off elements of the ER for degradation (Perlmutter, 2011). Some aggregated proteins that accumulate in the ER have been reported to be degraded via this pathway (Teckman and Perlmutter, 2000; Kamimoto et al., 2006; Hidvegi et al., 2010).

Cellular stress responses

Destabilising mutations or PN impairment can lead to the accumulation of misfolded or unfolded proteins. This in turn often causes a vicious cycle of further misfolding and aggregation due to progressive overburdening of the PN that eventually leads to proteostasis collapse (Figure 3). Cells have evolved specialised response pathways that sense disturbances in proteostasis and increase the cellular capacity to deal with the stress by inducing the expression of PN factors (Figure 3).

The cytosolic stress response

The accumulation of misfolded proteins in the cytosol induces the heat shock response (HSR) that stimulates the upregulation of proteostasis factors, most prominently molecular chaperones that assist protein folding and counteract aggregation. Other factors induced by the HSR include degradation factors, nucleic acid-modifying enzymes, metabolic enzymes, transcription factors, and kinases as well as proteins involved in transport, membrane modulation and in maintaining intracellular structures (Richter et al., 2010). The cellular HSR is characterised by activation of heat shock factor 1 (HSF1) that induces the expression of HSPs (Parker and Topol, 1984; Kingston et al., 1987). As its name suggests, the heat shock response was originally discovered as a cellular response to elevated temperatures (Ritossa, 1962); however, the HSR is not exclusive induced by heat stress but can also be activated by oxidative stress, heavy metals or chemicals that cause similar cellular damage (Bauman et al., 1993; McDuffee et al., 1997). Cellular recovery from such stress is accompanied by an acquired tolerance to more severe stress (Richter et al., 2010). However, prolonged, severe stress may lead to cell death.

The unfolded protein response

Protein folding stress in the ER induces a distinct stress response, namely the unfolded protein response (UPR) (Figure 6) (Walter and Ron, 2011). Protein folding in the ER can be disturbed

by a range of endogenous and external conditions including destabilising mutations, protein overload, alterations in Ca^{2+} levels, hypoxia, and glucose deprivation that causes a drop in ATP levels. Conditions that disrupt protein folding and maturation lead to accumulation of misfolded proteins in the ER and are referred to as ER stress. UPR factors sense ER stress and transmit a signal to the cytosol and nucleus to activate specific transcription factors that induce a coordinated stress response (Walter and Ron, 2011). The UPR relieves stress by inhibiting general translation, while simultaneously up-regulating proteins involved in protein degradation, folding, processing and trafficking as well as lipid biosynthesis in order to re-establish ER homeostasis. The UPR is thus an important physiological adaptation mechanism. However, during conditions of severe or prolonged ER stress that cannot be resolved, the UPR induces cell death via apoptosis (Puthalakath et al., 2007).

ER stress is first sensed by activating transcription factor 6 (ATF6), inositol requiring enzyme 1 α (IRE1 α , Endoplasmic reticulum-to-nucleus signalling 1, ERN1) and the PKR-like ER kinase (PERK) that are located in the ER membrane and transmit the stress signal to the cytosol (Walter and Ron, 2011). In the absence of stress, the three sensors are present in an inactive BiP-bound state. Upon accumulation of misfolded proteins in the ER, BiP is sequestered by misfolded substrates and dissociates from the UPR sensors allowing for their activation.

The ATF6 branch

The transcription factor ATF6 is retained as an ER transmembrane protein by association with BiP. Upon ER stress, BiP dissociates allowing for ATF6 translocation to the Golgi apparatus, where the transmembrane domain is cleaved releasing a transcription factor, which subsequently translocates to the nucleus to activate target genes (Figure 6) (Chen et al., 2002). ATF6 targets include genes involved in ER protein processing and ERAD (Adachi et al., 2008; Shoulders et al., 2013). ATF6 activity is thus cytoprotective as it improves ER

proteostasis. ATF6 also transcriptionally induces X-box binding protein 1 (XBP1) that is activated by cleavage of its mRNA by IRE1 α (Yoshida et al., 2001). Furthermore, ATF6 collaborates with XBP1 in transcriptional activation (Yamamoto et al., 2004).

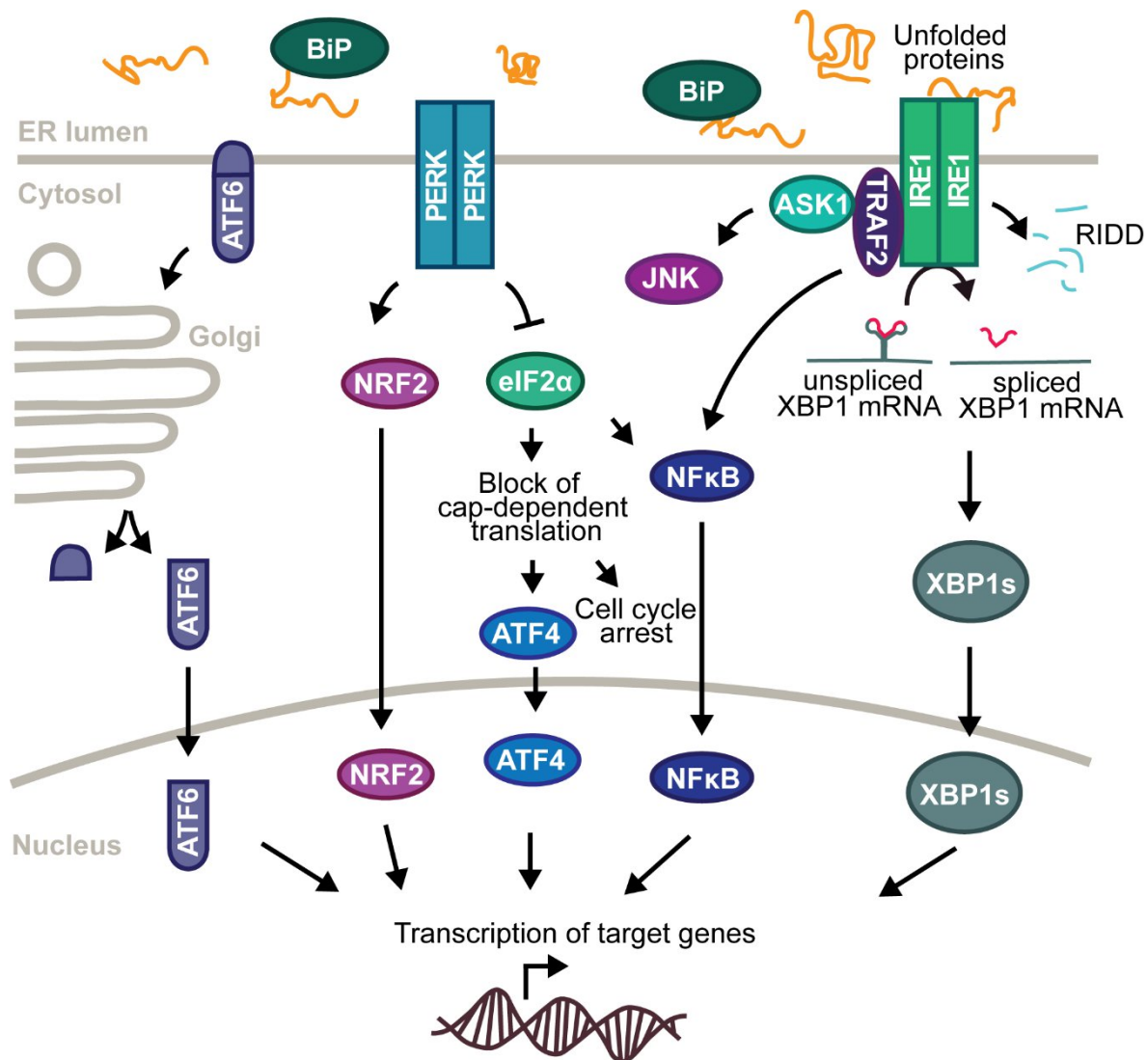


Figure 6. The unfolded protein response. The accumulation of misfolded proteins in the ER causes the activation of the ER stress sensors ATF6, PERK and IRE1 α that transmit a signal into the cytosol and nucleus to induce a coordinated stress response.

The IRE1 α branch

IRE1 is a type I ER transmembrane protein that has serine-threonine kinase as well as endoribonuclease activity owing to a cytosolic kinase-extension nuclease (KEN) domain (Lee et al., 2008b; Ali et al., 2011). IRE1 is present in two different isoforms: the extensively

studied and ubiquitously expressed IRE1 α , and IRE1 β , which has so far only been found in epithelial cells of the gastrointestinal tract and in the bronchi (Wang et al., 1998; Bertolotti et al., 2001; Martino et al., 2013). BiP dissociation during stress leads to oligomerisation and subsequent trans-autophosphorylation of IRE1 α . Phosphorylation activates the endoribonuclease domain, which then splices the pre-mRNA of XBP1 (Figure 6) (Cox and Walter, 1996; Kawahara et al., 1997; Calfon et al., 2002). The XBP1 pre-mRNA is recruited to the ER membrane co-translationally together with the stalled translation complex and the emerging nascent chain of the unspliced XBP1 (Yoshida et al., 2001; Yanagitani et al., 2009; Plumb et al., 2015). At the ER membrane, IRE1 α cuts a 26 nucleotide intron out of XBP1 mRNA (Yoshida et al., 2001). The spliced XBP1 (XBP1s) mRNA is then ligated by RtcB (Lu et al., 2014). The resulting frame shift allows for translation of the active transcription factor XBP1s and down-stream induction of its target genes that are involved in protein folding, trafficking, degradation and glycosylation, and in lipid synthesis and thus increase the ER's capacity to deal with misfolded proteins (Lee et al., 2003; Yoshida et al., 2003; Oda et al., 2006; Acosta-Alvear et al., 2007; Lee et al., 2008a; Shoulders et al., 2013). During recovery, XBP1s activity is regulated by a negative feedback loop that involves the translational product of the unspliced mRNA (XBP1u) (Yoshida et al., 2006; Guo et al., 2010). Activated IRE1 α also splices certain mRNAs in order to degrade them, a mechanism referred to as IRE1-dependent decay (RIDD) (Figure 6) (Han et al., 2009; Hollien et al., 2009; Gaddam et al., 2013). The purpose of this mechanism is to reduce translation of secretory proteins and in this way lower the burden on the ER (Hollien et al., 2009). On the other hand, RIDD may also contribute to ER stress-induced cell death as it was reported to activate pro-apoptotic signalling (Han et al., 2009)

IRE1 α also recruits the adaptor protein E3 ubiquitin ligase TNF-receptor-associated factor 2 (TRAF2), which links the apoptosis signalling kinase-1 (ASK1) to IRE1 α kinase

activity (Nishitoh et al., 1998; Nishitoh et al., 2002). ASK1 in turn induces the mitogen-activated protein (MAP) kinase member c-Jun N-terminal kinase (JNK) (Figure 6), which is associated with pro-apoptotic signalling (Urano et al., 2000; Nishitoh et al., 2002). IRE1 α -induced TRAF2 also activates the transcription factor nuclear factor kappa-light-chain-enhancer of activated B-cells (NF- κ B), which is in this context associated with pro-survival signalling (Kaneko et al., 2003). IRE1 α has also been suggested to induce the extracellular signal-regulated kinases (ERK) and the MAP kinases p38 (Zhao et al., 2011). Thus, ER stress-induced IRE1 α signalling can induce both pro-survival and pro-apoptotic responses and it is not yet fully understood how these opposing effects are coordinated. Several cytosolic factors have been proposed to regulate the various functions of IRE1 α (Marcu et al., 2002; Lisbona et al., 2009; Gupta et al., 2010).

The PERK branch

In a similar manner as IRE1 α , the serine/threonine protein kinase PERK is also activated by dimerisation and trans-autophosphorylation after dissociation of BiP. Activated PERK phosphorylates the α -subunit of eukaryotic initiation factor 2 (eIF2 α) (Figure 6). The eukaryotic initiation factors play important roles in translation as they recognise either the m7G cap at the 5' end or the poly(A) tail at the 3' end of mRNA, which allows binding of the pre-initiation complex (PIC) that consists of the small ribosomal subunit carrying Met-tRNAⁱ. The PIC then searches for the start codon by scanning the mRNA sequence (Sonenberg and Hinnebusch, 2009). Phosphorylated eIF2 acts as an inhibitor of its own nucleotide exchange factor, eIF2B, because it has increased affinity for eIF2B but nucleotide exchange cannot occur in the phosphorylated state of eIF2. In this way, phosphorylation of eIF2 α prevents it to return into its active state and thus blocks the translation initiation process leading to translational arrest of most mRNAs and a reduction in ER protein load (Kao et al., 2007). However, a few mRNAs, including many UPR targets and transcription factors, contain so-

called internal ribosome entry sites (IRESs) near the start codon that allow for PIC binding and translation initiation independent of this scanning mechanism (Sonenberg and Hinnebusch, 2009). Another mechanism of translation that occurs after eIF2 α phosphorylation is that of the transcription factor ATF4. In fact, ATF4 translation occurs preferentially once eIF2 α is phosphorylated because its mRNA contains short upstream open reading frames (uORFs) in the 5' untranslated region that are predominantly targeted by the PIC under normal conditions. Ribosome initiation at these uORFs hinders translation of the further downstream coding sequence. Only after phosphorylation of eIF2 α this mechanism is blocked allowing for a stochastic bypass of the uORFs and ribosome access to the start codon of the downstream coding sequence of ATF4 (Hinnebusch, 2014; Starck et al., 2016). Thus, eIF2 α phosphorylation blocks general translation but induces the transcription factor ATF4 and allows translation of UPR target genes. Notably, PERK is not the only kinase that phosphorylates eIF2 α . Three related kinases, called general control nonderepressible 2 (GCN2), heme-regulated inhibitor kinase (HRI), and interferon-induced dsRNA-dependent kinase (PKR) phosphorylate eIF2 α in response to various conditions of stress that include heat shock, amino acid deprivation, osmotic shock, oxidative stress and viral infection (Donnelly et al., 2013). Induction of the eIF2 α kinases leading to ATF4 activation is collectively referred to as the integrated stress response (ISR). ATF4 target genes include factors involved in restoring ER homeostasis and also other cytoprotective genes that are not ERQC-related as well as pro-apoptotic factors including the transcription factor C/EBP-homologous protein (CHOP, also referred to as GADD153) (Harding et al., 2000; Bi et al., 2005; Blais et al., 2006). PERK was also reported to induce NF- κ B in an eIF2 α phosphorylation-dependent manner (Deng et al., 2004).

PERK also activates the transcription factor nuclear factor-erythroid 2-related factor 2 (NRF2) (Figure 6). After phosphorylation by PERK, NRF2 dissociates from its negative

regulator Kelch-like ECH-associated protein 1 (KEAP1). NRF2 target genes play a role in cytoprotective redox signalling (Cullinan et al., 2003).

The ordered protein response

Notably, ER luminal accumulation of some aggregation-prone mutant proteins does not induce the UPR. These proteins include disease mutants of the serpin proteins α 1-antitrypsin (A1AT) and neuroserpin (NRS) that form polymers within the ER (Graham et al., 1990; Hidvegi et al., 2005; Davies et al., 2009). One explanation for why these mutant serpin proteins do not induce the UPR, even though they are prone to aggregate, is that they may not be recognised as misfolded protein species because they closely resemble the native state of the monomer (Yamasaki et al., 2008; Perlmutter, 2011). However, ER-retained polymers of both mutant A1AT (Lawless et al., 2004; Hidvegi et al., 2005) and mutant NRS (Davies et al., 2009) induce the transcription factor NF κ B in a UPR-independent manner. At least in the case of NRS polymers, this UPR-independent NF κ B activation was caused by an increased flux of Ca²⁺ from the ER into the cytosol (Davies et al., 2009). NF κ B activation by serpin polymers was first described as the ER overload response (EOR) but later renamed the ordered protein response (OPR) to underline that it is distinct from the UPR (Davies et al., 2009).

Protein aggregation toxicity

Protein aggregation is associated with a large number of different human diseases, the so-called protein misfolding or protein conformational diseases (Chiti and Dobson, 2006; Knowles et al., 2014). Protein aggregation can be caused by the synthesis of folding-incompetent protein species or by defects in the protein quality control machinery. If such species are not efficiently degraded, they are prone to form insoluble aggregate conformations.

Human diseases that are characterised by protein aggregates exhibit a wide variety of clinical symptoms (Table 2). Despite the diverse identities and properties of the aggregating proteins the aggregate conformations they form are very similar and elicit common toxic effects and cellular responses. Among the most prominent aggregate conformations are amyloid-like fibrils that consist of cross- β structures. Amyloid-like aggregates are associated with a range of human diseases including neurodegenerative disorders, non-neuropathic localised amyloidoses and non-neuropathic systemic amyloidosis, including sporadic and hereditary forms (Chiti and Dobson, 2006).

Disease	Clinical Features	Aggregating protein	Cellular location of aggregates
Alpha 1-antitrypsin deficiency	Lung and liver disease	α 1-antitrypsin (A1AT)	Endoplasmic Reticulum
Alzheimer's disease (AD)	Progressive dementia	Amyloid- β (A β) and tau	Extracellular, cytoplasmic
Amyotrophic lateral sclerosis	Movement disorder	Superoxide dismutase	Cytoplasmic
Familial encephalopathy with neuroserpin inclusion bodies (FENIB)	Dementia	Neuroserpin (NRS)	Endoplasmic Reticulum
Huntington's disease (HD)	Dementia, motor and psychiatric symptoms	Huntingtin (Htt)	Nuclear
Parkinson's disease (PD)	Movement disorder	α -synuclein	Cytoplasmic
Transmissible spongiform encephalopathies	Dementia, ataxia, psychiatric problems	Prion protein (PrP)	Extracellular
Transthyretin amyloidosis	Progressive sensory and motor polyneuropathy	Transthyretin (TTR)	Extracellular

Table 2. Diseases associated with protein aggregation. Modified from (Soto, 2003).

Conformational diseases caused by mutant ER proteins

Aggregation toxicity can be caused by loss-of-function as well as gain-of-function effects and in many cases both effects contribute to the disease. Misfolded secretory proteins are recognised by the ERQC machinery and are retained in the ER until they reach their native

state or are targeted for degradation to protect cells from the accumulation of toxic aggregation-prone proteins. However, retention and degradation can cause disease due to loss-of-function toxicity (Figure 7). Loss-of-function toxicity is caused by the loss of important protein activities and can be mimicked by knockout of a specific gene. It should however be noted that this effect is distinct from specific loss-of-function mutations because even though destabilising mutations affect the folding efficiency of a protein, the protein may be functional if correct folding is assisted. Thus, in the case of conformational diseases, loss-of-function toxicity is not the result of non-functionality of a specific protein activity. Instead, it is caused by aggregation and/or degradation of a protein before it can reach its native state (Hebert and Molinari, 2007; Molinari, 2007). The important difference is that loss-of-function disorders that are caused by folding-deficient mutants could potentially be treated by therapies that increase protein folding efficiency or protein trafficking. For example in the autosomal recessive disorder cystic fibrosis, folding deficient mutants of the membrane protein cystic fibrosis transmembrane conductance regulator (CFTR) do not reach their native state and target location and are degraded by ERAD (Cheng et al., 1990; Jensen et al., 1995; Ward et al., 1995). Other examples of diseases caused by loss-of-function toxicity are diabetes mellitus, familial hypercholesterolemia and retinitis pigmentosa (Hebert and Molinari, 2007).

If the ERQC fails to target folding-deficient secretory proteins for degradation they can cause gain-of-function toxicity (gain-of-toxicity) (Figure 7). Gain-of-function toxicity is caused by the sheer presence of aggregate conformations independent of the native identity of the aggregating proteins. Secretion of toxic misfolded protein species can lead to disorders such as the light chain and the transthyretin amyloidoses (Sorgjerd et al., 2006; Blancas-Mejia and Ramirez-Alvarado, 2013). However, ER retention of such aggregation-prone proteins causes intracellular gain-of-toxicity such as in the case of the serpinopathies, in which destabilised mutant serpin proteins accumulate in the ER as ordered polymers that interact

with each other via mobile loops and β -sheets. Serpinopathies are caused by point mutations in neuroserpins (NRS), α 1-antitrypsin (A1AT), antithrombin or 1-antichymotrypsin, all of which are members of the serine proteinase inhibitor (serpin) superfamily (Fitton et al., 1997; Gooptu et al., 2000; Sivasothy et al., 2000; Davis et al., 2002; Irving et al., 2011). Single point mutations in the NRS gene (S49P, S52R, H338R, or G392E) cause the dementia familial encephalopathy with neuroserpin inclusion bodies (FENIB). NRS proteins with any one of these mutations polymerise and are retained in the ER of neurons, where they cause toxicity leading to progressive dementia (Davis et al., 2002; Miranda et al., 2004). Mutations in the serpin A1AT cause A1AT deficiency that manifests itself in lung and liver disease (Perlmutter, 2011).

Notably, FENIB and A1AT deficiency are associated with both loss-of-function and gain-of-function toxicity. A1AT normally inhibits neutrophil proteases and loss of A1AT function leads to uncontrolled activation of these proteases resulting in damage to lung tissue (Perlmutter, 2011). Conversely, in this case A1AT replacement therapy has not proven effective and it is thus suspected that in addition to loss-of-function effects, gain-of-toxicity of A1AT mutants affects respiratory epithelial cells (Perlmutter, 2011). A1AT mutants have been shown to block the mobility of ER proteins, causing gain-of-toxicity that is thought to be responsible for liver disease at later stages of A1AT deficiency (Ordonez et al., 2013).

In Alzheimer's disease, amyloid β protein ($A\beta$) forms amyloid fibrils predominantly in the extracellular space as well as within cells leading to gain-of-toxicity. The aggregation-prone $A\beta$ is generated by cleavage of the amyloid precursor protein (APP) at the plasma membrane and the late Golgi (O'brien and Wong, 2011). In addition, intracellularly accumulated $A\beta$ is thought to be generated in the ER (LaFerla et al., 2007; Skovronsky et al., 1998; Wild-Bode et al., 1997).

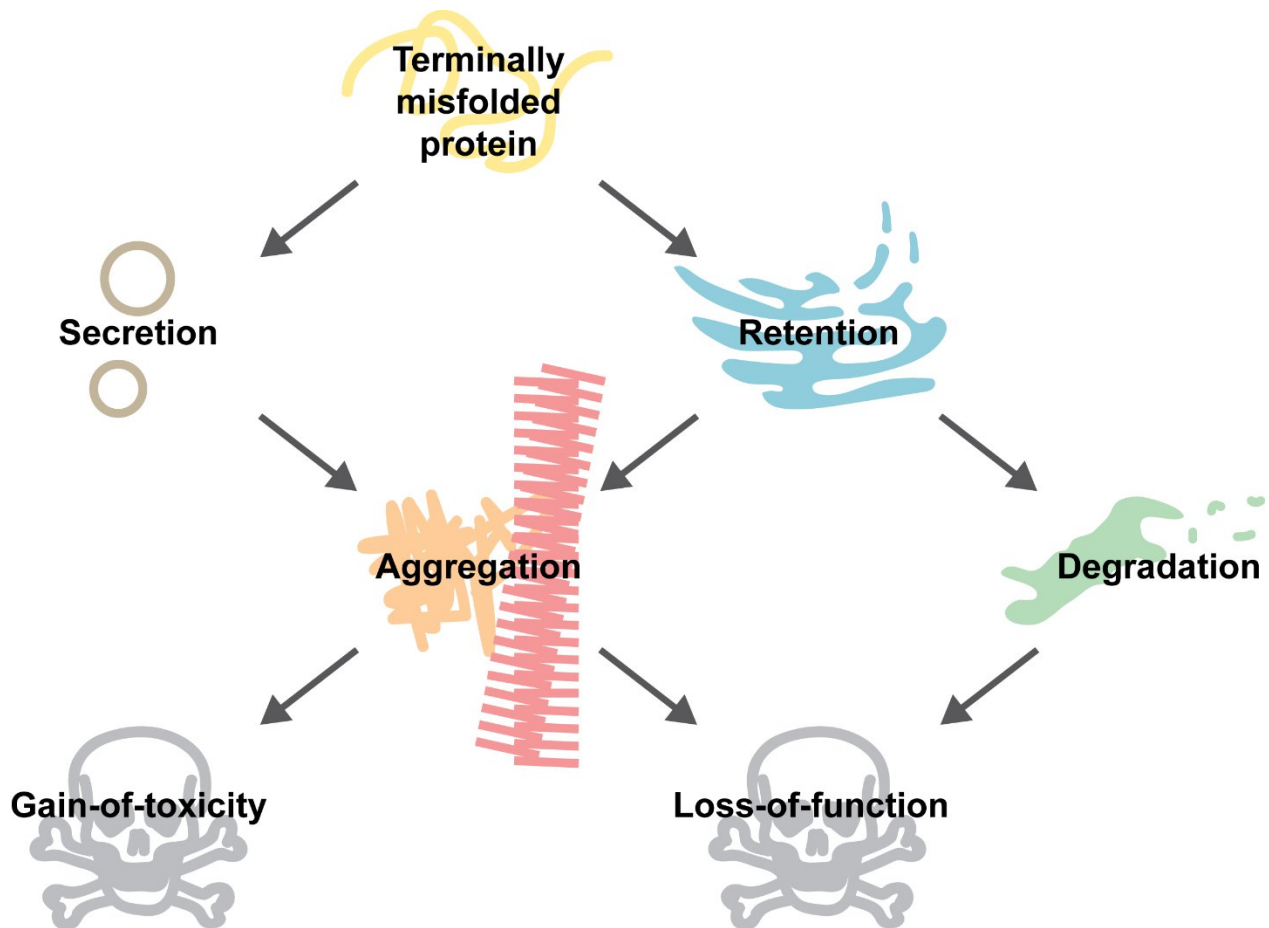


Figure 7. The different fates and potential modes of toxicity of terminally misfolded proteins in the ER. Some destabilised disease proteins aggregate in the ER or are secreted and form toxic aggregates in the extracellular space. Protein aggregation can cause gain-of-function and loss-of-function toxicity. If misfolded proteins are retained in the ER and efficiently targeted for degradation via ERAD, this can also cause loss-of-toxicity.

Even though protein aggregation is associated with cytotoxicity in many diseases it should be noted that it is unclear whether toxicity is caused by large aggregates or rather by smaller oligomeric conformations *en route* to formation of larger inclusions. It has been suggested that the formation of large aggregates may serve as a protective mechanism, whereby toxic protein species are deposited in large inert inclusions, even though large aggregates have also been demonstrated to cause toxicity in various contexts (Haass and Selkoe, 2007).

Mutations in ERQC factors can cause diseases

The importance of the ERQC for human health is exemplified by the detrimental symptoms of the multisystem disorder Marinesco-Sjögren syndrome (MSS) that include cataracts, cerebellar ataxia, growth-restriction, mental retardation and myopathy. MSS is caused by mutations in *Sil1* (Senderek et al., 2005). Other examples include bleeding disorders that are caused by mutations in *ERGIC53*, a protein trafficking factor, leading to reduced secretion of blood coagulation factors (Nichols et al., 1998).

ER stress responses in disease

In cancer, the proteostasis network is often co-opted to promote cancer cell growth and survival. Increased rates of protein synthesis during tumorigenesis can overburden the ERQC leading to ER stress. Cancer cells adapt to such conditions by up-regulating components of the ERQC machinery or the ER stress response. In particular, factors of the UPR are often up-regulated in cancer cells (Healy et al., 2009). For example, in multiple myeloma (MM), a cancer of B lymphocytes, which are highly specialised in antibody production and secretion, the ERQC is burdened by massive production of paraprotein, an abnormal immunoglobulin fragment. Due to the increased requirement for protein folding in the ER, MM cells depend on the ERQC system as well as on the activity of the UPR (reviewed in (Vincenz et al., 2013)). In addition to relieving the stress caused by high rates of protein synthesis, the UPR also promotes adaptation of cancer cells to conditions of hypoxia that are usually present in solid tumours.

In neurodegenerative diseases, ER stress can contribute to neuroprotection but also to neuronal loss. For example, XBP1s is induced by A β and has neuroprotective activity in models of AD (Casas-Tinto et al., 2011). However, A β as well as the Prion disease protein PrP^{Sc} have been demonstrated to induce apoptosis via ER stress in cortical neurons (Ferreiro et al., 2006; Hetz et al., 2003; Nakagawa et al., 2000).

ER quality control in aging

Aging is accompanied by the progressive accumulation of irreparable damage to cellular components and concurrently an impairment of the ability to induce cellular stress responses. This leads to compromised cellular homeostasis, particularly under conditions of stress, and to vulnerability to certain diseases. Proteostasis is especially affected by aging, which is exemplified by the progressive accumulation of protein aggregates in diseases such as Alzheimer's (AD), Parkinson's (PD) and Huntington's disease (HD). Studies of aging nematodes have revealed the global effects of aging on cellular proteostasis, which include protein misfolding, aggregation, proteome imbalances, and severe impairment of the HSR and UPR (Ben-Zvi et al., 2009; Walther et al., 2015).

ER proteostasis is impaired during aging due to several factors. First, total levels of ER chaperones and folding factors are decreased during aging. For example BiP, CNX and PDI have been reported to be down-regulated in aging rats (Paz Gavilan et al., 2006; Hussain and Ramaiah, 2007; Naidoo et al., 2008). Second, these factors accumulate irreparable damage leading to impairments in protein folding. For example, BiP, PDI and also CRT have been found to acquire oxidative damage in aging mice (Rabek et al., 2003). This age-related oxidative damage was shown to impair the ATPase activity of BiP as well as the enzymatic activity of PDI (Nuss et al., 2008). Third, the ability of cells to adapt to ER stress declines with age. In rodents the UPR-mediated activation of ER chaperones is impaired during aging leading to an increased induction of the apoptotic cell death pathway upon exposure to stressors (Paz Gavilan et al., 2006; Hussain and Ramaiah, 2007; Naidoo et al., 2008). It has also been demonstrated in nematodes that the activity of the IRE1 axis of the UPR declines with aging (Taylor and Dillin, 2013).

Increased UPR activity is thought to promote life span extension and thus the ERQC may represent a therapeutic target in age-related diseases (Taylor, 2016). In particular, XBP1s

activity has been demonstrated to promote longevity. In *C. elegans*, activation of XBP1s in nerve cells was shown to be sufficient to extend nematode life spans (Taylor and Dillin, 2013). XBP1s acts in collaboration with the transcription factor DAF-16 to promote longevity by increasing the resistance to ER stress in long-lived *C. elegans* mutants (Henis-Korenblit et al., 2010). It has also been shown that downstream induction of the ERAD pathway as well as autophagy by the XBP1s-induced hexosamine biosynthetic pathway (HBP) extends the life span of *C. elegans*, diminishes the toxicity of aggregation-prone proteins, and protects mice from oxidative stress and Ca²⁺ overload (Denzel et al., 2014; Vincenz and Hartl, 2014; Wang et al., 2014). This protective pathway may represent a promising therapeutic strategy because it can be induced simply by supplementation of cells with HBP metabolites.

Aims of the study

Aim of part 1

The aim of the work described in part 1 of this thesis was to better understand gain-of-toxicity and how cells deal with the accumulation of aggregation-prone proteins. Aggregating proteins in different diseases vary in their native function and do not share common amino acid sequences or structural homology (Chiti and Dobson, 2006). However, the aggregates that are formed are strikingly similar in their conformation and biochemical properties; they often form amyloid-like fibrils based on cross- β structures (Chiti and Dobson, 2006). Since gain-of-toxicity is independent of the specific native structure and function of a disease protein but rather depends on the aggregate conformation, studying gain-of-toxicity of aggregating proteins will enable us to better understand cellular mechanisms that may be relevant for a range of different disorders.

In order to study protein aggregation independently of a specific disease protein's identity, we use artificial model proteins that were *de novo* designed to form β -sheet structures that spontaneously aggregate into amyloid-like fibrils (Figure 8) (West et al., 1999; Olzscha et al., 2011). The β -strand secondary structure of these proteins is driven by an alternating pattern of polar and nonpolar amino acid residues (Figure 8) (Xiong et al., 1995; West et al., 1999).

Since these proteins were *de novo* designed, they lack physiological function and thus enable us to study gain-of-function effects of amyloidogenic proteins and at the same time exclude loss-of-function effects and other indirect effects caused by the overexpression of natural disease mutants. In previous studies these *de novo* β -proteins have been demonstrated to form amyloid-like aggregates also when expressed in mammalian cells (Olzscha et al., 2011; Woerner et al., 2016). The formation of these amyloid-like fibrils was toxic and experiments using β -protein constructs of similar size but with varying hydrophobicities

revealed that aggregation propensity correlated with the cytotoxicity of these proteins due to an increased ability to promote aberrant protein interactions with metastable cellular proteins leading to their sequestration (Olzscha et al., 2011).

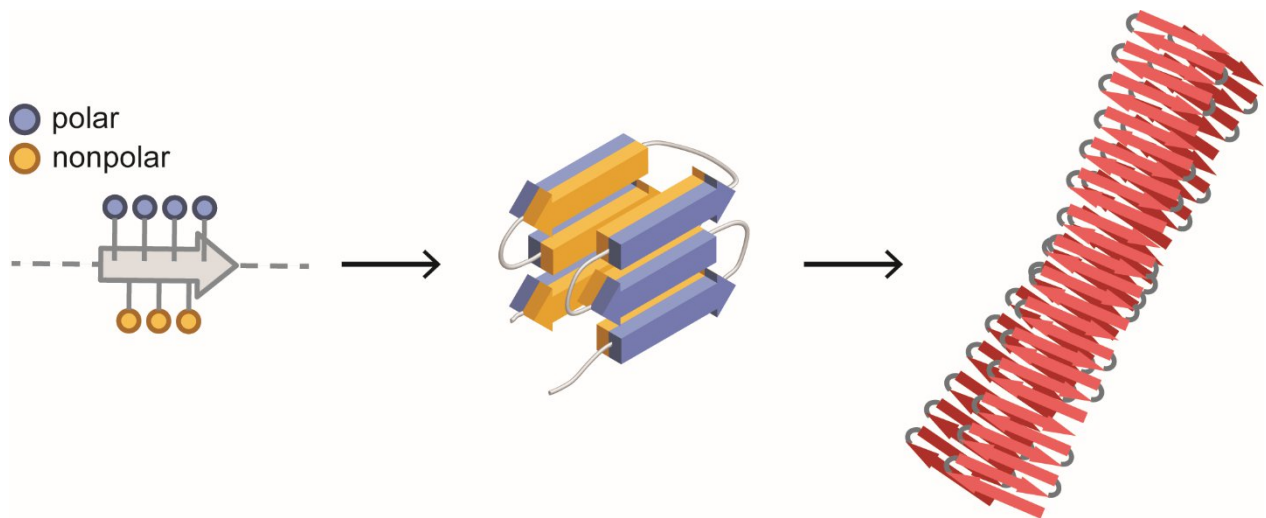


Figure 8. Designed β -sheet proteins form amyloid-like fibrils. An alternating pattern of polar (blue) and nonpolar (yellow) amino acid residues determine the β -sheet secondary structure of the *de novo* designed β -proteins that consist of six β -strands and spontaneously form amyloid-like aggregates.

The aggregation propensity of a protein as well as the biochemical properties and toxicity of aggregates vary depending on the subcellular location. For example, it was shown that in the cytosol toxic amyloid-like aggregates block nucleo-cytoplasmic transport of proteins and RNA but nuclear aggregates of the same proteins are much less toxic and do not block nucleo-cytoplasmic transport (Liu et al., 2015; Zhang et al., 2015; Woerner et al., 2016). As mentioned above, the ER is the site of synthesis of one third of the proteome including many disease-related proteins with protein aggregation occurring in the ER lumen or extracellularly (Table 2). Since the ER is characterised by a unique folding environment and a proteostasis network distinct from that of the cytosol, aggregation-prone proteins may be handled differently than in other cellular compartments. Indeed, it was reported that targeting amyloidogenic polyQ proteins to the ER or to mitochondria renders them more

soluble (Rousseau et al., 2004). However, the fate of amyloidogenic proteins in the ER and how exactly aggregation is modified by the ERQC system are poorly understood. In order to gain a more in-depth understanding of the underlying cellular mechanisms of protein aggregation, the aim of this work was to better understand the fate of amyloidogenic proteins in the ER. Such an understanding may provide new insights that will be beneficial for the development of novel therapeutic strategies.

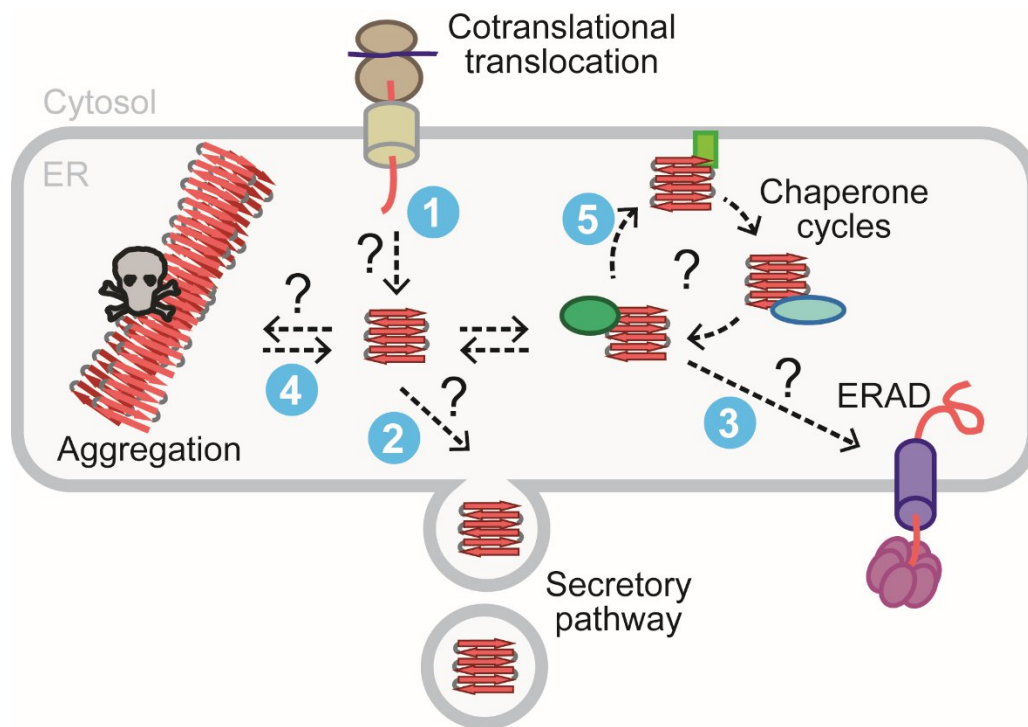


Figure 9. Potential fates of ER-targeted β -sheet proteins. ER-directed β -proteins are targeted for co-translational translocation into the ER via an N-terminal signal sequence (1). Without an ER retention signal, proteins that pass the ERQC may potentially be secreted (2). Proteins that are recognised as terminally misfolded and aggregation-prone may instead be targeted for degradation via ERAD (3). In the ER lumen, β -proteins may show different aggregation behaviour than in the cytosol (4). Aggregation-prone β -proteins may interact with molecular chaperones and other factors of the ERQC system (5).

Specifically, the aim of this project was to investigate the fate of the *de novo* designed β -proteins when targeted to the mammalian secretory pathway and to determine how they are handled by the ER proteostasis network. To this end, β -sheet constructs with an N-terminal signal sequence, but importantly no ER retention sequence, were utilised to address the

questions (1) whether amyloidogenic β -proteins can be efficiently targeted to the ER, (2) whether they can be secreted, (3) whether they are targeted for degradation, (4) whether they form toxic amyloid-like aggregates in the ER similarly to those found in the cytosol, (5) which factors of the ERQC system recognise amyloidogenic β -proteins (Figure 9). Furthermore, we addressed the question of how amyloidogenic β -proteins affect ER proteostasis and whether they induce the UPR.

Aim of part 2

The aim of the work presented in part 2 of this thesis was to analyse the effects of small molecule proteostasis modulators. The proteostasis network has emerged as a therapeutic target for a variety of diseases ranging from neurodegenerative conditions, to metabolic diseases and cancers. Therapeutic strategies include both proteostasis enhancement and inhibition. Proteostasis enhancement may be a promising therapeutic strategy in diseases that are caused by misfolded proteins. In some diseases, mutant proteins are folding-deficient leading to their rapid degradation or aggregation before the proteins can reach their native conformations. In such cases, the proteins could potentially still carry out their native function if proper folding and trafficking was assisted. Mutant misfolded proteins whose functionality could potentially be rescued by assisted folding include the class II mutations of CFTR that cause cystic fibrosis (Kerem, 2005), mutations of alpha-galactosidase in Fabry disease, a rare genetic lysosomal storage disease (Okumiya et al., 1995), and mutants of A1AT that cause A1AT deficiency (Burrows et al., 2000). A number of compounds including so-called chemical chaperones have been reported to increase protein folding and trafficking efficiency and to have therapeutic potential in disease models and also in clinical trials (Bernier et al., 2004; Hebert and Molinari, 2007; Molinari, 2007). However, the clinical feasibility of using such compounds is not yet clear because many of them seem to act by a rather non-specific mechanism of action and are effective only at high dosages (Hebert and Molinari, 2007).

Enhancement of proteostasis does not only include improved protein folding efficiency but also improved clearance of toxic protein aggregates. For example, induction of autophagy has been demonstrated to relieve liver damage in a mouse model of A1AT (Hidvegi et al., 2010). Thus, proteostasis enhancement has the potential to target both loss-of-function and gain-of-function toxicity and there is great interest in identifying and developing more potent proteostasis modifiers.

A screen for small molecule proteostasis enhancers that was carried out previously in our group led to the identification of a set of drugs that were already approved by the US Food and Drug Administration (FDA) for medical purposes, owing to properties other than proteostasis modulation. We tested the effects of the antipsychotic drug fluphenazine and the epidermal growth factor receptor (EGFR) inhibitor gefitinib on the proteostasis network in the presence of a Huntington's-disease-causing mutant of the protein huntingtin (Htt) (Table 2). Huntington's disease (HD) is caused by genetic mutations in the *Htt* gene that lead to an extension of a trinucleotide repeat sequence (CAG) encoding a polyglutamine (polyQ) stretch. This polyQ stretch is present in the Htt protein of healthy individuals and can vary in length. However, polyQ extensions over around 40 repeats cause neurodegeneration. Extended polyQ proteins aggregate into large inclusions that disturb the proteostasis network leading to exhaustion of the ubiquitin proteasome system (UPS) and accumulation of ubiquitinated proteins (Hipp et al., 2012). The first aim of the work presented in part 2 was to test whether the compounds could alleviate UPS impairment induced by polyQ aggregates. To this end, we utilized a UPS reporter cell line. Furthermore, we tested the effect of the compounds on polyQ protein aggregation and whether the compounds may act on the proteostasis network via induction of the HSR.

Materials and Methods

Materials

Chemicals

Acetic acid	Merck, Darmstadt, Germany
Acetone	Sigma-Aldrich, St. Louis, MO, USA
Acetonitrile (ACN)	VWR International, Radnor, PA, USA
Acrylamide:Bisacrylamide; 37.5:1; 30%	Serva, Heidelberg, Germany
Agar	Sigma-Aldrich, St. Louis, MO, USA
Agarose LE	Biozym Scientific, Oldendorf, Germany
Ammonium Persulfate (APS)	Sigma-Aldrich, St. Louis, MO, USA
Ampicillin	Carl Roth, Karlsruhe, Germany
Arg ⁰ HCl	Sigma-Aldrich, St. Louis, MO, USA
Arg ⁶ HCl	Cambridge Isotope Laboratories, MA, USA
Arg ¹⁰ HCl	Cambridge Isotope Laboratories, MA, USA
Bacto-Tryptone	BD Biosciences, CA, USA
Bacto-Yeast Extract	BD Biosciences, CA, USA
BCA Protein Assay Kit	Pierce, Thermo Fisher Scientific, MA, USA
Bis-Tris	Fluka, Buchs, Switzerland
Boric acid	VWR International, Radnor, PA, USA
Bovine albumin Fraction V (BSA)	Serva, Heidelberg, Germany
Brefeldin A (BFA)	Sigma-Aldrich, St. Louis, MO, USA
Bromophenol Blue Sodium Salt	Sigma-Aldrich, St. Louis, MO, USA
BSA Standard	Pierce, Thermo Fisher Scientific, MA, USA
Calcium chloride-dihydrate	VWR International, Radnor, PA, USA

Complete Protease Inhibitor Cocktail	Roche, Basel, Switzerland
CutSmart buffer	New England Biolabs, Ipswich, MA, USA
Cycloheximide	Sigma-Aldrich, St. Louis, MO, USA
4',6-Diamidino-2-Phenylindole (DAPI) dihydrochloride	Life Technologies, Carlsbad, CA, USA
DharmafectDuo Transfection Reagent	GE Healthcare Dharmacon, Lafayette, CO, USA
DharmaFECT Transfection Reagent	GE Healthcare Dharmacon, Lafayette, CO, USA
N,N-Dimethylformamide (DMF)	Sigma-Aldrich, St. Louis, MO, USA
Dimethylsulphoxide (DMSO)	Sigma-Aldrich, St. Louis, MO, USA
3-(4,5-Dimethylthiazol-2-yl)-2,5-diphenyltetrazoliumbromide (MTT)	Sigma-Aldrich, St. Louis, MO, USA
Dithiothreitol (DTT)	Sigma-Aldrich, St. Louis, MO, USA
DNA Loading Buffer	Fermentas, St. Leon-Rot, Germany
dNTP Set	Metabion, Martinsried, Germany
Droperidol	Sigma-Aldrich, St. Louis, MO, USA
Dulbecco's Modified Eagle's medium (MEM)	Biochrom AG, Merck Millipore, Darmstadt, Germany
Dulbecco's Modified Eagle's medium (MEM) without phenol red	Biochrom AG, Merck Millipore, Darmstadt, Germany
Dulbecco's Modified Eagle's medium (MEM), High glucose, without Arg, Lys, l-glutamine	PAA Laboratories, Dartmouth, MA, USA
Erlotinib HCl	Selleck Chemicals, TX, USA
Ethanol Absolute	Merck, Darmstadt, Germany
Fetal Bovine Serum (FBS)	Gibco, Thermo Fisher Scientific, MA, USA
Fluorescent Mounting Medium	DAKO, Hamburg, Germany
Fluphenazine HCl	Sigma-Aldrich, St. Louis, MO, USA
Formic acid	Merck, Darmstadt, Germany

FuGENE 6 Transfection Reagent	Promega, WI, USA
Gefitinib	Biotang, Thermo Fisher Scientific, MA, USA
GeneRuler 100bp DNA ladder	Fermentas, Thermo Fisher Scientific, MA, USA
GeneRuler 1kb DNA ladder	Fermentas, Thermo Fisher Scientific, MA, USA
Geneticin (G418)	Calbiochem, Merck Millipore, Darmstadt, Germany
Glycerol	Carl Roth, Karlsruhe, Germany
Immersion oil	VWR International, Darmstadt, Germany
Iodoacetamide	Sigma-Aldrich, St. Louis, MO, USA
Kanamycin	Sigma-Aldrich, St. Louis, MO, USA
L-Glutamine	Gibco, Thermo Fisher Scientific, MA, USA
Low fat milk powder	Saliter, Obergünzburg, Germany
Lumigen ECL Ultra	Lumigen Inc., MI, USA
Luminata Classico Western HRP substrate	Merck Millipore, Darmstadt, Germany
Lys ⁰ HCl	Sigma-Aldrich, St. Louis, MO, USA
Lys ⁴ 2HCl	Cambridge Isotope Laboratories, MA, USA
Lys ⁸ HCl	Cambridge Isotope Laboratories, MA, USA
Manganese chloride	Merck Millipore, Darmstadt, Germany
2-(N-Morpholino)ethanesulfonic acid (MES)	Sigma-Aldrich, St. Louis, MO, USA
Methanol p.a.	Merck, Darmstadt, Germany
β-Mercaptoethanol	Merck, Darmstadt, Germany
MG132	Cayman Chemical, MI, USA
3-(N-Morpholino) propanesulfonic acid (MOPS)	Sigma-Aldrich, St. Louis, MO, USA

N,N',N'-Tetramethyl-ethane-1,2-diamine (TEMED)	Sigma-Aldrich, St. Louis, MO, USA
NuPAGE Antioxidant	Thermo Fisher Scientific, MA, USA
Opti-MEM I	Gibco, Thermo Fisher Scientific, MA, USA
PageRuler Prestained Protein Ladder	Thermo Fisher Scientific, MA, USA
Paraformaldehyde, 16%	Thermo Fisher Scientific, MA, USA
Penicillin-streptomycin (Pen Strep)	Gibco, Thermo Fisher Scientific, MA, USA
Phenylmethanesulfonylfluoride (PMSF)	Serva, Heidelberg, Germany
Phosphate Buffered Saline (PBS) pH 7.2	Gibco, Thermo Fisher Scientific, MA, USA
Phosphoric acid	Sigma-Aldrich, St. Louis, MO, USA
Ponceau S solution	Sigma-Aldrich, St. Louis, MO, USA
Potassium acetate (KAc)	Sigma-Aldrich, St. Louis, MO, USA
1-Propanol p.a.	Merck, Darmstadt, Germany
Rubidium chloride (RbCl)	Sigma-Aldrich, St. Louis, MO, USA
Sodium bisulphite	Sigma-Aldrich, St. Louis, MO, USA
Sodium chloride	Merck, Darmstadt, Germany
Sodium deoxycholate	Sigma-Aldrich, St. Louis, MO, USA
Sodium hydroxide	Merck, Darmstadt, Germany
Sodiumdodecylsulfate (SDS)	Serva, Heidelberg, Germany
Sodium-Ethylenediaminetetraacetic acid (EDTA)	Merck, Darmstadt, Germany
Stable glutamine (dipeptide Gln-Ala)	PAA Laboratories, Dartmouth, MA, USA
Steady-Glo Luciferase Assay System	Promega, Madison, WI, USA
Sybr Safe DNA gel stain	Life Technologies, Carlsbad, CA, USA
T4 DNA ligase buffer	New England Biolabs, Ipswich, MA, USA
Trichloric acid (TCA)	Sigma-Aldrich, St. Louis, MO, USA
Trifluoroacetic acid (TFA)	VWR International, Radnor, PA, USA

Tris (Trizma base)	Sigma-Aldrich, St. Louis, MO, USA
Triton X-100	Sigma-Aldrich, St. Louis, MO, USA
TrypLE Express	Gibco, Thermo Fisher Scientific, MA, USA
Tween 20	Sigma-Aldrich, St. Louis, MO, USA

Antibodies

For immunoblotting

Primary antibodies

Anti-BiP/GRP78 (rabbit pAB, ab21685)	Abcam, Cambridge, United Kingdom
Anti-Calnexin (rabbit pAB, SPA860)	Enzo Life Sciences Inc., Farmingdale, New York, USA
Anti-Erlin-2/SPFH2 (rabbit mAB, ab128924)	Abcam, Cambridge, United Kingdom
Anti-GAPDH (mouse mAB, MAB374)	Merck Millipore, Billerica, MA, USA
Anti-GFP (mouse, mAB, 11814460001)	Roche, Basel, Switzerland
Anti-GRP94 (rat mAB, MA3-016)	Thermo Fisher Scientific, Waltham, MA, USA
Anti-HYOU1 (rabbit, mAB, ab134944)	Abcam, Cambridge, United Kingdom
Anti-mCherry (rat, mAB, M11217)	Life Technologies, Carlsbad, CA, USA
Anti-Myc (mouse mAB produced in hybridoma cell line Myc-9E10)	Max Planck Institute of Biochemistry, Martinsried, Germany
Anti-Neuroserpin (mouse mAB, ab55587)	Abcam, Cambridge, United Kingdom
Anti-OS-9 (rabbit mAB, ab109510)	Abcam, Cambridge, United Kingdom
Anti-PDIA6 (rabbit mAB, ab154820)	Abcam, Cambridge, United Kingdom
Anti-SEL1L (rabbit pAB, S3699)	Sigma Aldrich, St. Louis, MO, USA
Anti- α -Tubulin (mouse mAB, T5168)	Sigma Aldrich, St. Louis, MO, USA

Secondary antibodies

Anti-mouse IgG-Peroxidase (goat pAB, A4416)	Sigma Aldrich, St. Louis, MO, USA
Anti-rat (goat pAB, A9037)	Sigma Aldrich, St. Louis, MO, USA

Anti-rabbit (goat pAB, A9169) Sigma Aldrich, St. Louis, MO, USA

For immunofluorescence

Primary antibodies

Anti-Calreticulin (chicken pAB, ab14234) Abcam, Cambridge, United Kingdom

Anti-ERp57 (rabbit pAB, ab10287) Abcam, Cambridge, United Kingdom

Anti-Giantin (rabbit pAB, ab24586) Abcam, Cambridge, United Kingdom

Anti-Myc (mouse mAB, sc-40) Santa Cruz Biotechnology, Dallas, TX, USA

Secondary antibodies

Anti-mouse Cy3 (goat pAB, 115-165-062) Jackson ImmunoResearch Laboratories, West Grove, PA, USA

Anti-rabbit FITC (goat pAB, F2765) Invitrogen by Thermo Fisher Scientific, Waltham, MA, USA

Anti-rabbit Alexa Fluor 405 (goat pAB, A-31556) Life Technologies, Carlsbad, CA, USA

Anti-chicken Alexa Fluor 488 (goat pAB, A-11039) Life Technologies, Carlsbad, CA, USA

Enzymes

AgeI New England Biolabs, Ipswich, MA, USA

Benzonase Max Planck Institute of Biochemistry, Martinsried, Germany

DpnI New England Biolabs, Ipswich, MA, USA

Endo H New England Biolabs, Ipswich, MA, USA

KpnI New England Biolabs, Ipswich, MA, USA

PNGase F New England Biolabs, Ipswich, MA, USA

Q5 High Fidelity polymerase	New England Biolabs, Ipswich, MA, USA
T4 DNA Ligase	New England Biolabs, Ipswich, MA, USA
Trypsin, proteomics grade	Roche, Basel, Switzerland

Bacterial strains

DH5 α F ^{''}	F'/endA1 hsdR17 (rk-, mk+) glnV44 thi-1 recA1 gyrA (NA1r) relA1 Δ (lacIZYA-argF) U169 deoR [ϕ 80dlac Δ (lacZ)M15]
------------------------------	---

Mammalian cell lines

Human embryonic kidney cells 293T (HEK293T)	American Type Culture Collection (ATCC), Manassas, VA, USA
Human epithelial cervix adeno carcinoma (HeLa)	American Type Culture Collection (ATCC), Manassas, VA, USA

Buffers

All buffers are water-based.

Britton & Robinson Buffer (BRUB): 20 mM acetic acid, 20 mM phosphoric acid, 20 mM boric acid, at pH 3, 4, 5, 6, 8, and 11 (pH adjusted with 1 M NaOH).

CAPS/methanol transfer buffer: 10 mM CAPS, 20% (v/v) methanol, final pH 11.

Laemmli sample buffer: 300 mM Tris-HCl, pH 6.8, 10% (w/v) SDS, 20% (v/v) Glycerol, 25% (v/v) β -Mercaptoethanol, 5 mM PMSF, 0.1 % (w/v) Bromophenolblue.

MES buffer: 50 mM MES, 50 mM Tris, 1 mM EDTA (pH 8), 0.1% SDS.

MOPS buffer: 50 mM MOPS, 50 mM Tris, 1 mM EDTA (pH 8), 0.1% SDS.

MTT stop buffer: 40% DMF and 20% SDS.

PBS: 137 mM NaCl, 27 mM KCl, 10 mM Na₂HPO₄, 1.76 mM KH₂PO₄, pH 7.2.

RIPA buffer: 25 mM Tris pH 7.6, 150 mM NaCl, 1% NP-40, 1% sodium deoxycholate, 0.1% SDS.

TAE buffer: 40 mM Tris, 20 mM acetic acid, 1 mM EDTA.

TBS: 50 mM Tris-Cl, pH 7.6, 150 mM NaCl.

TBS-T: 50 mM Tris-Cl, pH 7.6, 150 mM NaCl, 0.1% (v/v) Tween 20.

Transformation buffer (TfB) I: 100 mM RbCl, 50 mM MnCl₂X2H₂O, 10 mM CaCl₂X2H₂O, 30 mM KAc, 15% glycerol, pH 5.8 (by addition of acetate), filter sterilised.

TfB II: 10 mM MOPS, 10 mM RbCl, 75 mM CaCl₂X2H₂O, 15% glycerol, pH 7 (by addition of NaOH), filter sterilised.

UA buffer: 8 M urea, 0.1 M Tris, pH 8.5.

Urea sample buffer: 8 M urea, 5% SDS, 200 mM Tris at pH 6.8, 0.1 mM EDTA, 0.1% Bromophenolblue, 5% β-mercaptoethanol, 10% glycerol

Polyacrylamide Bis-Tris gels

Resolving gel: 360 mM Bis-Tris pH 6.8, 0.07% APS, 0.2% TEMED, 8-16% polyacrylamide (Acrylamide:Bisacrylamide; 37.5:1)

Stacking gel: 360 mM Bis-Tris pH 6.8, 0.07% APS, 0.35% TEMED, 4-8% polyacrylamide (Acrylamide:Bisacrylamide; 37.5:1)

Media

Full growth medium: DMEM supplemented with 10% FBS, 1% penicillin-streptomycin and 1% L-glutamine.

LB agar: 15 mg ml⁻¹ agar, 10 mg ml⁻¹ NaCl, 10 mg ml⁻¹ bacto-tryptone, 5 mg ml⁻¹ bacto-yeast extract, in H₂O, autoclaved and supplemented with either 100 µg ml⁻¹ ampicillin or 35 µg ml⁻¹ kanamycin.

LB medium: 1% bacto-tryptone, 1% NaCl, 0.5% bacto-yeast extract in H₂O, autoclaved.

SILAC media: DMEM with 4.5 g l⁻¹ glucose without arginine, lysine and glutamine, supplemented with 10% dialysed FBS (dialysed against 0.15 M NaCl), Pen/Strep and stable glutamine (dipeptide Gln-Ala), the following combinations of different isotopes of arginine (0.28 mM) and lysine (0.56 mM) were added:

Light: Arg⁰HCl and Lys⁰HCl

Medium: Arg⁶HCl and Lys⁴HCl

Heavy: Arg¹⁰HCl and Lys⁸HCl

Kits

BCA Protein Assay Kit	Thermo Fisher Scientific, MA, USA
EndoFree Plasmid Maxi Kit	Qiagen, Hilden, Germany
HiSpeed Plasmid Maxi Kit	Qiagen, Hilden, Germany
MemCodeReversible Protein Stain Kit	Thermo Fisher Scientific, MA, USA
NativePAGE Sample Prep Kit	Thermo Fisher Scientific, MA, USA
Steady Glo Luciferase Assay System	Promega, Madison, WI, USA
Wizard SV gel and PCR Clean Up System	Promega, Madison, WI, USA

Other materials and Instruments

AG285 and PB602 Balances	Mettler Toledo, Gießen, Germany
Avanti J-25 Centrifuge with Rotors JLA 10.500 and JA 25.50	Beckman, Munich, Germany
Plate reader Synergy HT	BioTek Instruments, Winooski, VT, USA
C18 Empore disks	IVA, Analysentechnik, Meerbusch, Germany
Centrifuge 5415 R	Eppendorf, Hamburg, Germany
Confocal laser scanning microscope LSM780	ZEISS, Jena, Germany
Cryo-tubes	Nunc, Roskilde, Denmark
DU 640 UV/VIS Spectrophotometer	Beckman, Munich, Germany
Empore High Performance Extraction Disks	IVA Analysentechnik, Meerbusch, Germany
End-over-end rotor, stuart rotator SB3	Bibby Scientific, Staffordshire, UK
Exactive orbitrap mass spectrometer	Thermo Fisher Scientific, MA, USA
FACSAriaIII	BD Biosciences, San Jose, CA, USA
FACSCalibur	BD Biosciences, San Jose, CA, USA
Gel Documentation System BioCapt	MWG BiotechAG, Göttingen, Germany
Gene Pulser cuvette, 0.4 cm	Biorad, CA, USA
Gene Pulser Xcell electroporations system	Biorad, CA, USA

ImageReader LAS-3000	FUJI, Tokyo, Japan
Innova 4430 Incubator	New Brunswick Scientific, Nürtingen, Germany
LAS 3000 image reader	FujiFilm, Tokio, Japan
Light Microscope Diavert	Leitz, Wetzlar, Germany
Luminometer Lumat LB 9507	Berthold, Bad-Wildbad, Germany
Magnetic rack	Miltenyi Biotec, Bergisch Gladbach, Germany
μMacs anti-Myc beads	Miltenyi Biotec, Bergisch Gladbach, Germany
μMACS 20μ columns	Miltenyi Biotec, Bergisch Gladbach, Germany
Millex SV Filter Units, pore size 0.22 μM	Merck Millipore, Darmstadt, Germany
MilliQ Plus Deionization System	Merck Millipore, Darmstadt, Germany
MiniProtean2 Electrophoresis Chamber	Bio-Rad, Munich, Germany
Mini Sub Cell	Bio-Rad, Munich, Germany
Nanodrop 1000 Spectrophotometer	Thermo Fisher Scientific, MA, USA
Nano-HPLC autosampler	Thermo Fisher Scientific, MA, USA
NativePAGE Novex 4-16% Bis-Tris Protein Gels, 1.0 mm, 10-well	Thermo Fisher Scientific, MA, USA
Nitrocellulose Amersham PROTRAN Blotting Membrane, 0.45 μm pore size	GE Healthcare, Chicago, IL, USA
NuPAGE™ Novex™ 4-12% Bis-Tris Protein Gels, 1.0 mm, 10-well	Thermo Fisher Scientific, MA, USA
OMIX96 C18 tips	Agilent Technologies, Oberhaching, Germany
PCR Tubes AB-0266	Thermo Fisher Scientific, MA, USA
pH-Meter pH538	WTW, Weilheim, Germany
PicoTip Emitter Silica Tip, ID 75 μm, 30 cm long, 8 μm tip opening,	New Objective, Woburn, MA, USA
Pipettes Eppendorf Research	Eppendorf, Hamburg, Germany

Poly-L-Lysine (PLL) Round Coverslips, 12mm	BD Biosciences, CA, USA
Polyvinylidene difluoride (PVDF) Western Blotting Membrane, 0.2 µm pore size	Roche, Basel, Switzerland
Proxeon EASY-nLC 1000 nano-HPLC system	Thermo Fisher Scientific, MA, USA
QIAprep Spin Miniprep Kit	Qiagen, Hilden, Germany
Reprosil-Pur C18-AQ	Dr. Maisch HPLC, Ammerbuch, Germany
Safe Imager 2.0 Blue-Light Transilluminator	Life Technologies, Carlsbad, CA, USA
Scepter™ Automated Cell Counter	Millipore, MA, USA
Scepter™ Sensors - 60µM	Millipore, MA, USA
µ-Slide 8 Well Plates	Ibidi, Martinsried, Germany
Sonicator Sonorex RK100	Bandelin electronic GmbH, Berlin, Germany
Tank Blot System	Bio-Rad, Munich, Germany
Thermocycler PCR T3	Biometra, Göttingen, Germany
Thermomixer Comfort	Eppendorf, Hamburg, Germany
Tissue Culture Dish 100 X 20 mm	Becton and Dickinson, New Jersey, USA
Falcon Tissue Culture Plates, flat bottom, 6 well, 12 well, 24 well, 48 well and 96 well	Thermo Fisher Scientific, MA, USA
Transformer for Electrophoresis PAC300	Bio-Rad, Munich, Germany
Vacuum concentrator Speedvac SPD121P	Thermo Fisher Scientific, MA, USA
Vivacon 10 kDa, ultrafiltration devices	Sartorius, Göttingen, Germany
Vortex-Genie 2	Scientific Industries, NY, USA
Weighing Balance CP3202P	Sartorius, Göttingen, Germany

Plasmids

Name	Description	Backbone	Antibiotic resistance	Source
CMV-Luc	Firefly luciferase under the CMV promoter	pcDNA3.1(+) myc/His	Amp	Gupta et al., 2011
CPY*-mCh	ER-targeted CPY*-mCherry	pShooter pCMV/myc/ER	Amp	Rajat Gupta, see methods
ER- α	α -S824 with N-terminal SP-B signal peptide	pcDNA3.1(+) myc/His	Amp	Dolfe et al., 2015
ER- β 4	β 4 with N-terminal SP-B signal peptide	pcDNA3.1(+) myc/His	Amp	Dolfe et al., 2015
ER- β 17	β 17 with N-terminal SP-B signal peptide	pcDNA3.1(+) myc/His	Amp	Dolfe et al., 2015
ER- β 23	β 23 with N-terminal SP-B signal peptide	pcDNA3.1(+) myc/His	Amp	Dolfe et al., 2015
ER-mCh	ER-targeted mCherry, see methods section	pcDNA3.1(+) myc/His	Amp	This study, see methods
ER- α -mCh	ER- α cloned into mCherry N1 upstream of mCherry	mCherry N1	Kan	This study, see methods
ER- β 23-mCh	ER- β 23-mCh cloned into mCherry N1 upstream of mCherry	mCherry N1	Kan	This study, see methods
ER- β 23-mCh ^A	ER- β 23-mCh cloned into pcDNA3.1(+) with point mutation C24A	pcDNA3.1(+) myc/His	Amp	This study, see methods
ER-GFP	pShooter vector pCMV/Myc/ER/ GFP	pShooter	Amp	Life Technologies, Carlsbad, CA, USA
ERSE I-Luc	Firefly luciferase under the ERSE I promoter	pGL3 luciferase reporter	Amp	Bouman et al., 2011
ERSE II-Luc	Firefly luciferase under the ERSE II promoter	pGL3 luciferase reporter	Amp	Bouman et al., 2011
Hsp70-Luc	Firefly luciferase under the HSPA1A promoter	pUB/Bsd	Amp	Prof. H. Wagner, Technical University of Munich, Germany
mCherry	pmCherry N1	mCherry N1	Kan	Clontech, CA, USA
NRS	Neuroserpin (SERPIN1)	pcDNA3.1(+)	Amp	Schipanski et al., 2014
NRS ^{G392E}	Neuroserpin mutant G392E	pcDNA3.1(+)	Amp	Schipanski et al., 2014
NRS ^{G392E} -GFP	Neuroserpin G392E mutant with C-terminal EGFP tag	pcDNA3.1(+)	Amp	Schipanski et al., 2014

NRS ^{G392E} ^{ANN}	Neuroserpin-G392E-N157/3211	pcDNA3.1(+)	Amp	Schipanski et al., 2014
NRS-GFP	Neuroserpin with C-terminal EGFP tag	pcDNA3.1(+)	Amp	Schipanski et al., 2014
NRS ^{ANN}	NeuroserpinN157/3211	pcDNA3.1(+)	Amp	Schipanski et al., 2014
nt- α	α -S824	pcDNA3.1(+) myc/His	Amp	Olzscha et al., 2011
nt- β 17	β 17	pcDNA3.1(+) myc/His	Amp	Olzscha et al., 2011
nt- β 23	β 23	pcDNA3.1(+) myc/His	Amp	Olzscha et al., 2011
nt- β 4	β 4	pcDNA3.1(+) myc/His	Amp	Olzscha et al., 2011
pcDNA3.1	Empty vector	pcDNA3.1(+) myc/His	Amp	Thermo Fisher Scientific, MA, USA
Q25	Exon 1 fragment of huntingtin Q25 fused N-terminally to mCherry	pcDNA3.1(+) myc/His	Amp	Gupta et al., 2011
Q97	Exon 1 fragment of huntingtin Q97 fused N-terminally to mCherry	pcDNA3.1(+) myc/His	Amp	Gupta et al., 2011
SEL1L	Human full length SEL1L	pcDNA3.1(+) myc/His	Amp	This study, see methods section
UPRE-Luc	Firefly luciferase under the UPRE promoter	pGL3 luciferase reporter	Amp	Bouman et al., 2011

siRNAs

Non-targeting control siRNA 3

GE Healthcare Dharmacon, Lafayette, CO, USA

OS-9 siRNA smart pool

GE Healthcare Dharmacon, Lafayette, CO, USA

SEL1L siRNA smart pool

GE Healthcare Dharmacon, Lafayette, CO, USA

Softwares

Adobe Illustrator CS6

Adobe Systems, San Jose, USA

Chromas (Version 1.45)

Griffith University, Queensland, Australia

FlowJo (Version 9.9)

FlowJo, LLC, Ashland, OR, USA

ImageJ (Version 1.49v)

National Institutes of Health, MD, USA

MaxQuant (Version 1.3.0.5)

Max Planck Institute of Biochemistry, Martinsried, Germany

Perseus (Version 1.5.2.12)

Max Planck Institute of Biochemistry,
Martinsried, Germany

Methods

Production of chemically competent *E. coli*

DH5 α cells were pre-cultured in LB medium at 37 °C, overnight, shaking. The OD was then measured at 600 nm, cells were diluted to an OD of 0.05 in a total of 100 ml LB medium and cultured further until an OD of 0.5 was reached. Cells were then incubated shortly on ice before centrifugation at 2,500 xg for 10 min at 4 °C. The cell pellet was re-suspended in 30 ml ice-cold TfBI buffer and incubated on ice for 1 h. Cells were then again pelleted by centrifugation before resuspension in 9 ml ice-cold TfBII buffer. Cell suspensions were then aliquoted, frozen in liquid N₂ and stored at -80 °C.

Plasmid preparation

To 100 μ l chemically competent DH5 α cells, 100-200 ng plasmid DNA were added. Cells were incubated on ice for 20 min, heat shocked at 42 °C for 90 s and again incubated on ice. After 5-10 min on ice, 900 μ l LB medium were added and cells were cultured at 37 °C, shaking, for 45-60 min before plating 0.1-100% of the culture on LB agar plates supplemented with either ampicillin (Amp) or kanamycin (Kan) and overnight incubation at 37 °C. Single colonies were picked, added to 5 ml LB medium supplemented with appropriate antibiotics (50 μ g ml⁻¹ Amp or 10 μ g ml⁻¹ Kan) and incubated at 37 °C, overnight, shaking. For cloning purposes, plasmids were purified from 5 ml cultures using the QIAprep Miniprep Kit following the manufacturer's instructions. To prepare plasmids for transfection of mammalian cells, 200-500 μ l of the 5 ml overnight cultures were added to 100-200 ml LB medium and cultured for an additional night before plasmid preparation using the EndoFree Plasmid Maxi Kit or the HiSpeed Plasmid Maxi Kit following the manufacturer's

instructions. Plasmids were sequenced by the Max Planck Institute sequencing core facility (Martinsried, Germany).

PCR amplification and purification of PCR products

All PCR amplifications were carried out using the Q5 polymerase following the manufacturer's instructions. PCR products were resolved on 1% agarose gels containing SyBr Safe DNA gel stain in TAE buffer. For purification, gel pieces containing resolved PCR products were cut from gels and the DNA was extracted using the Wizard SV gel and PCR Clean Up System following the manufacturer's instructions.

DNA Restriction Digestion and Ligation

Restriction digestions were carried out using 1 μ g DNA and 1 μ l each of the required restriction enzymes in 5 μ l CutSmart buffer in nuclease-free water at 37 °C for 2 h. DNA ligations were carried out at a molar ratio of 1:4 of backbone to insert using T4 DNA ligase in 1X T4 DNA ligase buffer at 16 °C for 18 h.

Cloning of expression plasmids

The signal peptide of human pulmonary surfactant-associated protein (SP-B) (MAESHLLQWLLLLLPTLCGPGTA) was inserted upstream of the Myc-tag of pcDNA3.1(+) plasmids containing α S-824, β 4, β 17 and β 23 (Olzscha et al., 2011) (here named nt- α , nt- β 4, nt- β 17 and nt- β 23) by (Dolfe et al., 2015) to generate ER- α , ER- β 4, ER- β 17 and ER- β 23, respectively. To generate mCherry-tagged constructs for live cell imaging, ER- β 23 and ER- α were excised from the pcDNA3.1(+) plasmids using KpnI and AgeI after generation of a downstream AgeI site via the QuikChange PCR method (Agilent Technologies) and inserted into mCherry N1 vectors. To generate the ER- β 23^{C24A}-mCherry construct (ER- β 23-mCh^A) for FLIP experiments, a point mutation (C24A) was introduced into the ER- β 23-mCh construct using Quik change. The insert was then amplified by PCR, simultaneously adding a 5' BamHI and a 3' NotI digestion site. Amplified inserts were then

inserted it into the pcDNA3.1(+) vector using BamH1 and Not1. To generate the control ER-mCh construct for FLIP, the signal peptide of SP-B followed by one alanine residue and a Myc-tag was fused upstream to mCherry by PCR amplification. A C-terminal KDEL sequence, as well as a 5' BamH1 and a 3' Not1 digestion site were also added by PCR amplification. The purified PCR product was then inserted into the pcDNA3.1(+) plasmid using BamH1 and Not1. The ER-targeted CPY*-mCherry construct (CPY*-mCh) was generated by Rajat Gupta by insertion of the insert of non-targeted CPY*-mCherry (CmCh*) (Park et al., 2013) into the pShooter vector pCMV/Myc/ER via XhoI/NotI. The insert encoding human SEL1L flanked by BamH1 and Not1 digestion sites was purchased from Thermo Fisher Scientific and inserted into the pcDNA3.1(+) plasmid via BamH1/Not1. DNA was sequenced by the Max Planck Institute sequencing core facility (Martinsried, Germany).

Cell culture and transfections

Human HEK293T and HeLa cell lines were cultured in full growth medium at 37 °C in an atmosphere of 5% CO₂. Cell lines were regularly tested for mycoplasma contamination. Cells were transfected with a total of 1 µg plasmid DNA in 6-well plates using 3 µl FuGene 6 transfection reagent prepared in Opti-MEM I buffer following the manufacturer's instructions. After preparation of the transfection reagent mix, this was added dropwise to cells in full growth medium. For transfection of cells in other culturing containers, amounts of transfection reagents were up- or down-scaled accordingly.

Immunofluorescence imaging

Cells were seeded in µ-Slide chambered coverslips (for live cell imaging) or on poly-L-lysine-coated glass coverslips (for immunofluorescence experiments) 24 h prior to transfection. Transfected cells were either directly analysed in chambered coverslips or fixed with 4% paraformaldehyde, washed with PBS, permeabilised with 0.1% Triton X-100 in PBS for 5 min followed by additional washes in PBS, blocked with 1% BSA and labelled with

primary antibodies diluted 1:500 in 1% BSA in PBS. After three washes in PBS, the cells were stained with fluorescently-labelled secondary antibodies at dilutions of 1:200 in 1% BSA in PBS. For live cell imaging, cells were grown in μ -Slide 8 Well plates in DMEM without phenol red supplemented with 10% FBS, 1% penicillin-streptomycin and 1% L-glutamine. Throughout analysis cells were kept in a chamber at 37 °C, 5% CO₂.

Images were recorded at the Imaging Facility of the Max Planck Institute of Biochemistry, Martinsried, on a ZEISS LSM780 confocal laser scanning microscope equipped with a ZEISS Plan-APO 63x/NA1.46 oil immersion objective and analysed using ImageJ software (ImageJ 1.49v, <http://imagej.nih.gov/ij/>). Representative images or videos of at least three independent experiments are shown.

Immunoblotting

Denaturing electrophoresis

Cells were harvested after one wash in PBS and lysed in RIPA buffer supplemented with cComplete Protease Inhibitor Cocktail and benzonase. After lysis for at least 20 min on ice with occasional vortexing, cell debris was removed by centrifugation at 5,000 xg for 5 min at 4 °C and transfer of lysates to fresh tubes. Protein concentrations were measured using the BCA assay kit. Lysates were denatured in Laemmli sample buffer at 70 °C for 10 min and then 20 μ g of protein were resolved on 8%, 10% or 12% Bis-Tris gels (homemade) or on commercial NuPAGE 4-12% Bis-Tris gels in MES or MOPS buffer supplemented either with 5 mM sodium bisulphite or with NuPAGE Antioxidant following the manufacturer's instructions.

Native electrophoresis

Cells were lysed using the NativePAGE Sample Prep Kit supplemented with cComplete Protease Inhibitor Cocktail and benzonase. After lysis for 30 min on ice, cell debris was removed by centrifugation at 5,000 xg for 5 min at 4 °C and lysates were transferred to fresh

tubes. Protein concentrations were measured using the BCA assay kit. Per sample, 45 μ g protein were resolved on 4-16% NativePAGE Novex Bis-Tris gels.

Transfer and staining

Proteins were transferred to nitrocellulose or PVDF (preferred for β -sheet proteins) membranes in 3-(Cyclohexylamino)-1-propanesulfonic acid (CAPS)/methanol buffer at 110 V for 60-90 min at 4 °C. Membranes were blocked for 1 h in 5% low fat dry milk in TBS-T and then incubated with primary antibodies diluted in 5% low fat dry milk at 4 °C overnight at the indicated dilutions: BiP (1:1,000, Abcam #ab21685), calnexin (1:500, Enzo Life Sciences, #SPA860), Erlin-2 (1:1,000, Abcam, #ab128924), GAPDH (1:1,000, Millipore #MAB374), GFP (1:1,000, Roche, #11814460001), GRP94 (1:1,000, Pierce, #MA3-016), HYOU1 (1:1,000, Abcam #ab134944), mCherry (1:1,000, Life Technologies, #M11217), Myc (1:200, mouse monoclonal produced in hybridoma cell line Myc-9E10), OS-9 (1:1,000, Abcam, #ab109510), PDIA6 (1:500, Abcam #ab154820), SEL1L (1:1,000, Sigma #S3699), α -tubulin (1:1,000, Sigma #T5168). Membranes were washed three times with TBS-T and then incubated with HRP-conjugated secondary antibodies diluted in TBS-T (anti-mouse, 1:5,000, Sigma #A4416; anti-rat, 1:2,000, Sigma #A9037) or 5% milk (anti-rabbit, 1:20,000, Sigma #A9169) for 1.5 h at RT. After additional washing in TBS-T, HRP substrate was added and chemiluminescence was quantified using a Fuji LAS 3000 image reader. Protein bands from at least three independent experiments were quantified using ImageJ software. Representative blots from at least three independent experiments are shown.

Solubility analysis

Cells were lysed in 1% Triton X-100 in PBS supplemented with cComplete Protease Inhibitor Cocktail and benzonase for 1 h at 4 °C with end-over-end rotation. Protein concentrations were measured using the BCA assay. A fraction of each lysate was put aside for analysis of total protein content; the remainder was centrifuged at 14,000 \times g for 10 min at 4 °C to

separate soluble from insoluble proteins. The supernatant containing soluble protein was transferred to a fresh tube. Both soluble and total fractions were denatured by addition of concentrated Urea sample buffer to give a concentration corresponding to 1x sample buffer. The pellet was re-suspended directly in 1x sample buffer. All samples were heated to 70 °C for 10 min and subsequently analysed by denaturing immunoblotting as described above.

Cell viability assay

HEK293T cells were trypsinised at exponential growth rate and 4×10^6 cells were re-suspended in 400 μ l DMEM supplemented with 25% FBS and electroporated with 30 μ g plasmid DNA in a 0.4 cm Gene Pulser cuvette in the Gene Pulser Xcell electroporations system at 225 V, 950 μ F. After electroporation, cells were allowed to recover for 10 min in full growth medium before seeding at 2×10^5 cells ml^{-1} into 24 well plates (1 ml cells in full growth medium per well). After 72 h, 500 μ l of 0.5 mg ml^{-1} MTT was added (0.17 mg ml^{-1} final) and cells were incubated at 37 °C for 1 h before the reaction was stopped by the addition of MTT stop buffer. Concentrations of formazan, the product of the reduction of MTT by cellular reductases, were analysed by measuring absorbance at 570 nm in a plate reader.

Analysis of secreted proteins

HEK293T cells were seeded and transfected in a 6 well plate and media was exchanged 24 h after transfection to 600 μ l full growth medium in the presence or absence of 1 $\mu\text{g ml}^{-1}$ brefeldin A (BFA). After overnight incubation, media and cells were harvested separately. Cell pellets were washed, lysed, quantified and denatured as described above. Media samples were centrifuged at 5,000 $\times g$ for 5 min at 4 °C and transferred to fresh tubes to ensure elimination of any floating cells. Then, 6 μ l 2% sodium deoxycholate were added to media samples followed by vortexing and incubation at 4 °C for 30 min before addition of 60 μ l trichloric acid (TCA) and incubation at 4 °C overnight. Precipitated proteins from media

samples were then collected by centrifugation at 16,000 xg for 14 min at 4 °C. Pellets were dried and then resuspended in 1x Urea sample buffer. TrisCl at pH 8.8 was added dropwise until the pH was neutralised. Proteins were denatured at 70 °C for 10 min. Samples from conditioned media and cell lysates were brought to the same volumes. For immunoblotting, equal volumes of concentrated protein from media samples were loaded per well (equivalent to 20 µg of cell lysates). After transfer, PVDF membranes were stained using the MemCodeReversible Protein Stain Kit and nitrocellulose membranes using Ponceau to provide loading controls.

Cycloheximide chase

Cells were transfected in one dish and after 24 h trypsinised and reseeded into 12 well plates. After a recovery period of 24-48 h, cells were treated with 0.5 mM cycloheximide (CHX). Cells were harvested at indicated time points for analysis by immunoblotting. Images were analysed using the ImageJ software.

SILAC labelling

SILAC media for light (L), medium (M) or heavy (H) labelling were prepared as follows: DMEM with 4.5 g L⁻¹ glucose and without arginine, lysine, and glutamine (PAA Laboratories #E15-086) was supplemented with 10% dialyzed FBS, Pen/Strep and stable glutamine (dipeptide Gln-Ala) (PAA Laboratories). Combinations of different isotopes of arginine (0.28 mM) and lysine (0.56 mM) were added. HEK293T cells were cultured in either L, M or H media for at least 5 passages and efficient incorporation of amino acid isotopes was confirmed by mass spectrometry (MS).

Sample preparation for SILAC-MS analysis

SILAC-labelled HEK293T cells were transfected by lipofection with Fugene 6 (L: pcDNA3.1, M: ER- α and H: ER- β 23), harvested 48 h later and lysed in 1% Triton X-100 in PBS supplemented with cComplete Protease Inhibitor Cocktail and benzonase. After 1 h of

end-over-end rotation at 4 °C, cell debris was removed by centrifugation at 2,000 xg for 5 min at 4 °C and lysates were transferred to fresh tubes. 1.5 mg protein (in a total of 1 ml) were incubated with 50 µl µMacs anti-Myc beads at 4 °C on an end-over-end rotor overnight. Samples were then applied to µMACS columns that were equilibrated with 200 µl lysis buffer on a magnetic rack. Columns were washed once with 200 µl lysis buffer and then three times with 200 µl 0.1% Triton X-100/PBS and once with PBS. Proteins were eluted by addition of 70 µl hot Urea sample buffer. Eluates from H, M and L samples were mixed 1:1:1 before separation on a NuPAGE Bis-Tris gradient gel in MES buffer according to the manufacturer's instructions. For analysis of total protein, input lysates were directly mixed (1:1:1) and separated on a gradient gel. Gels were sliced into 12 equal slices per lane and proteins were reduced, alkylated, and digested within the gel as described in (Ong and Mann, 2006). After extraction, peptides were desalted using homemade columns of 200 µl tips containing C18 Empore disks. Peptides were eluted with 1% formic acid in 70% acetonitrile (ACN) and dried in a vacuum concentrator.

Sample preparation for label-free MS analysis

For analysis of total amounts of ER-β23-mCh in cell lysates, cells were transfected as above. Cells were lysed in RIPA buffer and after quantification using the BCA assay, proteins were reduced with 1 mM DTT and denatured in 2% SDS at 96 °C for 5 min. Proteins were digested using the filter-aided sample preparation (FASP) method (Wisniewski et al., 2011). Vivacon filtration columns were equilibrated with UA buffer before applying 100 µg of protein lysates. After three washes with UA buffer, proteins were reduced with 10 mM DTT (45 min, RT), acetylated with 50 mM Iodoacetamide (30 min, RT) and again washed twice with UA buffer before elution with 40 mM NH₄HCO₃ and digestion with trypsin at 37 °C overnight. Trypsin was then inactivated by acidification with TFA and peptides dried in a speedvac. Peptides were then fractionated using homemade SAX microcolumns (6 layers of Empore High

Performance Extraction Disks in 200 μ l pipette tip) using BRUB at decreasing pH (11-3). After extraction of the last peptide fraction with MeOH/H₂O (1:1)/1% formic acid, all fractions were acidified with TFA. Peptides were then desalted using homemade columns containing C18 Empore disks or commercial OMIX96 C18 tips. Peptides were eluted with 1% formic acid in 70% ACN and dried in a vacuum concentrator.

LC-MS/MS

Peptides eluted from desalting tips were dissolved in 5% (v/v) formic acid and sonicated for 5 min. Samples were analysed on a Proxeon EASY-nLC 1000 nano-HPLC system coupled to a Q-Exactive orbitrap mass spectrometer. Peptides were separated on home-made spray-columns (PicoTips packed with 1.9 μ m Reprosil-Pur C18-AQ) using a 2 h linear gradient between 5 % solvent A (0.2 % formic acid in water) and 30 % solvent B (0.2 % formic acid in ACN). Samples were loaded on the column by the nano-HPLC autosampler at a flow rate of 0.5 μ L per minute. No trap column was used. The HPLC flow rate was set to 0.25 μ L per minute during analysis. MS/MS analysis was performed with standard settings using cycles of 1 high resolution (70,000 FWHM) MS scan followed by 10 MS/MS scans of the most intense ions with charge states of 2 or higher at a resolution setting of 17,500 (FWHM).

Analysis of MS data

Protein identification and SILAC-based quantitation was performed with MaxQuant (version 1.3.0.5) (Tyanova et al., 2014) using default settings. The human sequences of UNIPROT (version 2012-06-14) were selected as the database for protein identification. MaxQuant used a decoy version of the specified UNIPROT database to adjust the false discovery rates for proteins and peptides below 1%. The protein OS-9 was identified in one replicate with SILAC ratios of 6.57 but could not be quantified by the MaxQuant algorithm in two other experimental replicates. However, this protein was also enriched in these replicates as judged based on the extracted ion intensities of light and heavy labelled peptides, which was

confirmed by visual inspection of the mass spectra. OS-9 was thus included in the interactor set. Normalized ratios (H/L) and combined ratios (H/L) from three independent experiments as calculated by MaxQuant were used for analysis. Identified interactors were further analysed using Perseus (1.5.2.12). For the label-free analysis of the proteome from ER- β 23-mCh-expressing cells, three independently prepared and measured samples were analysed by MaxQuant.

Fluorescence-activated cell sorting (FACS)

Transfected cells were detached using TrypLE Express 48 h after transfection followed by suspension in PBS. Cells were kept on ice until analysis. Cells were analysed using the BD FACSCalibur or the BD FACSAriaIII instruments. FACS data were analysed using the FlowJo software (Version 9.9).

siRNA knockdowns

HEK293T cells were transfected with 100 nM non-targeting control siRNA 3 (Ctrl), OS-9 siRNA smart pool or SEL1L siRNA smart pool and CPY*-mCh using DharmafectDuo transfection reagent following the manufacturer's instructions. Protein levels were analysed 48 h after transfection.

Luciferase assays

HEK293T cells were co-transfected with the luciferase constructs and either empty pcDNA3.1, ER- β 23 or ER- α in a ratio of 1:1. 24 h after transfection cells were trypsinised and seeded in 96-well plates in 100 μ l DMEM. After indicated treatments 30 μ l of Steady-Glo Luciferase Assay system buffer were added directly to the wells followed by incubation for 15 min in the dark at room temperature. Luminescence was recorded in a luminometer (2 s acquisition time). Untransfected cells incubated with Steady-Glo served as blanks.

Deglycosylation

Transfected HEK293T cells were lysed in RIPA buffer supplemented with protease inhibitors and benzonase. After removal of cell debris by centrifugation and quantification using the BCA assay, 40 µg protein were denatured and incubated with 2 µl Endo H or PNGase F following the manufacturer's instructions.

Analysis of Q97 inclusions by fluorescence microscopy

HEK293T cells were transfected with Q97 or Q25 using FuGene6 as described above and 24 h later trypsinised and reseeded on PLL-coated coverslips in 12 well plates. Cells were allowed to settle for 24 h before treatment with 20 µM gefitinib, 20 µM fluphenazine, 20 µM erlotinib or 50 µM droperidol for 20 h. After the treatment, cells were washed twice with PBS and fixed with 4% paraformaldehyde for 1 h at RT. Cells were again washed twice with PBS followed by DAPI staining (300 nM DAPI in PBS) for 5 min at RT. Cells were washed a further 3 times in PBS and mounted on glass slides with DAKO fluorescent mounting medium. Cells were analysed by confocal microscopy using a Zeiss LSM confocal microscope. 15 random images were taken per sample each using the 516 nm laser (mCherry) at two different laser strengths (0.7 and 7%) and the 405 nm laser (DAPI) at only one laser strength (1.0). The images with the lower 516 nm laser strength were used to analyse inclusion size and number and the images with the high laser strength were used only to count the total number of transfected cells. 5 random images per sample were analysed (about 300 transfected cells in total) using ImageJ. The total number of transfected cells was manually counted using the cell counter plugin. Inclusions were analysed using a macro following the same automated steps for each sample to ensure unbiased analysis: a Gaussian Blur (sigma=2) and the Renyi Entropy dark threshold were applied. Automatic watershedding was applied to separate overlapping particles. Particles of pixel sizes 7.00 to 44117.4 with a circularity of 0.00 to 1.00 were analysed by size (in pixels) and total number per image.

Results

Part 1 - How the ER handles aggregation-prone β -sheet proteins

Targeting an aggregation-prone β -protein to the ER

The model proteins β 4, β 17 and β 23 have been *de novo* designed to fold into six β -strands and form amyloid-like fibrils with cross- β structure *in vitro* and when expressed in the mammalian cytosol (West et al., 1999; Olzscha et al., 2011). To determine how the ERQC machinery handles aggregation-prone β -sheet proteins, we targeted these β -sheet proteins to the ER. The most aggregation-prone of these, β 23, was chosen as the primary model protein for this study. In addition, initial experiments addressing the fate of these proteins in the ER were performed also with β 4 and β 17 to test whether the observed behaviour was sequence-specific or common to all β -sheet proteins. As a control protein we used α -S824, a *de novo* designed α -helical protein, similar in amino acid composition to the designed β proteins, that folds into a 4-helical bundle (Wei et al., 2003; Olzscha et al., 2011) (ER- α , Figure 10A). The model proteins were targeted to the ER by addition of an N-terminal signal peptide derived from the secretory pulmonary surfactant-associated protein B (SP-B) (Dolfe et al., 2015) (Figure 10A). This signal peptide targets SP-B for co-translational translocation into the ER followed by processing and transport through the secretory pathway (Ueno et al., 2004).

The ER-targeted proteins had the same apparent molecular weight on SDS-PAGE as their cytosolic counterparts after expression in human embryonic kidney cells (HEK293T) (Figure 10B), suggesting that the signal peptide was efficiently cleaved by the signal peptide peptidase in the ER membrane and thus pointing towards efficient ER-targeting. Furthermore, this result suggests that the ER-targeted model proteins were not subjected to any specific post-translational modifications that would affect their mobility in SDS-PAGE and would allow them to be discriminated from their cytosolic counterparts.

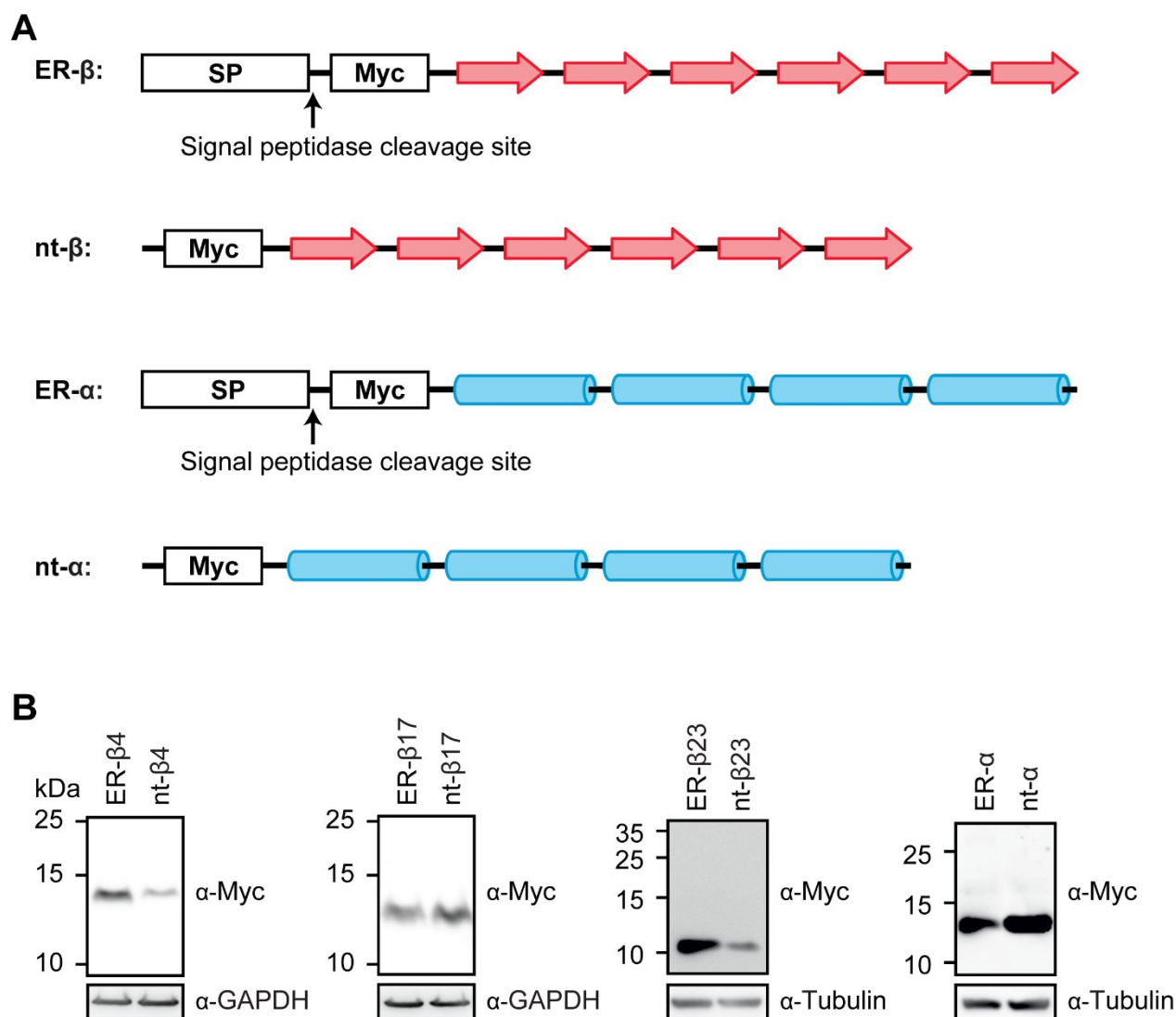


Figure 10. Targeting β -proteins to the ER. (A) Model β -proteins were designed to form a β -sheet consisting of six β -strands (indicated by red arrows), and α -proteins were designed to form 4-helical bundles (indicated by blue rods). ER-targeted constructs were designed by addition of an N-terminal signal peptide upstream of the Myc-tag of the non-targeted constructs (nt- β and nt- α , respectively). The signal peptidase cleavage sites are indicated by arrows. (B) Immunoblot analysis of ER-targeted (ER) model proteins after 48 h of expression in HEK293T cells revealed no shifts in mobility compared to the non-targeted (nt) proteins.

Analysis by confocal microscopy confirmed localisation of the ER-targeted model proteins to the ER. Human epithelial adenocarcinoma cells (HeLa) were used here as an additional model cell line for microscopy because their flat morphology facilitates clearer distinction of cellular organelles.

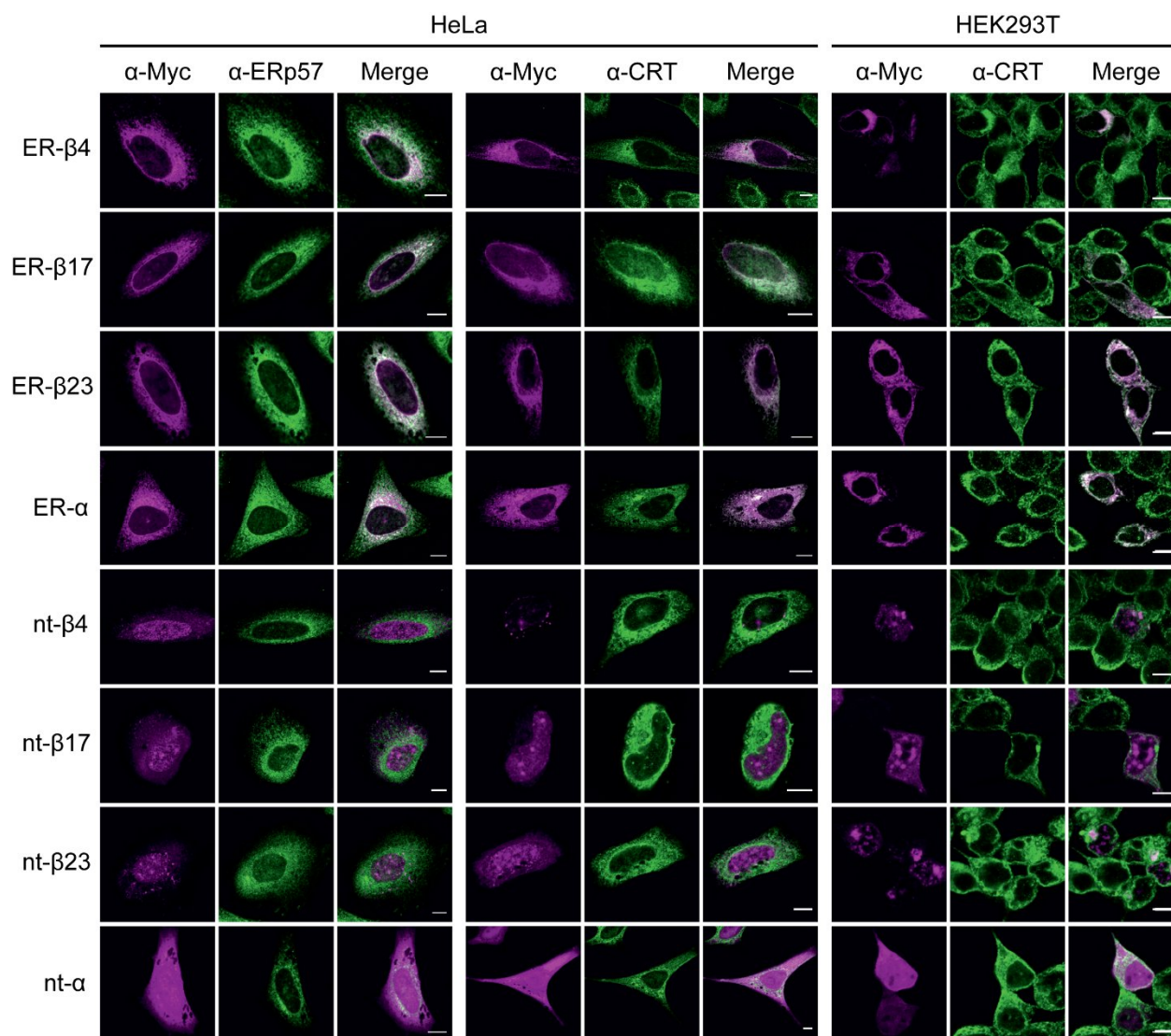


Figure 11. Model α - and β -proteins are efficiently targeted to the ER. HeLa or HEK293T cells were fixed after 48 h expression of the indicated model proteins and stained with anti-Myc (magenta) and either anti-ERp57 or anti-calreticulin (CRT) (green) antibodies, followed by fluorescently labelled secondary antibodies and analysis by confocal microscopy. Representative images from at least 3 independent experiments are shown. Scale bars represent 10 μ m.

All four proteins, ER- β 4, ER- β 17, ER- β 23 and ER- α , co-localised with the ER marker proteins ERp57 and CRT in HeLa and in HEK293T cells (Figure 11). In contrast, the non-targeted proteins, nt- β 4, nt- β 17, nt- β 23 and nt- α , did not co-localise with ER markers (Figure 11).

Taken together, the SP-B signal peptide efficiently targets the model proteins for co-translational translocation into the ER.

ER- β proteins are retained in the ER

After removal of the signal peptide, correct folding and modification, secretory proteins are transported in vesicles to the Golgi and subsequently to the plasma membrane for secretion, whereas proteins that fail to fold properly are usually retained in the ER until correct folding is completed or, should they fail to fold correctly, they are targeted for degradation (Araki and Nagata, 2011). The model α - and β -proteins did not contain an ER-retention signal and we thus wondered whether they could pass the ERQC for secretion. As expected, the majority of the control protein ER- α was detected in the conditioned medium of HEK293T cells two days after transfection (2-fold higher levels than intracellular, $p < 0.01$) (Figure 12A-B). The possibility of non-specific protein leakage into the media could be excluded because media samples did not contain any GAPDH or α -tubulin (Figure 12A-B). Furthermore, secretion of ER- α was strongly reduced by treatment of cells with brefeldin A (BFA), which inhibits protein transport from the ER to the Golgi (Klausner et al., 1992), indicating that ER- α exits the cell via the classic secretory pathway (Figure 12B). In contrast, ER- β 4, ER- β 17 and ER- β 23 were not detectable in the media, indicating that the β -proteins are retained in the secretory pathway, despite their high intracellular concentration (Figure 12A-B).

The observed defect in the secretion of ER- β proteins prompted the question at what stage of the secretory pathway trafficking may be impaired. To test whether ER- β 4, ER- β 17 or ER- β 23 were transported from the ER to the Golgi, the Golgi was stained with an antibody against the Golgi membrane protein giantin.

As expected, ER- α clearly co-localised with giantin in both HeLa and HEK293T cells (Figure 12C). In contrast, no co-localisation between giantin and ER- β 4, ER- β 17 or ER- β 23 could be detected (Figure 12C), indicating that all three ER- β proteins were retained within the ER.

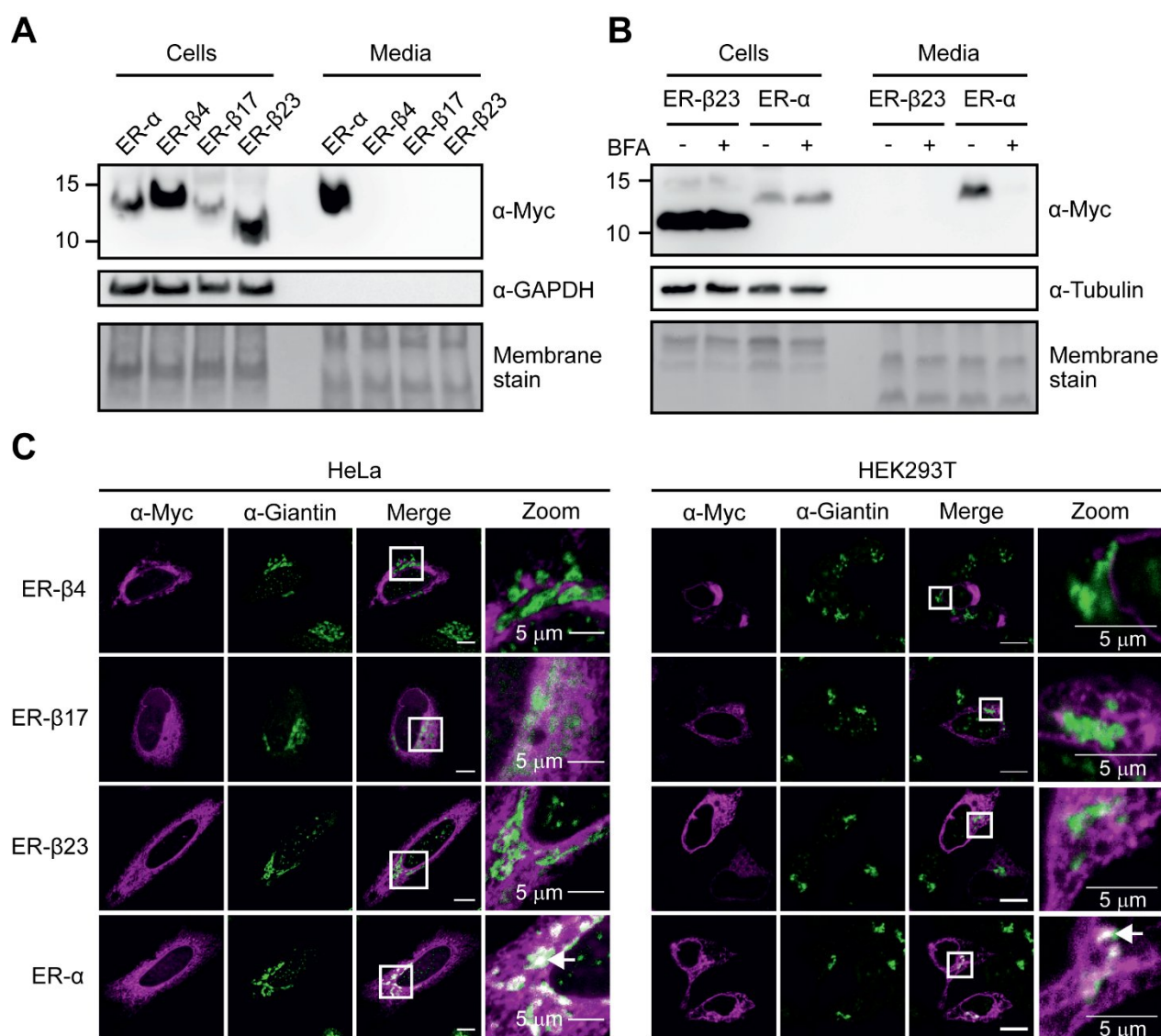


Figure 12. β -proteins are retained in the ER. (A) Conditioned media were collected after overnight incubation with HEK293T cells expressing the indicated model proteins for 48 h. Proteins from media were TCA-precipitated and equal fractions of protein from media and cell lysates were analysed by immunoblotting against the Myc-tag. GAPDH levels demonstrated the absence of cell leakage. Membrane staining was performed to provide a loading control. (B) HEK293T cells expressing the indicated model proteins were treated with $1 \mu\text{g ml}^{-1}$ brefeldin A (BFA) for 18 h. Proteins from conditioned media and cell lysates were analysed as in (A). Tubulin levels demonstrated absence of cell leakage. Membrane staining is used as a loading control. (C) HeLa or HEK293T cells were fixed after 48 h expression of the indicated model proteins and stained with anti-Myc (magenta) and anti-giantin (green) antibodies, followed by fluorescently labelled secondary antibodies and analysis by confocal microscopy. Representative images from at least three independent experiments are shown. Scale bars represent $10 \mu\text{m}$.

Misfolded proteins that are retained in the ER are usually recognised by ER chaperones and targeted for degradation (Olzmann et al., 2013). Since ER-targeted β -proteins do not seem to pass the ERQC for secretion, they may instead be targeted for degradation. Thus, the stability of ER- β 23 was tested by inhibiting protein synthesis using cycloheximide (CHX). Strikingly, ER- β 23 was found to be a remarkably stable protein with a half-life of more than 24 h (Figure 13), considerably exceeding the half-life of classic ERAD substrates (Finger et al., 1993). For example, mutant carboxypeptidase Y (CPY*) fused to mCherry (CPY*-mCh) was rapidly degraded, with a half-life of less than 3 h, (Figure 13). Thus, ER- β 23 is retained in the ER, but is not successfully targeted for degradation by ERAD.

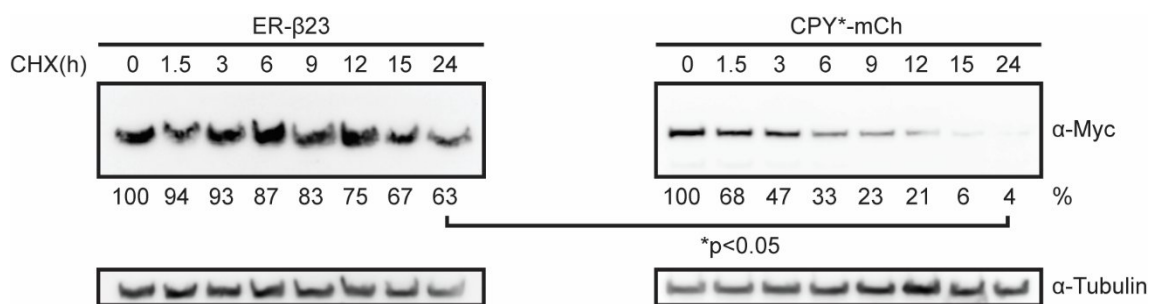


Figure 13. ER- β 23 is more stable than ERAD substrate CPY*-mCh. HEK293T cells expressing either ER- β 23 or CPY*-mCh for 72 h were treated with 0.5 mM cycloheximide (CHX) and harvested after indicated times of treatment. Protein levels were analysed by immunoblotting against the Myc-tags. Mean protein levels of ER- β 23 and CPY*-mCh from three independent experiments were quantified and shown as percentage of levels in untreated cells (0 h). The p value shown was determined using the Student's t-test (unpaired t-test).

Retention of ER- β 23 was also determined by live cell imaging. To enable detection, a fluorescent C-terminal mCherry-tag was added to ER- β 23 (ER- β 23-mCh) and ER- α (ER- α -mCh). The mCherry-tag did not alter the localisation of ER- α and ER- β 23. As observed for the myc-tagged constructs, ER- β 23-mCh was retained in the ER, whereas ER- α -mCh was detected in conditioned media and in the Golgi of HEK293T cells (Figure 14A-B).

Imaging of cells over a 192 s time span revealed that ER- β 23-mCh mostly localised to large network-like structures (Figure 14C), whereas ER- α -mCh was mainly present in vesicle-like structures that rapidly moved laterally through the cell (Figure 14C).

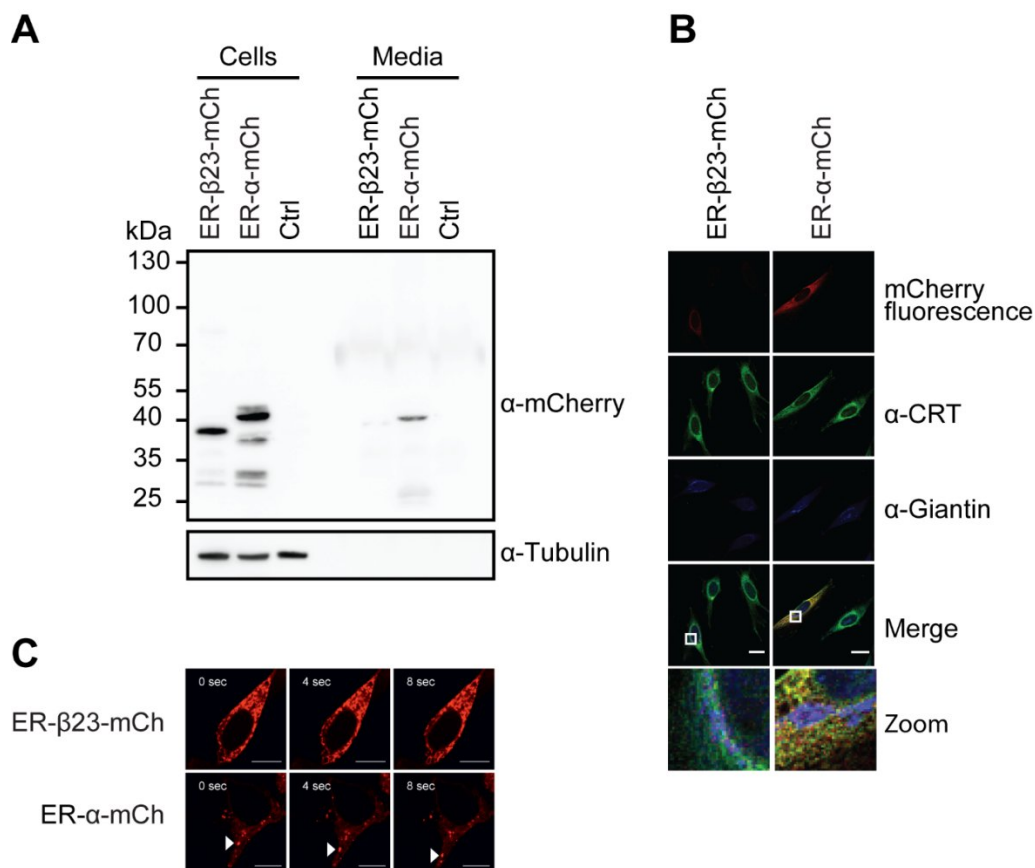


Figure 14. ER- β 23-mCh is retained in the ER. (A) Proteins from conditioned media of HEK293T cells after 48 h expression of the indicated proteins were concentrated by TCA precipitation and equal fractions of media and cell lysate samples were analysed by immunoblotting with anti-mCherry antibody. (B) HeLa cells expressing ER- β 23-mCh or ER- α -mCh were fixed and stained with anti-calreticulin (CRT) (green) and anti-giantin (blue) antibodies, followed by fluorescently labelled secondary antibodies and analysis by confocal microscopy. Scale bars represent 30 μ m. Enlarged regions (zoom) are indicated by white boxes. (C) Live HEK293T cells expressing ER- β 23-mCh or ER- α -mCh for 48 h were analysed by confocal microscopy. The movement of mCherry-tagged proteins was recorded over 192 s. The movement of a vesicle containing ER- α -mCh is indicated by white arrow heads. Scale bars represent 10 μ m.

Targeting β -protein to the ER reduces toxicity and aggregation propensity

The non-targeted β -proteins nt- β 4, nt- β 17, and nt- β 23 formed inclusion bodies (IBs) in the cytosol and nucleus, whereas nt- α distributed diffusely throughout the cytosol (Figure 11), as

described previously (Olzscha et al., 2011). The β -protein inclusions were markedly larger in HEK293T cells than in HeLa most likely due to higher expression levels. However, no clear inclusions could be observed after expression of the ER-targeted β -proteins (Figure 11). Furthermore, the ER-targeted β -proteins were almost completely soluble in buffer containing 1% Triton, in contrast to the largely insoluble non-targeted β -proteins that fractionated mostly to the pellet fraction after centrifugation (Figure 15A-B).

Non-targeted β -proteins were previously shown to reduce cell viability and this toxicity correlated with their aggregation propensity, nt- β 23 being the most toxic (Olzscha et al., 2011). However, expression of ER- β 23 did not result in significant toxicity (Figure 15C). This observation is in line with its increased solubility. Notably, the reduced toxicity and aggregation propensity was not due to lower expression levels of ER- β 23. In fact, intracellular ER- β 23 levels were more than 4-fold higher than the levels of nt- β 23 (Figure 15D). Thus, despite high concentrations the ER has a much higher capacity to maintain aggregation-prone β -sheet proteins in a more soluble and less toxic state.

The observations that ER-targeting renders β -proteins more soluble and less toxic regardless of their specific amino acid sequence indicates the existence of a potent ER quality control pathway independent of specific amino acid composition that retains proteins rich in β -structure in the ER and prevents them from forming amyloid-like, insoluble aggregates.

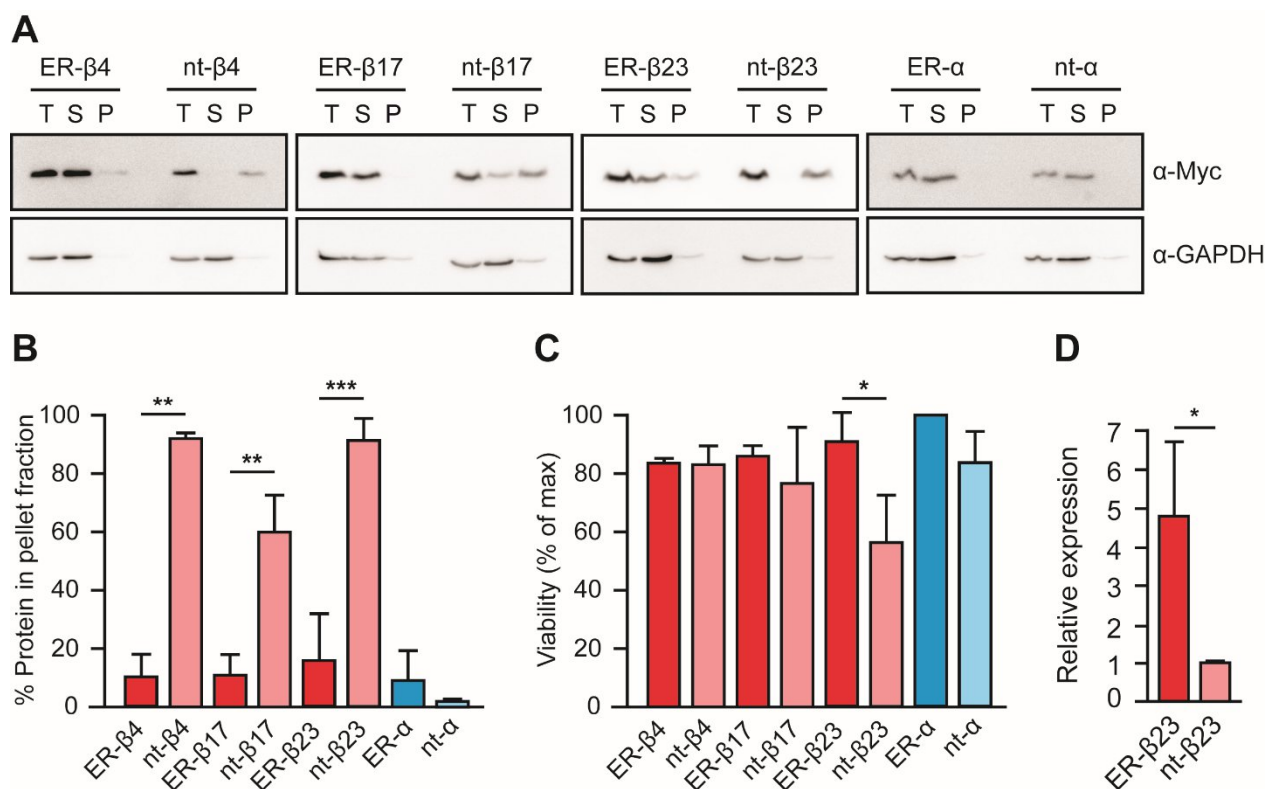


Figure 15. ER-targeting prevents β -protein aggregation and toxicity. (A) Solubility of ER-targeted model proteins (ER) and their non-targeted counterparts (nt) was analysed after 48 h of expression in HEK293T cells. Lysates were fractionated by centrifugation and fractions analysed by immunoblotting with anti-Myc antibody. T: total lysate, S: soluble fraction, P: pellet fraction. (B) Protein levels in P versus S from four independent experiments were quantified and mean values plotted. (C) Viability of HEK293T cells was measured by the MTT assay after 72 h of expression of the indicated constructs. Mean cell viability from three independent experiments was calculated as percentage of the max (ER- α). (D) The relative expression levels of ER- β 23 and n- β 23 in HEK293T cells was quantified based on immunoblotting described in Figure 10B. Total levels of ER- β 23 were quantified and shown as fold increase over nt- β 23. Mean values from four independent experiments are shown. Error bars represent SD and p values are based on the Student's t-test (unpaired t-test). * $p < 0.05$; ** $p \leq 0.01$; *** $p \leq 0.001$.

To test whether ER- β 23 forms higher-order macromolecular assemblies, cell extracts were analysed by blue native PAGE (Figure 16A). A small fraction of ER- β 23 migrated as a monomeric band, but a larger fraction migrated as higher molecular weight species above 200 kDa (Figure 16A), indicating the presence of a range of oligomers.

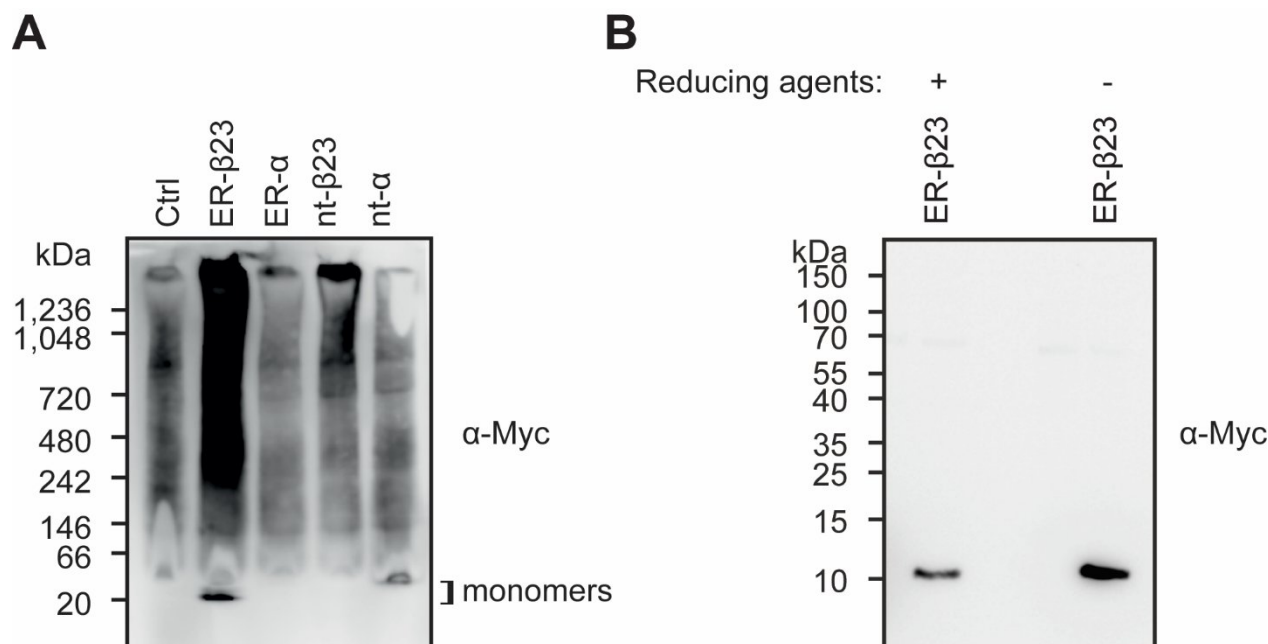


Figure 16. ER-β23 forms oligomers. (A) Lysates from HEK293T cells expressing either pcDNA (Ctrl), ER-β23, ER-α, nt-β23 or nt-α for 48 h were separated on blue native PAGE and analysed by immunoblotting with anti-Myc antibody. (B) Lysates from HEK293T cells expressing ER-β23 for 48 h were either treated with reducing agents (1 mM DTT and 5% β-mercaptoethanol) or left unreduced, separated on denaturing PAGE and analysed by immunoblotting against the Myc-epitope.

In contrast, the majority of nt-β23 formed large complexes that did not move into the gel and no monomeric protein was detectable. As expected, a monomeric band was detected for nt-α but no high molecular weight signal over background could be observed for the secreted protein ER-α. Taken together, these findings indicate that nt-β23 and ER-β23 have markedly different aggregation properties: nt-β23 forms predominantly large, insoluble aggregates, whereas ER-β23 accumulates mainly as soluble oligomers that are significantly less toxic. Notably, ER-β23 only contains one cysteine residue at the very N-terminus excluding the possibility of disulphide-linked polymers. Furthermore, no higher molecular bands could be observed by SDS-PAGE under non-reducing conditions confirming the absence of intramolecular disulphide bridges (Figure 16B).

Since ER-β23 is not permitted to exit the ER, the polymer formation might reduce the diffusion mobility of ER-β23. To test the mobility of ER-β23, fluorescence loss in

photobleaching (FLIP) experiments were performed and the behaviour of mCherry-tagged ER- β 23 (ER- β 23-mCh) was compared to ER-mCh-KDEL (ER-mCh), which contains the same signal sequence but also a C-terminal ER retention signal to prevent secretion. A small area within the ER of transfected cells was continuously bleached and images recorded after each bleaching cycle. ER-mCh fluorescence rapidly decreased within the whole cell as expected for a soluble monomeric protein. Strikingly, ER- β 23-mCh fluorescence only decreased within the area where the bleaching laser was pointed (Figure 17A) but remained relatively constant in a more distant ER area within the same cell (FLIP area, Figure 17A-B) demonstrating that ER- β 23-mCh was immobilised. Over time, the bleached area increased, which may indicate slow local movement.

The reduced mobility of ER- β 23-mCh indicates either that the protein is immobilised due to formation of immobile oligomers, or alternatively, that ER- β 23-mCh accumulation leads to fragmentation of the ER restricting the exchange of luminal components through the ER network. To distinguish between these two possibilities, the mobility of ER-targeted GFP (ER-GFP) was analysed in the presence of ER- β 23-mCh. After continuous photobleaching of a small area of the ER, ER-GFP fluorescence rapidly decreased within the whole ER both in the presence of ER- β 23-mCh (Figure 17A-B) and in the control ER-mCh (Figure 17A and C) indicating that ER-GFP freely moved through a connected ER network. Thus, even though ER- β 23-mCh is immobilised compared to monomeric ER-mCh, it allows for free movement of other ER-localised proteins. Taken together, this indicates that ER- β 23-mCh forms a network of soluble oligomers that fills the ER like a gel.

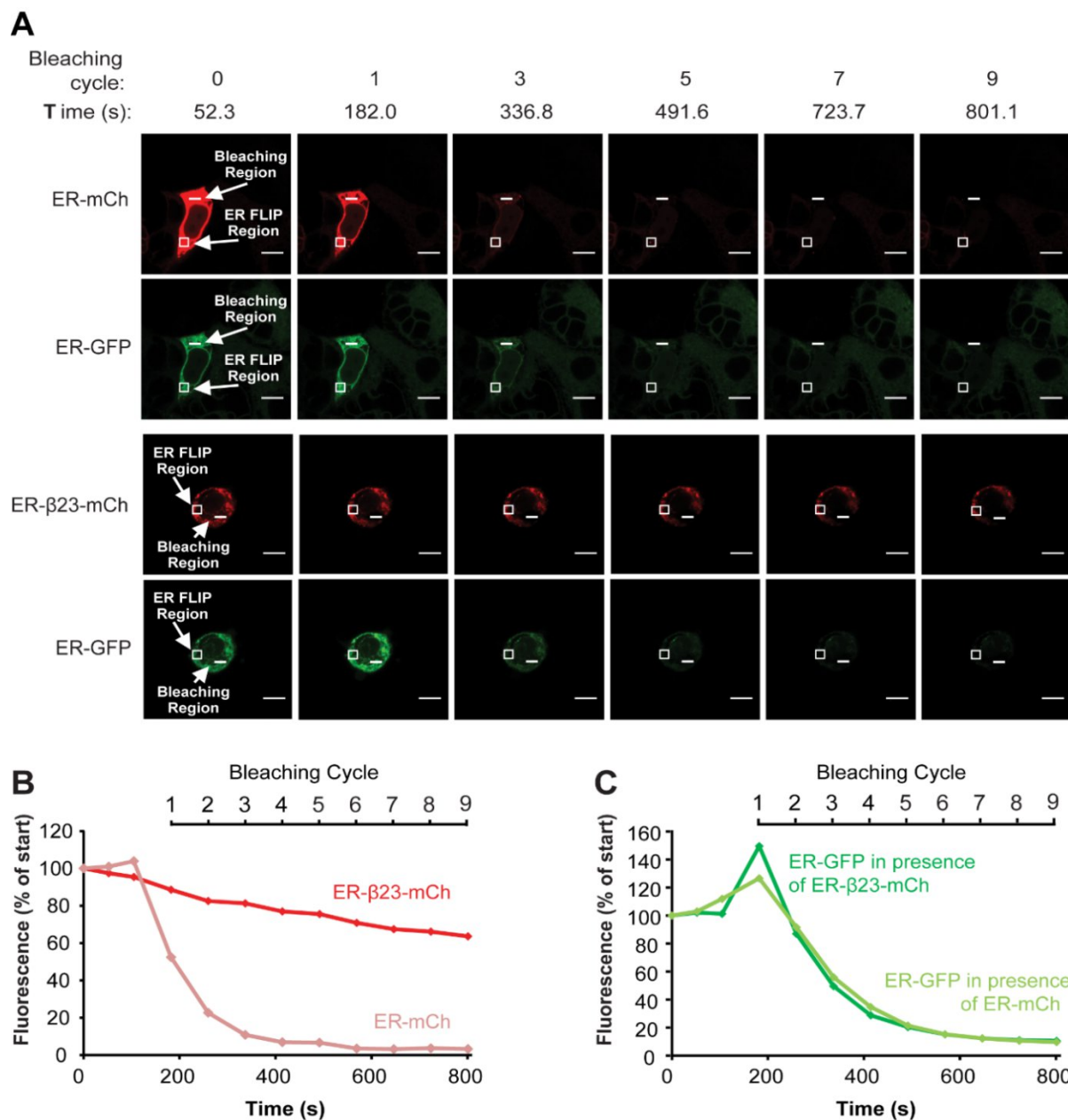


Figure 17. ER-β23-mCh forms oligomers with restricted mobility. (A) Fluorescence loss in photobleaching (FLIP) was performed in HEK293T cells after 48 h of expression of ER-GFP-KDEL (ER-GFP) in combination with either ER-β23-mCherry (ER-β23-mCh) or ER-mCherry-KDEL (ER-mCh). Before bleaching, three images were recorded by confocal microscopy to control for variations and possible bleaching during image recording. Then, small areas within the ER of cells (bleaching region) were repeatedly bleached using the 561 nm (for mCherry), 488 nm and 458 nm (for GFP) lasers and images recorded after each bleaching cycle (every 77.4 s). Relative changes in mean fluorescence of areas within the ER of the same cells (ER FLIP region) were plotted for (B) mCherry and (C) GFP, each normalised to the fluorescence measured at the first data point. Representative data from four independent experiments are shown. Scale bars represent 10 μm.

However, it should be noted that ER- β 23 may be more dynamic than the mCherry-tagged version because the cellular concentrations of ER- β 23-mCh were higher than those of non-tagged ER- β 23, and consequently, ER- β 23-mCh showed increased insolubility (Figure 18).

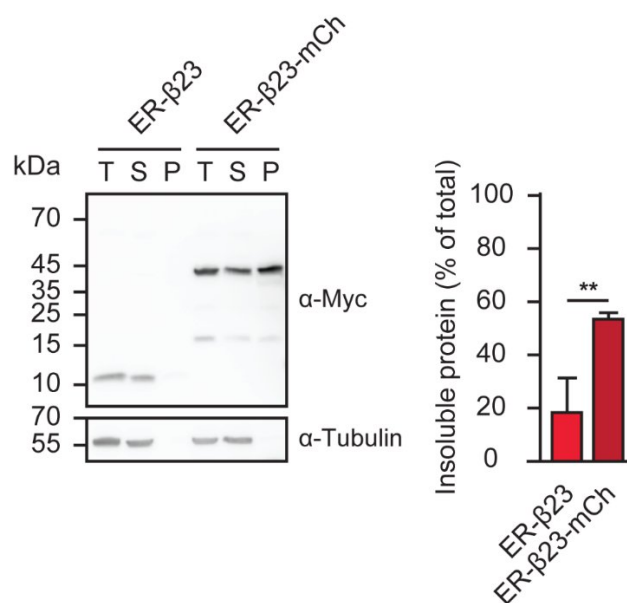


Figure 18. ER- β 23-mCh is expressed at higher levels than ER- β 23. Solubility of ER- β 23 and ER- β 23-mCh in HEK293T cells was analysed 48 h after transfection by centrifugation of lysates and immunoblotting against the Myc-tag. T: total lysate, S: soluble fraction, P: pellet fraction. Right panel: Protein amounts in the pellet fraction were quantified and presented as % of total (S+P). Error bars represent SD from four independent experiments and p values are based on the student's t-test (unpaired t-test). ** $p \leq 0.01$.

Nevertheless, non-tagged ER- β 23 was efficiently retained in the ER where it accumulated at high concentrations and formed oligomers. The reduced mobility of the mCherry-tagged construct indicates that this type of oligomer may have restricted mobility.

ER- β 17 is also retained in a detergent-soluble state in stably expressing cell lines

It has recently been reported that a small fraction of ER- β 17 expressed in stable HEK293 cell lines may be insoluble and that a small amount could be detected extracellularly after immunoprecipitation (Dolfe et al., 2015).

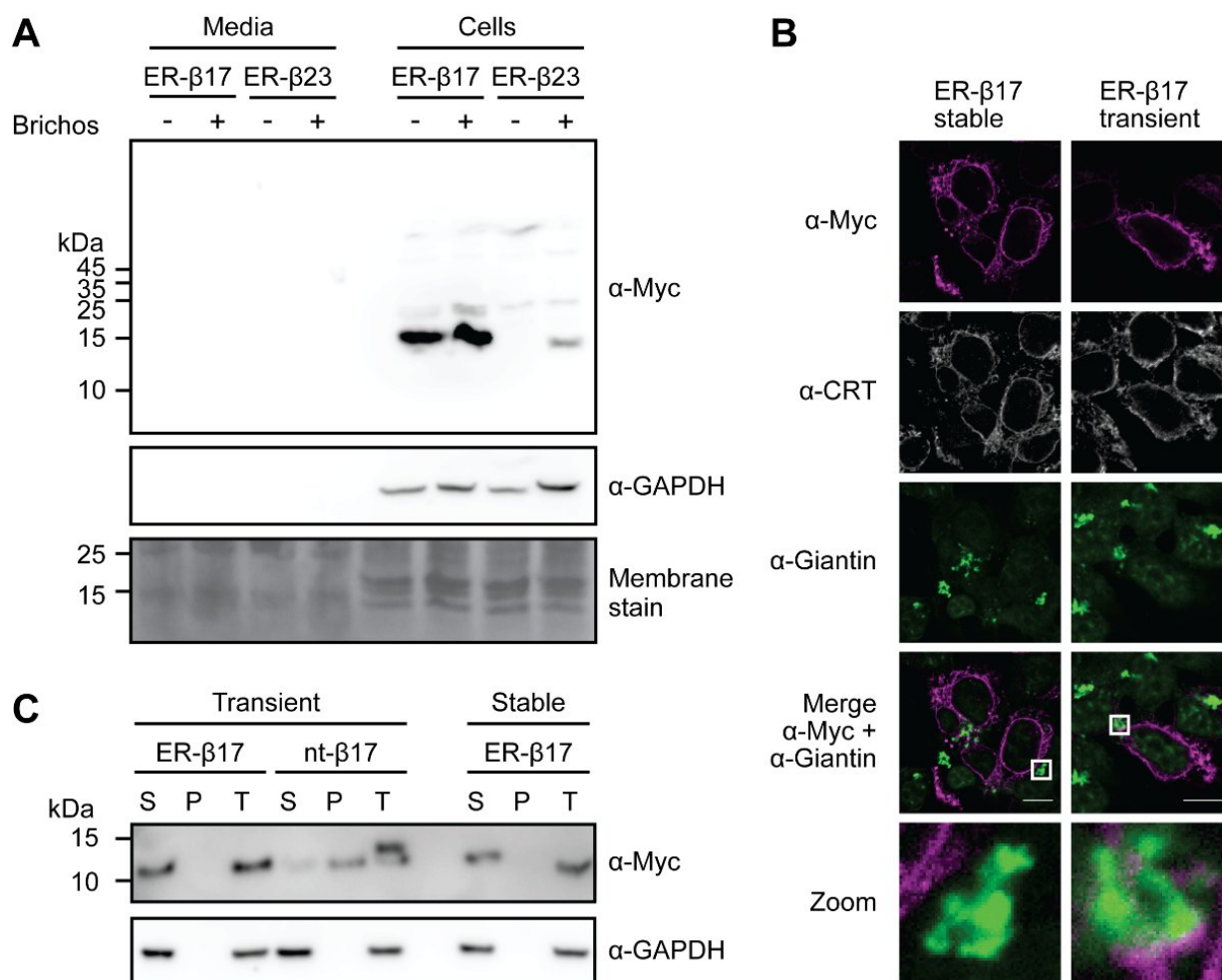


Figure 19. ER-β17 is detergent-soluble and retained in the ER in stably expressing cell lines. (A) Lysates and conditioned media samples from HEK293T cells stably expressing the indicated model proteins were analysed as described in Figure 12A. (B) HEK293T cells stably expressing ER-β17 or transiently transfected with ER-β17 were fixed and stained with anti-Myc (magenta), anti-CRT (gray) and anti-giantin (green) antibodies, followed by fluorescently labelled secondary antibodies and analysis by confocal microscopy. Scale bars represent 10 μm. Enlarged regions (Zoom) are indicated by white boxes. (C) Solubility of nt-β17 and ER-β17 from transiently transfected cells or from the stably expressing HEK293T cells was analysed 48 h after transfection as described in Figure 15A. T: total lysate, S: soluble fraction, P: pellet fraction.

We thus set out to determine whether ER-β17 may be handled differently after prolonged and increased expression in stable cell lines compared to transiently transfected cells. However, no differences between stably or transiently expressed ER-β17 were detectable in conditioned medium or in co-localisation studies with the Golgi marker giantin (Figure 19A-B). Similar to the transiently expressed ER-β17, ER-β17 from stable cell lines

was mostly soluble in 1% Triton (Figure 19C). We conclude that insoluble ER- β 17 represents only a minor fraction (less than 10%) of total ER- β 17 and that ER- β proteins seem to be handled in a similar manner in a stably expressing HEK293 cell line as in transiently transfected cells.

Analysis of the ER- β 23 interactome

To identify the components of the ERQC machinery that interact with ER- β 23, we performed a quantitative proteomic analysis using stable isotope labelling with amino acids in cell culture (SILAC) (Ong and Mann, 2006). After labelling HEK293T cells with amino acid isotopes in cell culture and verification of full incorporation of amino acids by mass spectrometry, labelled cells were transfected with ER- β 23, ER- α or the empty pcDNA vector (Figure 20A). Myc-tagged proteins were immuno-precipitated and equal amounts of eluates were mixed before preparation for mass spectrometry. Immuno-precipitation (IP) of ER- β 23 resulted in an enrichment of about 6-fold with minimal loss of protein in the flow-through (Figure 20B). However, ER- α could not be isolated as efficiently with almost 60% of protein lost in the flow-through and minimal (less than 0.1 fold) enrichment (Figure 20B). Not surprisingly, therefore, no specific ER- α interactors over the control (pcDNA) could be detected. Comparison of protein levels on a coomassie-stained gel confirmed equal amounts of total protein contents and specific band patterns for input versus eluate samples (Figure 20C).

A total of 3,317 proteins were identified in the mixed eluate sample by mass spectrometry in three independent experiments (Figure 20D and Appendix Suppl. Table 2). Of these, 83 proteins were more than 2-fold (up to 8.9-fold) enriched in ER- β 23 compared to the control (pcDNA) in at least two of three independent experiments and were thus defined as specific ER- β 23 interactors (Figure 20D and Appendix Suppl. Table 2).

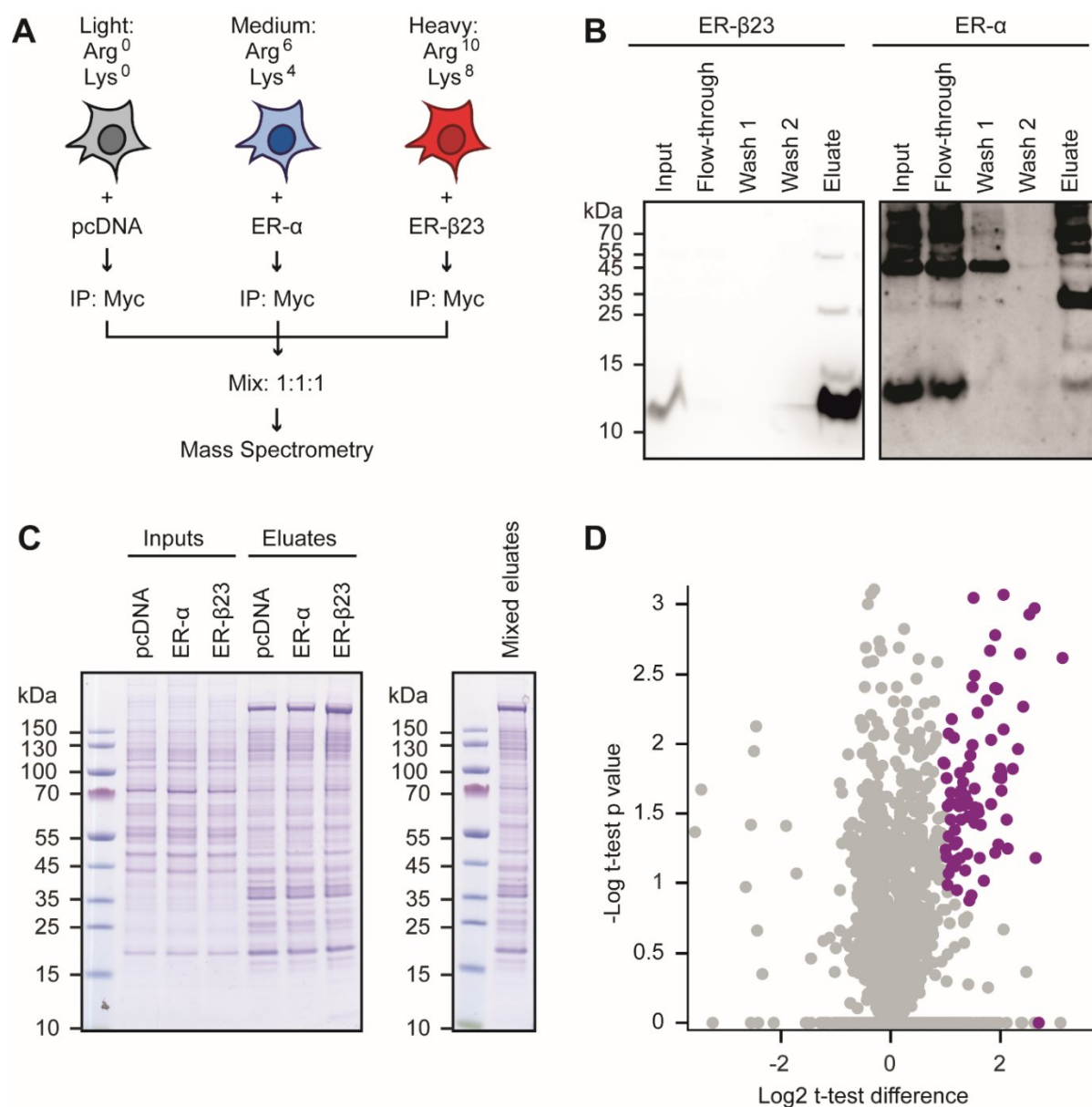


Figure 20. Analysis of the ER-β23 interactome. (A) Design of SILAC-based MS analysis to identify proteins that preferentially interact with ER-β23. (B) ER-β23 and ER-α were immuno-precipitated from HEK293T cell lysates after 48 h of expression using anti-Myc antibody coupled magnetic beads. The IP input lysates, flow-through, wash fractions and eluates were analysed by immunoblotting using a different anti-Myc antibody. (C) Input lysates and IP eluates were separated by SDS-PAGE and analysed by Coomassie staining. (D) The H/L ratios (ER-β23 over control) of all proteins identified in IP eluates were analysed using Perseus (1.5.2.12) to generate a volcano plot showing the mean H/L ratio in log₂ (Log₂ t-test difference) versus the negative log of the p value for all identified proteins. Proteins that were enriched more than 2-fold in ER-β23 eluates over the control in at least two out of three experiments were defined as ER-β23 interactors (indicated as purple dots, all other proteins shown as grey dots).

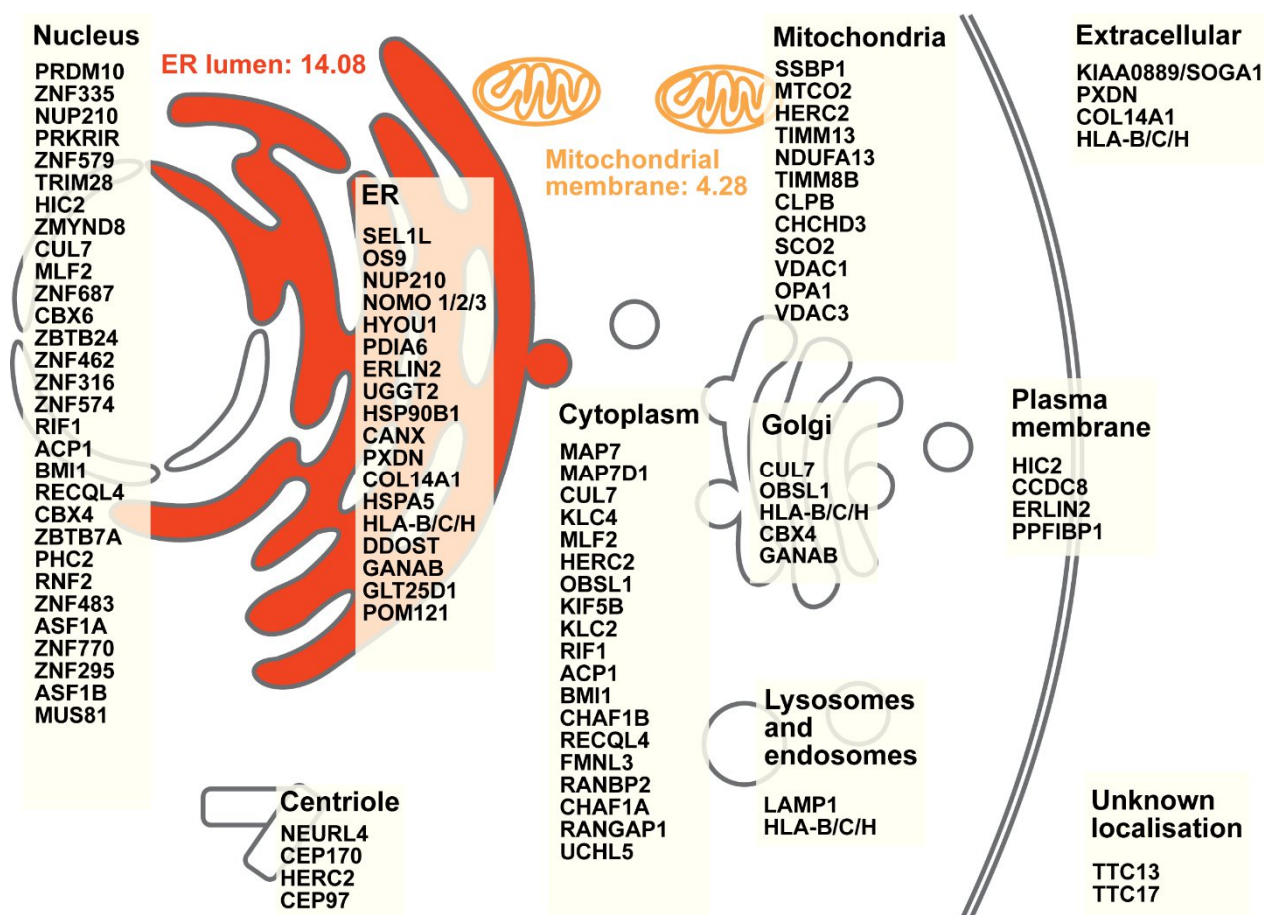


Figure 21. Cellular localisation of ER-β23 interactors. Gene Ontology Cellular Component (GOCC) annotations were assigned to ER-β23 interactors using Perseus (1.5.2.12). All interactors are listed grouped by their main localisations and sorted by their SILAC enrichment. The enrichment of the GOCC category annotations among the set of interactors was calculated over the background of GOCC category annotations of all proteins identified using the Fisher exact test. Enrichment factors of the significantly enriched organelle parts (ER lumen and mitochondrial membrane) are shown in red and orange.

Analysis of total protein levels in the input lysates revealed that the 83 interactors of ER-β23 were not significantly up-regulated (Appendix Suppl. Table 2), indicating that the observed interactions are not due to altered total protein levels.

ER-β23 interacts with a distinct set of ER chaperones and ERAD factors

The set of ER-β23 interactors is significantly enriched for ER luminal proteins and with lower significance for mitochondrial and ER membrane proteins when comparing gene ontology annotations of ER-β23 interactors to the background of all identified proteins (Figure 21 and

Appendix Suppl. Table 3). Interactions of ER- β 23 with mitochondrial membrane proteins could be due to localisation to ER-mitochondria contact sites. Other components of the secretory pathway were not significantly enriched, consistent with the finding that ER- β 23 is retained in the ER. ER- β 23 also interacted with a large set of cytosolic and nuclear proteins, including proteins of the nuclear envelope, but neither the cytosol nor the nucleus were significantly enriched as cellular components.

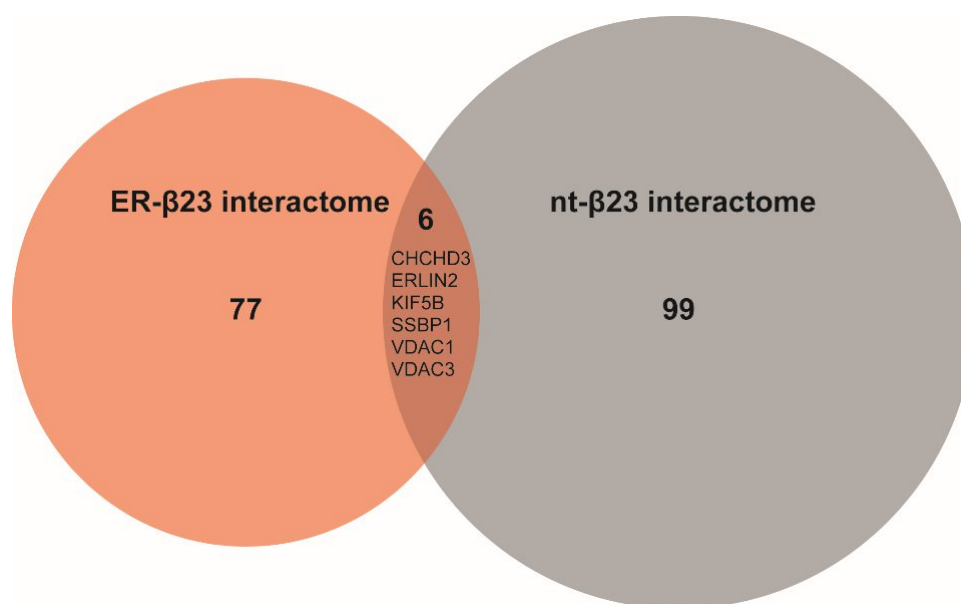


Figure 22. Overlap of the ER- β 23 and the nt- β 23 interactomes. Comparison of the identified interactors of ER- β 23 (83 proteins, represented by red circle) and the interactors of nt- β 23 (Olzscha et al., 2011) (105 proteins, represented by grey circle) revealed six common interactors (gene names listed).

Less than 10% (6 proteins) of the ER- β 23 interactors were previously found to interact with nt- β 23 (Olzscha et al., 2011) (Figure 22). This confirms that the proteins have distinct cellular localisations and that the majority of identified interactions are not due to post-lysis artefacts. Interestingly, 4 of the 6 interactors common to ER- β 23 and nt- β 23 are mitochondrial proteins.

Amongst the interactors of ER- β 23 we identified several ER-resident chaperones (Figure 23A-B). These include the HSP90 family member GRP94, the HSP70 BiP, the lectin chaperone calnexin (CNX), the nucleotide exchange factor of the HSP110 family HYOU1

and the protein disulphide-isomerase A6 (PDIA6). The latter has recently been demonstrated to play a role in protein folding as well as regulation of the UPR (Eletto et al., 2014). Surprisingly, we also identified several interactors of ER- β 23 that are part of the ERAD machinery: the substrate binding protein OS-9, the adapter protein SEL1L and the intramembrane adapter protein Erlin-2 (Figure 23A-B and Appendix Suppl. Table 2). These interactions were striking because ER- β 23 does not seem to be efficiently degraded via the ERAD pathway (Figure 13). Notably, no cytosolic members of the ERAD pathway interacted with ER- β 23 suggesting that ER- β 23 may be targeted for ERAD and recognised by substrate recognition factors but not be efficiently dislocated into the cytosol for degradation by the UPS.

Of the 83 ER- β 23 interactors, 90% contributed less than 2% each to the total amount (in ppm) of proteins found in the IP eluate (relative abundance calculated using IBAQ values) (Appendix Suppl. Table 4). However, BiP strikingly stood out as one of the most abundant interactors making up more than 20% of total interacting proteins in the eluate (Appendix Suppl. Table 4).

The specific interactions of ER- β 23 with SEL1L, OS-9, HYOU1, PDIA6, GRP94, Erlin-2, CNX and BiP were confirmed by immunoblotting. It is worth noting that for many chaperones only a small fraction (~0.2-3%) of the total amount of the protein present in cells could be immuno-precipitated (Figure 23B). Thus, even though the IP eluate contained a large amount of BiP, this reflected only a small fraction of total cellular BiP levels suggesting that a depletion of the free chaperone pool by ER- β 23 is unlikely. In contrast, high amounts of the ERAD components SEL1L and OS-9 compared to their total cellular levels interacted with ER- β 23 (about 10% of total SEL1L and about 50% of total OS-9). Notably SEL1L and OS-9 are very low-abundance proteins in HEK293T cells. Label-free MS quantification revealed that cellular levels of SEL1L and OS-9 were over 200-fold lower than the levels of GRP94

and BiP (Appendix Suppl. Table 5). Thus, sequestration of these factors by ER- β 23 may have functional consequences.

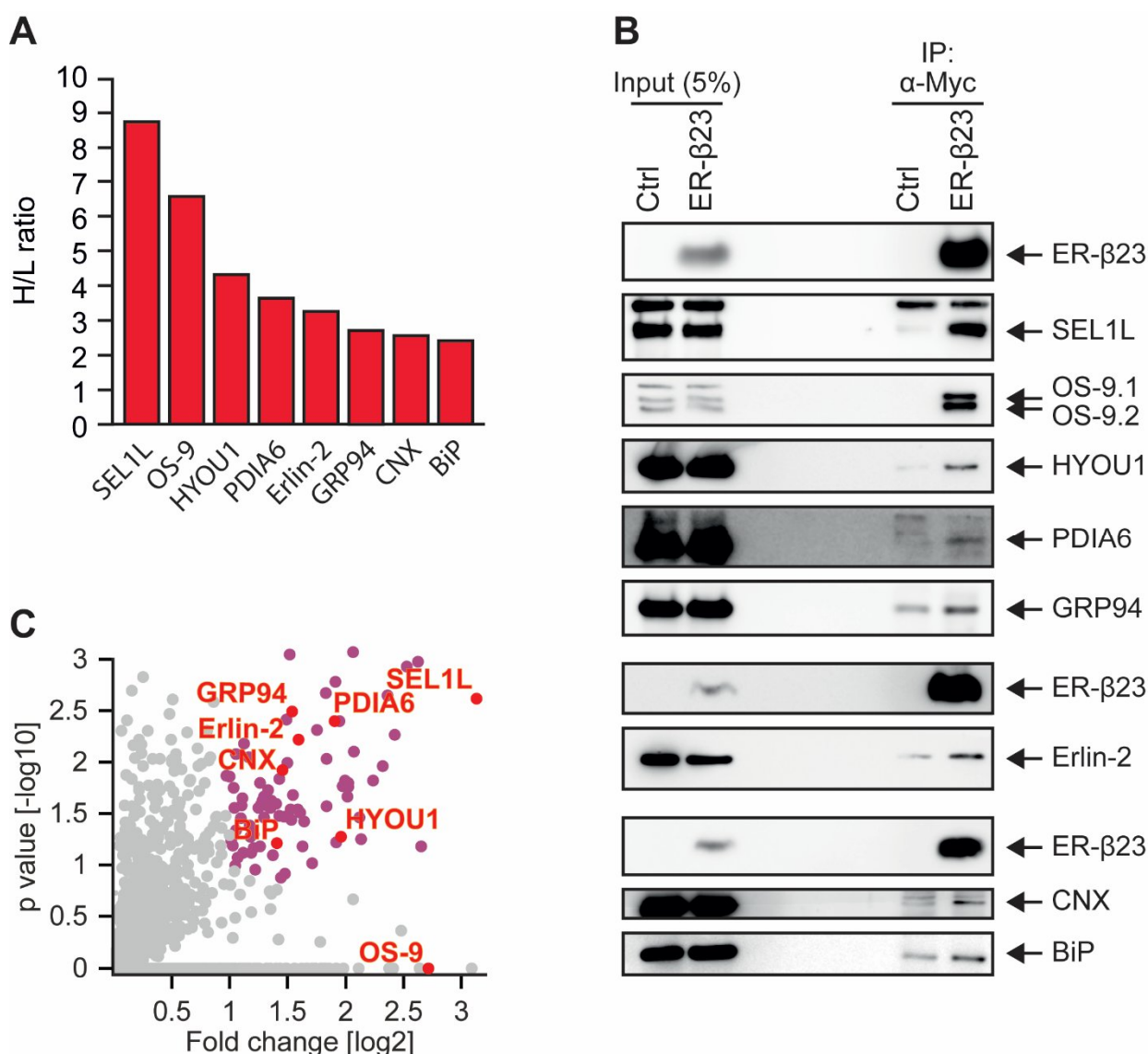


Figure 23. ER- β 23 is recognised by a set of ER chaperones and ERAD factors. (A) Enrichment ratios of ER- β 23-interacting ERQC factors (combined H/L ratios from three independent experiments calculated by MaxQuant (version 1.3.0.5)) are shown. (B) Detail of volcano blot described in Figure 20D. The ER- β 23-interacting chaperones and ERAD factors are indicated in red, all other ER- β 23 interactors as purple dots and non-enriched proteins that were identified as grey dots. (C) The interactions of SEL1L, OS-9, HYOU1, PDIA6, GRP94, Erlin-2, CNX and BiP with ER- β 23 were confirmed by immunoblotting after IP of ER- β 23 as described in Figure 20B.

ER- β 23 accumulates at levels exceeding those of interacting chaperones

Binding of ER- β 23 to ER-resident chaperones might contribute to its retention in the ER. To test whether HEK293T cells contained sufficient amounts of the ER chaperones BiP, CNX, GRP94, HYOU1 and PDIA6 to bind all ER- β 23 molecules, the abundance of ER chaperones relative to ER- β 23 was analysed by MS. Tryptic digestion of ER- β 23 did not produce any peptides that could be detected by MS, making it impossible to quantify ER- β 23 by proteomics. However, tryptic digestion of the mCherry-tagged version of ER- β 23 (ER- β 23-mCh) generated sufficient peptides to allow intensity-based absolute quantification (IBAQ) (Schwanhausser et al., 2011). Thus, relative chaperone levels were quantified in HEK293T cells expressing ER- β 23-mCh. The abundances of proteins were calculated as ppm of all identified proteins after normalisation for transfection efficiency (Figure 24A) to exclude proteins from untransfected cells from the analysis. Strikingly, ER- β 23-mCh levels were significantly higher than the levels of each individual interacting ER chaperone and even exceeded the combined amount of all interacting chaperones (Figure 24B).

BiP has previously been reported to reach low millimolar concentrations in the ER (up to 5 mM) (Weitzmann et al., 2007). This provides an estimate for the cellular concentration of ER- β 23, which must be in the millimolar range even after taking into account that the mCherry-tagged version is expressed at higher levels (Figure 18). Based on these high levels of ER- β 23, a 1:1 molar interaction between a major fraction of ER- β 23 and any interacting chaperone is very unlikely, especially because only a few percent of the total of each chaperone was co-immunoprecipitated (Figure 23B). Thus, chaperones may bind to only a small fraction of ER- β 23 at any given time, for example the monomeric form. A single chaperone molecule may also be able to bind and retain ER- β 23 oligomers. Alternatively, ER- β 23 may be retained due to the formation of oligomers and higher order polymers

(Figure 16A) that are immobilised (Figure 17A-B) preventing their packaging into secretory vesicles.

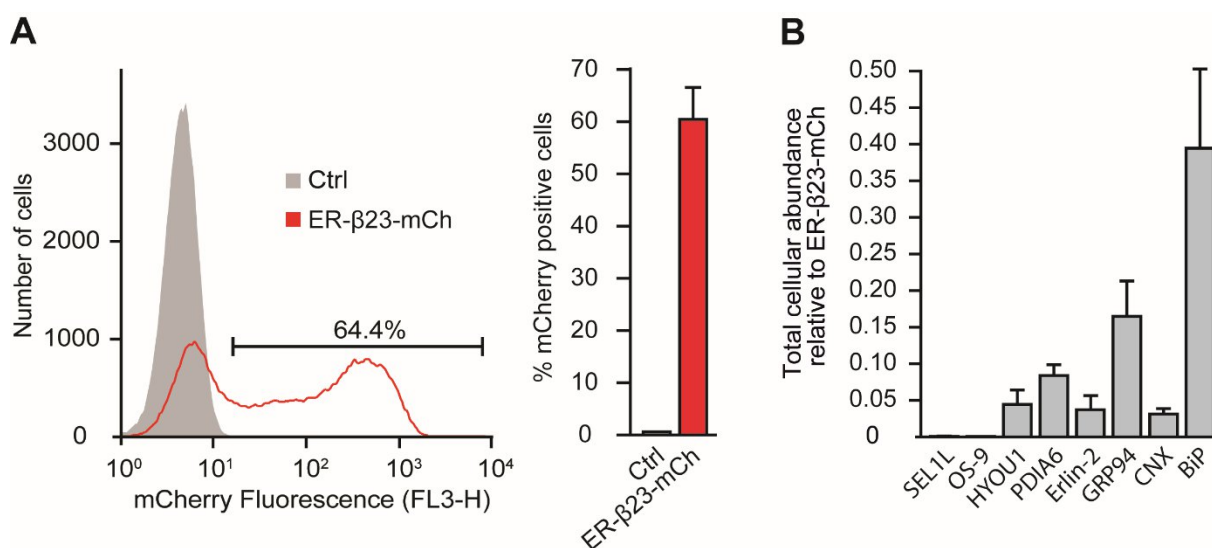


Figure 24. Total abundances of ER- β 23 interactors. (A) Transfection efficiency was analysed 48 h after transfection of HEK293T cells with ER- β 23-mCh by measuring mCherry fluorescence using fluorescence-activated cell sorting (FACS). The fraction of mCherry-positive cells (right panel) was calculated using the FlowJo software after generating a gate including all mCherry-positive cells and excluding the untransfected control cells (representative plot shown in left panel). (B) Cellular abundance values of ER chaperones and ERAD factors relative to the abundance of ER- β 23-mCh. IBAQ values of proteins measured in ER- β 23-mCh-expressing cells are plotted as fractions of the IBAQ value of ER- β 23-mCh after normalisation for transfection efficiencies shown in (A). Error bars represent SD of three independent experiments. Proteins are sorted from left to right in order of their enrichment in the ER- β 23 interactome (see Figure 23A).

ER- β 23 inhibits UPR induction

Since ER- β 23 is recognised by ER chaperones and retained within the ER lumen at high concentrations, it may induce the UPR. However, MS analysis revealed that ER- β 23 expression for 48 h did not lead to increased levels of UPR targets (Appendix Suppl. Table 6). To test further how ER- β 23 expression affected UPR signalling, cells were co-transfected with ER- β 23 and UPR sensor constructs that express firefly luciferase under the control of the UPR-induced UPRE, ERSE I and ERSE II promoters (Bouman et al., 2011), which are induced by the UPR transcription factors XBP1 (UPRE) and ATF6 (ERSE I and II)

(Yamamoto et al., 2004). We found that ER- β 23 expression did not lead to increased UPRE-induced luciferase activity but, on the contrary, resulted in a significantly reduced basal UPRE-regulated expression (Figure 25A). Tunicamycin (Tm) treatment, which causes ER stress by inhibition of protein glycosylation (Takatsuki and Tamura, 1971), resulted in induction of UPRE-luciferase in control cells but failed to cause a detectable induction in ER- β 23-expressing cells (Figure 25A). In contrast, the control protein ER- α did induce UPRE-luciferase. Indeed, it would be expected that high overexpression of a secretory protein requires the cell to increase its ERQC capacity via UPR induction (Calton et al., 2002).

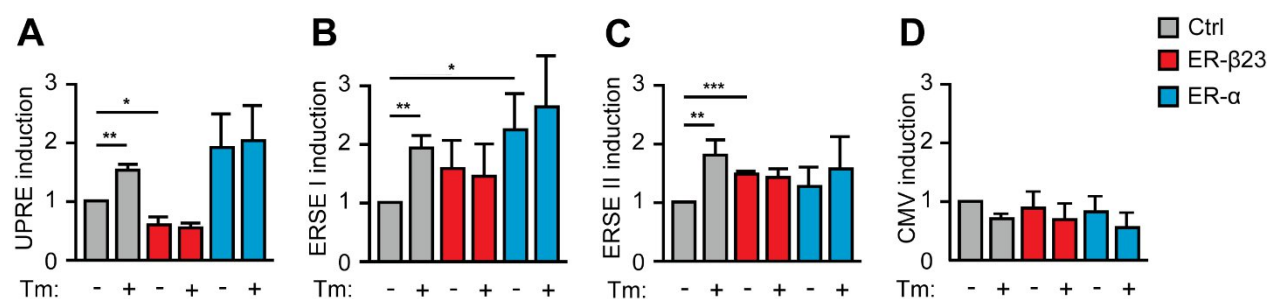


Figure 25. ER- β 23 inhibits UPR induction. HEK293T cells were co-transfected with a combination of pcDNA (Ctrl), ER- β 23 or ER- α and either (A) UPRE-, (B) ERSE I-, (C) ERSE II- or (D) CMV-promoter-driven-luciferase and 48 h later treated with 1 $\mu\text{g ml}^{-1}$ tunicamycin (Tm) for 24 h were indicated. Luciferase expression was then analysed by measuring luminescence. Mean luminescence values of three independent experiments are plotted as fold change from untreated control cells (Ctrl). Error bars represent SD and p values are based on the student's t-test (unpaired t-test). * $p < 0.05$; ** $p \leq 0.01$; *** $p \leq 0.001$.

The ERSE I- and ERSE II-promoters were, in contrast to UPRE, induced by ER- β 23 as well as ER- α (Figure 25B-C). Tm treatment led to a mild additional induction of the promoters in the presence of ER- α . Yet, in the presence of ER- β 23 no further induction by Tm treatment could be detected (Figure 25B-C), indicating a mild inhibitory effect of ER- β 23 also on the ERSE-promoters. Co-expression of ER- β 23 and CMV-driven luciferase verified that the observed effects were promoter-specific and not due to a general inhibition of translation or luciferase folding (Figure 25D). It was previously shown that nt- β 23 does not induce the cytosolic stress response and in fact inhibited its activation (Olzscha et al., 2011). ER- β 23

appears to have a similar inhibitory effect on the IRE1 α /XBP1 axis of the UPR and to some extent on the ATF6 axis.

ER- β 23 is not glycosylated

Many of the ER- β 23 interactors are known to bind glycosylated substrates. ER- β 23 contains several asparagines (Appendix Suppl. Table 1) but the NetNGlyc 1.0 Server algorithm (Blom et al., 2004) predicted no N-glycosylation sites. Furthermore, the fact that ER- β 23 migrates at the same size as nt- β 23 in electrophoresis strongly suggested that ER- β 23 was not subject to glycosylation (Figure 10B). In addition, ER- β 23 did not show any shift in electrophoretic mobility after treatment of lysates with the deglycosylating enzymes endoglycosydase H (Endo H) or peptide-N-glycosidase F (PNGase F). In contrast, the endogenous ER protein SEL1L was clearly deglycosylated under these conditions in the same lysates (Figure 26A). Thus, ER- β 23 is not glycosylated and is recognised by these lectins either via an additional client recognition mechanism such as a peptide binding domain or the lectins bind ER- β 23 indirectly as parts of larger protein complexes.

ER- β 23 inhibits ERAD

Surprisingly, even though ER- β 23 was degraded with very slow kinetics, it interacted strongly with ERAD factors OS-9, SEL1L and Erlin-2 that serve as substrate recognition and adaptor proteins, respectively. However, no downstream factors of the ERAD pathway involved in substrate translocation or ubiquitination were identified as interactors of ER- β 23. Together with the findings that ER- β 23 was very stable and was exclusively detected in the ER, these selective interactions with early ERAD factors suggest that ER- β 23 does not pass the dislocon for retro-translocation into the cytosol. Thus, ER- β 23 may interact with components of the early ERAD pathway in a non-productive manner and in this way block degradation of other ERAD substrates. To test this hypothesis, the effect of ER- β 23 on the degradation of the ERAD model substrate CPY*-mCh was analysed.

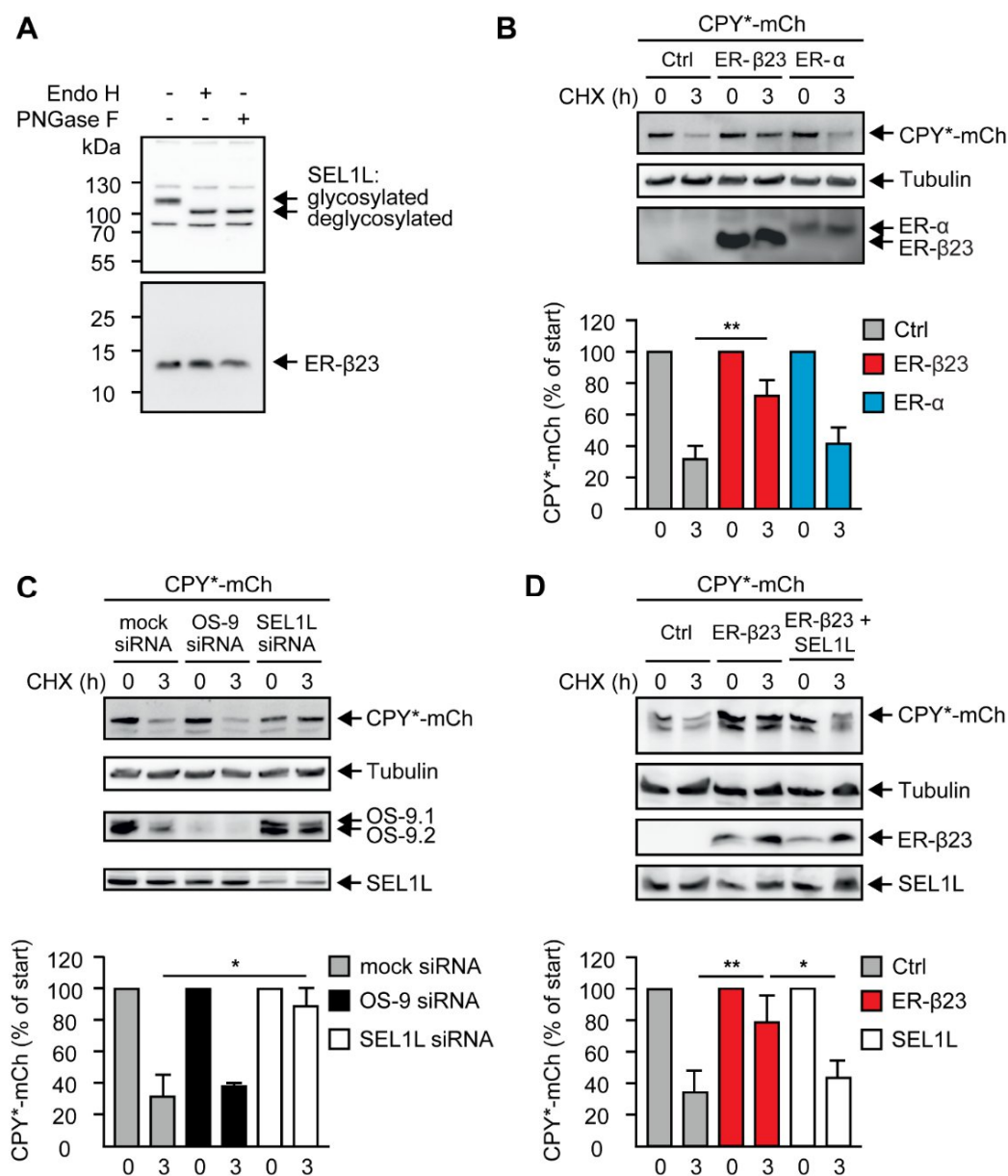


Figure 26. ER-β23 inhibits ERAD. (A) Lysates from ER-β23-expressing HEK293T cells were treated with deglycosylating enzymes Endo H or PNGase F before analysis by immunoblotting with anti-SEL1L and anti-Myc antibodies, using 8% and 12% Bis-Tris gels for SEL1L and ER-β23, respectively, to ensure maximum resolution. (B) HEK293T cells co-transfected with CPY*-mCh and either pcDNA (Ctrl), ER-β23 or ER-α were treated with 0.5 mM cycloheximide (CHX) for 3 h where indicated. Levels of CPY*-mCh, ER-β23 and ER-α were analysed by immunoblotting with anti-Myc antibody. CPY*-mCh levels were quantified, normalised with the loading control tubulin and presented as % of untreated cells (0 h). Error bars represent SD from three independent experiments and p values are based on the Student's t-test (unpaired t-test). (C) Cells were co-transfected with a combination of CPY*-mCh and non-targeting siRNA (mock) or siRNA pools targeting OS-9 or SEL1L. Stability of CPY*-mCh was analysed as in (B). (D) Cells were co-transfected with CPY*-mCh, pcDNA (Ctrl), ER-β23 plus pcDNA or ER-β23 plus SEL1L. Stability of CPY*-mCh was analysed as in (B). * $p < 0.05$, ** $p \leq 0.01$.

As expected from previous findings, only ~30% of CPY*-mCh remained after 3 h in pcDNA-transfected control cells and in cells expressing ER- α but strikingly, in the presence of ER- β 23, CPY*-mCh was stabilised to levels higher than 70% (Figure 26B). Thus, ER- β 23 inhibits degradation of ERAD substrate CPY*-mCh. The observed interactions of OS-9 and/or SEL1L with ER- β 23 might lead to depletion of these ERAD factors and in this way stabilise ERAD substrates such as CPY*, whose degradation, at least in yeast, is dependent on Yos9p and Hrd3p, the yeast homologues of OS-9 and SEL1L, respectively (Buschhorn et al., 2004; Bhamidipati et al., 2005; Gauss et al., 2006). However, it had so far not been demonstrated that CPY* degradation in mammalian cells is also dependent on these factors. To test whether degradation of CPY*-mCh by the mammalian ERAD system is dependent on OS-9 and SEL1L, knockdowns of these factors was performed using siRNAs.

Surprisingly, simultaneous knockdown of both OS-9 isoforms, OS-9.1 and OS-9.2, had no significant effect on CPY*-mCh stability (Figure 26C). This may be due to redundant activities of OS-9 and the ERAD substrate recognition lectin XTP3-B, at least for the degradation of soluble ERAD substrates (Bernasconi et al., 2010). In contrast, knockdown of SEL1L, which is thought to be required for mammalian ERAD (Sun et al., 2014), caused a significant stabilisation of CPY*-mCh with almost 90% of CPY*-mCh remaining after 3 h of CHX treatment (Figure 26C). Taken together, this strong dependence on SEL1L (Figure 26C), the large fraction of total SEL1L interacting with ER- β 23 non-productively (Figure 23B) and the low basal cellular abundance of SEL1L (Figure 24B), all indicate that the sequestration of SEL1L by ER- β 23 may be sufficient to block ERAD. Indeed, mild overexpression of SEL1L in combination with ER- β 23 and CPY*-mCh rescued ERAD of CPY*-mCh (Figure 26D). Thus, ER luminal accumulation of ER- β 23 inhibits ERAD by titration of SEL1L.

NRS^{G392E} interacts productively with SEL1L

Mutants of the neuroserpin (NRS) protein that form polymers within the ER cause the dementia familial encephalopathy with neuroserpin inclusion bodies (FENIB) (Davis et al., 2002; Miranda et al., 2004). The wild type NRS is a secretory protein but the disease mutant NRS^{G392E}, as well as the GFP-tagged version NRS^{G392E}-GFP, were reported to form polymers that are retained in the ER (Schipanski et al., 2014). We confirmed this specific retention of NRS^{G392E}-GFP and the formation of higher order oligomers in HEK293T cells (Figure 27A-B). Similar to ER- β 23, NRS^{G392E} was almost completely soluble in 1% Triton (Figure 27C).

Importantly, SEL1L interacted selectively with the NRS^{G392E} mutant but not with wild type NRS (Figure 27D). It has previously been reported that NRS^{G392E} is degraded via ERAD (Schipanski et al., 2014). Thus, in contrast to ER- β 23, NRS^{G392E} may interact with SEL1L in a productive manner without blocking ERAD of other substrates. Indeed, co-expression with NRS^{G392E} did not lead to stabilisation of CPY*-mCh (Figure 27E). The secretory wt NRS could not be detected by immunoblotting in this experiment, most likely due to its low intracellular levels, particularly under conditions of co-expression with another ER-targeted protein (Figure 27E). To test whether the productive interaction with SEL1L was dependent on glycosylation of NRS^{G392E}, a mutant that lacks two major N-glycosylation sites, NRS^{G392E Δ NN} was utilised. NRS^{G392E Δ NN} was also shown to form polymers in the ER and was previously reported to be more stable than the glycosylated protein and may thus block ERAD (Schipanski et al., 2014). Lack of glycosylation could be confirmed by an electrophoretic shift; however, NRS^{G392E Δ NN} did not affect stability of CPY*-mCh (Figure 27E). Taken together, mutant NRS proteins that accumulate in the ER in a similar manner as ER- β 23 do not cause a block of ERAD but interact with SEL1L in a productive manner leading to their clearance.

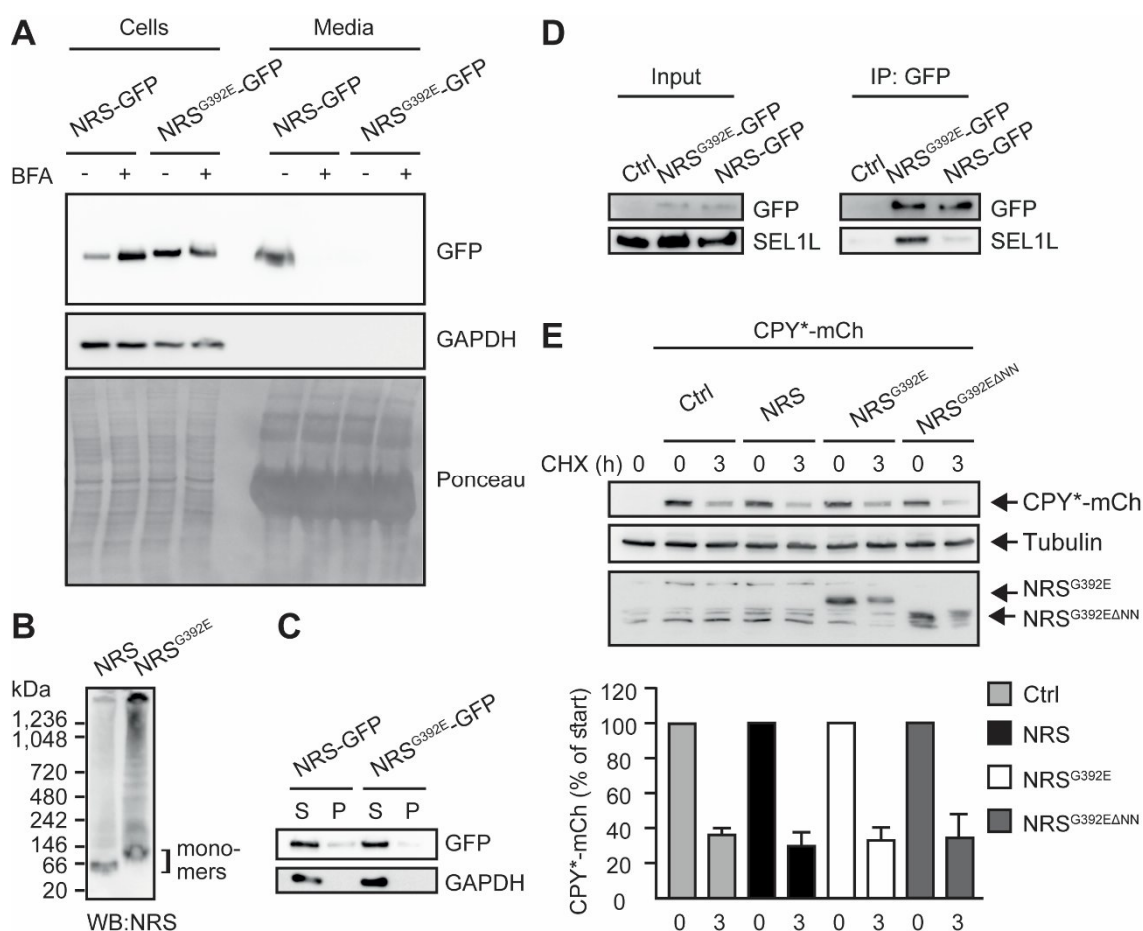


Figure 27. NRS^{G392E} interacts with SEL1L but does not inhibit ERAD of CPY*-mCh. (A) HEK293T cells expressing NRS-GFP or NRS^{G392E}-GFP were treated with 1 $\mu\text{g ml}^{-1}$ BFA for 18 h before collection of conditioned media and cells. Proteins from media were TCA-precipitated and equal fractions of protein from media and cell lysates were analysed by immunoblotting with anti-GFP antibody. GAPDH levels demonstrated the absence of cell leakage. Membrane staining was performed to provide a loading control. (B) Cell lysates from HEK293T cells transfected with NRS or NRS^{G392E} were separated on blue native PAGE and analysed by immunoblotting with an anti-NRS antibody. (C) Solubility of NRS-GFP and NRS^{G392E}-GFP expressed in HEK293T cells was analysed by fractionation of lysates and immunoblotting with anti-GFP antibody. T: total lysate, S: soluble fraction, P: pellet fraction. (D) NRS^{G392E}-GFP and NRS-GFP were immuno-precipitated from HEK293T cell lysates using anti-GFP antibody-coupled magnetic beads. The IP input lysates and eluates were analysed by immunoblotting using a different anti-GFP antibody. (E) HEK293T cells co-transfected with a combination of CPY*-mCh and either empty pcDNA (Ctrl), wt NRS (NRS), NRS^{G392E}, or NRS^{G392EΔNN} were treated with 0.5 mM CHX for 3 h where indicated. Levels of CPY*-mCh and NRS were analysed by immunoblotting with anti-Myc and anti-NRS antibodies, respectively. CPY*-mCh levels were quantified, normalised with the loading control tubulin and presented as % of untreated cells (0 h). Error bars represent SD from three independent experiments.

Part 2: Small molecule enhancers of proteostasis

Fluphenazine and gefitinib reduce HttQ97-induced UPS impairment

The FDA-approved drugs fluphenazine and gefitinib (Figure 28) were identified in a screen for small molecule modulators of the proteostasis network. Fluphenazine is an antipsychotic drug that is used to treat schizophrenia and other psychoses and gefitinib is an epidermal growth factor receptor (EGFR) inhibitor that is used in cancer treatment. We set out to better understand how these compounds modulate the PN.

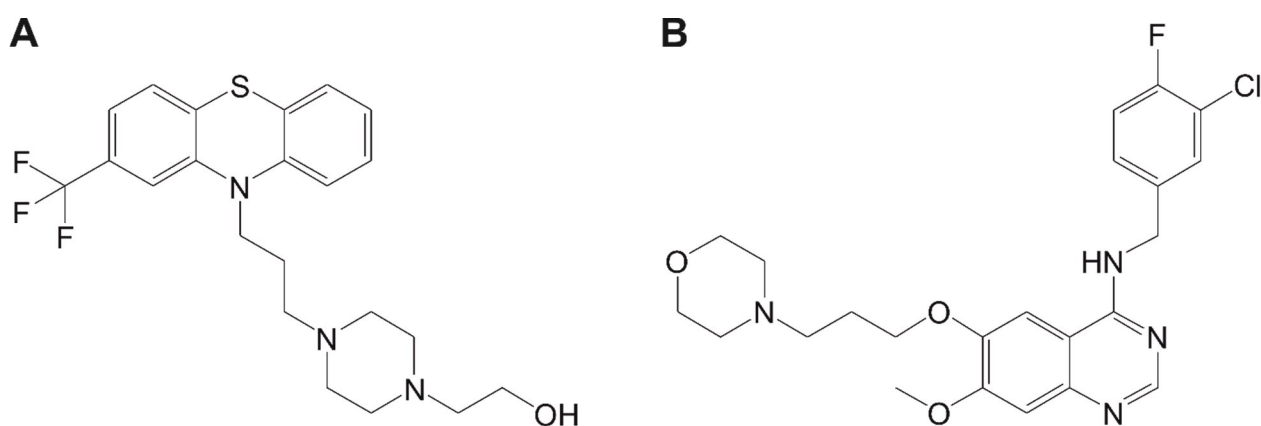


Figure 28. Chemical structures of the proteostasis modulators. (A) Structure of the antipsychotic drug fluphenazine. **(B)** Structure of the EGFR inhibitor gefitinib.

To better understand how these compounds may affect the PN, their potential to alleviate toxic effects of protein aggregates of the HD model protein HttQ97 (Q97) were tested. The HD model protein Q97 consists of the Htt exon 1 and includes a 97 residue polyQ stretch as well as a mCherry tag. As a control, a similar construct that contains only a 25 residue long glutamine stretch and is less aggregation-prone (Q25) was utilised. Accumulation of aggregation-prone polyQ repeat fragments leads to proteostasis imbalance and, as a result, to exhaustion of the UPS and an accumulation of UPS substrates (Hipp et al., 2012).

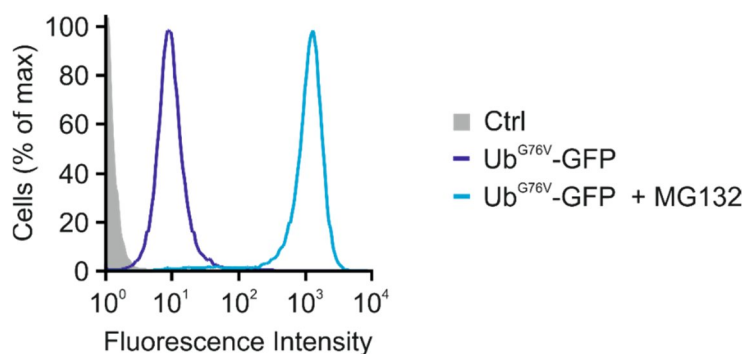


Figure 29. Proteasomal activity can be measured with the Ub^{G76V}-GFP reporter. HEK293 cells stably expressing Ub^{G76V}-GFP were treated with 10 μ M MG132 for 20 h or left untreated. Changes in GFP fluorescence intensity compared to wt cells (Ctrl) were then measured by FACS.

This toxic effect of Q97 can be measured using a reporter HEK293 cell line that stably expresses Ub^{G76V}-GFP. In healthy cells, the highly unstable Ub^{G76V}-GFP is rapidly degraded by the proteasome. Upon proteasomal inhibition, such as with the proteasomal inhibitor MG132, Ub^{G76V}-GFP accumulation can easily be measured by FACS (Figure 29).

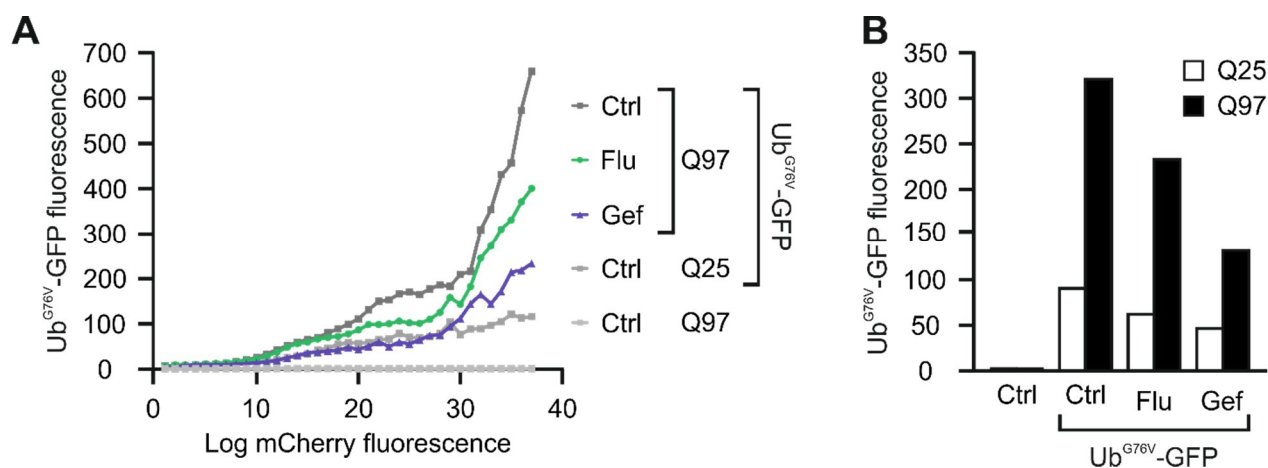


Figure 30. Fluphenazine and gefitinib reduce Q97-induced UPS impairment. Ub^{G76V}-GFP reporter or wt HEK293 (Ctrl) cells were transfected with HttQ25-mCherry (Q25) or HttQ97-mCherry (Q97) and 48 h later treated with 20 μ M fluphenazine (Flu), 20 μ M gefitinib (Gef) or DMSO (Ctrl) for 20 h. Accumulation of Ub^{G76V}-GFP in Htt-mCherry-expressing cells was analysed by FACS and (A) plotted against mCherry fluorescence. (B) After gating for transfected cells (mCherry expression), mean GFP fluorescence of 50,000 cells was quantified. Representative results of five independent experiments are shown.

After transfection with Q97, Ub^{G76V}-GFP accumulated in cells that highly expressed Q97 as measured by mCherry fluorescence and to a lesser extent in cells that expressed Q25 (Figure 30A), indicating strong inhibition of the UPS by Q97. This UPS inhibition by Q97 was alleviated by treatment with either fluphenazine (Flu) or gefitinib (Gef) (Figure 30A-B). Thus, these compounds clearly improve cellular proteostasis in the presence of protein aggregates.

Fluphenazine induces the heat shock response

One mechanism for how these compounds might improve proteostasis capacity could be via induction of cellular stress responses. To test whether either Flu or Gef may induce the HSR, a luciferase sensor consisting of firefly luciferase driven by the HSP70-promoter that is induced by HSF1 upon activation of the HSR was utilised. Strikingly, Flu significantly induced the HSR in a dose-dependent manner, whereas Gef did not (Figure 31A). This indicates that Flu may alleviate Q97-induced UPS impairment by inducing the HSR-driven upregulation of molecular chaperones, whereas Gef seems to alleviate the effect of Q97 by a different mechanism.

Droperidol also induced the HSR and improved proteostasis

Fluphenazine is a known dopamine antagonist and we thus asked whether other anti-dopaminergic compounds may have a similar effect on HSR induction and proteostasis improvement. To address this question, the effects of the anti-dopaminergic drug droperidol (Dro) (Figure 32A) were tested. Interestingly, Dro also mildly induced the HSR (Figure 31B) and alleviated UPS impairment in the presence of Q97 (Figure 31C) in a similar manner to Flu. This suggests that anti-dopaminergic drugs share common features that may induce the HSR leading to improved proteostasis under conditions of stress. Alternatively, the HSR may be induced via inhibition of dopamine receptor signalling. However, even though dopamine

receptors play important roles in the renal system (Hussain and Lokhandwala, 2003), it is unclear whether they are present in HEK293 cells.

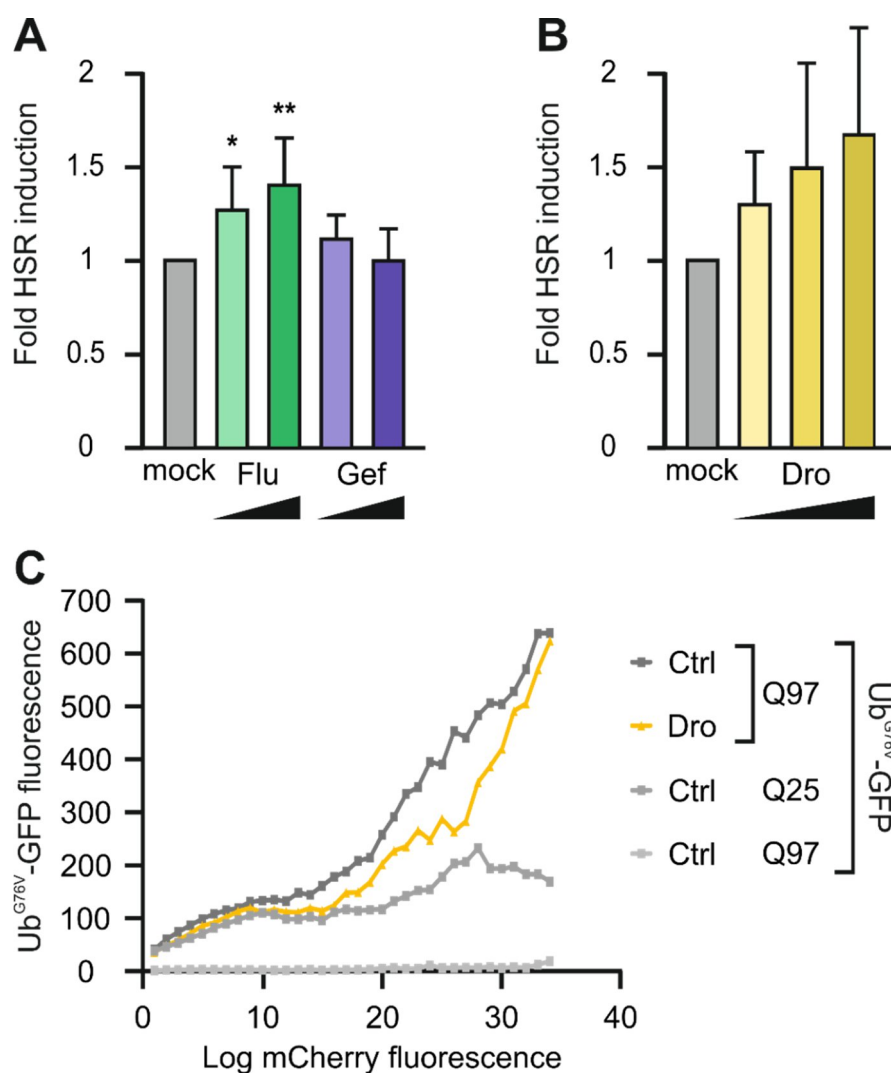


Figure 31. Fluphenazine and droperidol induce the heat shock response. HEK293 cells were transfected with a HSP70-promoter-luciferase construct and treated with (A) DMSO (Ctrl), or 5 or 20 μ M of either fluphenazine (Flu) or gefitinib (Gef) or (B) with 10, 20 or 50 μ M droperidol (Dro) for 20 h before measuring luciferase activity. (C) Ub^{G76V}-GFP reporter or wt HEK293 (Ctrl) cells were transfected with Q25 or Q97 and 48 h later treated with 50 μ M droperidol (Dro) or DMSO (Ctrl) 20 h. Accumulation of Ub^{G76V}-GFP in Htt-mCherry expressing cells was analysed by FACS and plotted against mCherry fluorescence. Representative results of three independent experiments are shown.

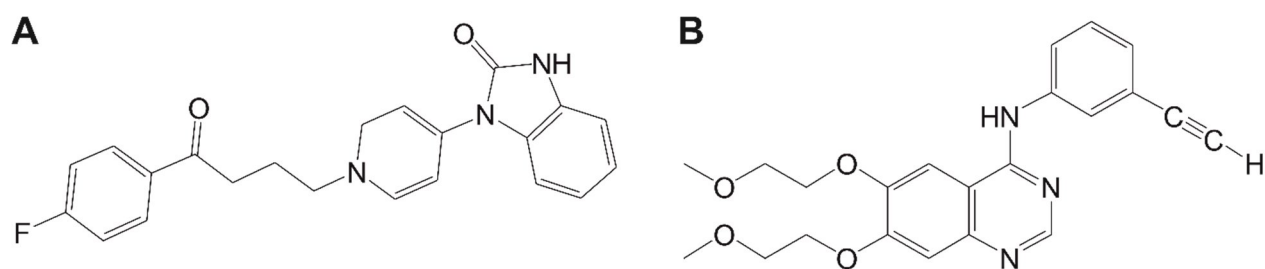


Figure 32. Chemical structures of droperidol and erlotinib. (A) Structure of the antipsychotic drug droperidol. (B) Structure of the EGFR inhibitor erlotinib.

Erlotinib also reduces HttQ97-induced UPS impairment

Gefitinib is an epidermal growth factor receptor (EGFR) tyrosine kinase inhibitor (TKI) (Maemondo et al., 2010). We were thus wondering whether other EGFR inhibitors may also improve proteostasis capacity in the presence of Q97. Interestingly, the EGFR inhibitor erlotinib (Erl) (Figure 32B) alleviated Q97-induced UPS impairment to the same extent as Gef (Figure 33). This may suggest that inhibition of EGFR, which we measured to be expressed in HEK293T cells at about 5 ppm as determined by quantitative proteomics, improves proteostasis by an unknown mechanism.

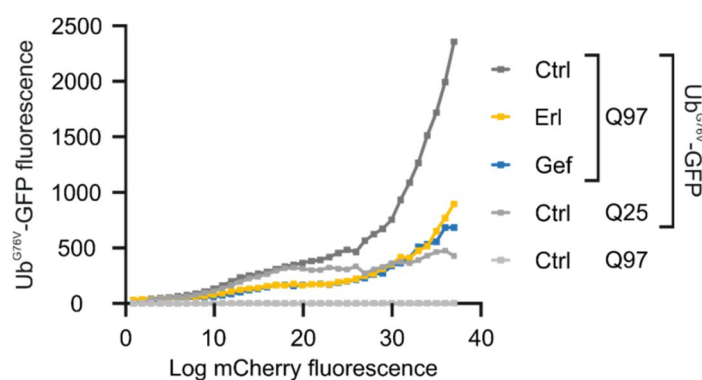


Figure 33. Erlotinib reduces Q97-induced UPS impairment. Ub^{G76V}-GFP reporter or wt HEK293 (Ctrl) cells were transfected with HttQ25-mCherry (Q25) or HttQ97-mCherry (Q97) and 48 h later treated with DMSO (Ctrl), 20 μ M Erl or Gef for 20 h. Accumulation of Ub^{G76V}-GFP in transfected cells was analysed by FACS and plotted against mCherry fluorescence.

Importantly, neither Flu, Dro, Gef nor Erl had an effect on the UPS in the absence of Q97 (Figure 34), thus confirming that the compounds alleviated an impairment that was caused by Q97 and did not directly affecting basal UPS activity.

Gefitinib reduces the size of Q97 aggregates

To understand in more detail how these compounds may alleviate the stress on the UPS caused by Q97, the effects on Q97 aggregate formation were tested. Neither of the compounds reduced the total number of cells with inclusions (Figure 35A-B). However, Gef treatment led to a mild but significant reduction in inclusion size (Figure 35C). This indicates that Gef may alleviate proteotoxic stress by increasing the capacity of cells to prevent Q97 aggregation.

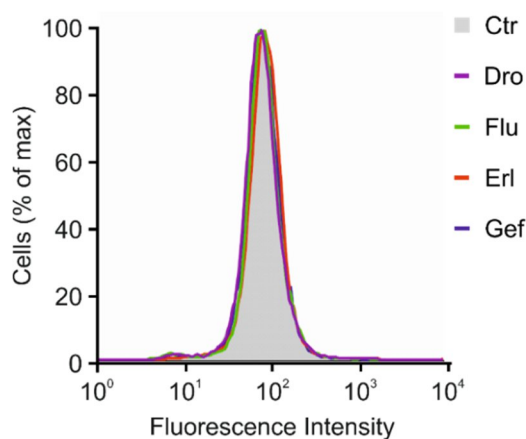


Figure 34. Treatments with Dro, Flu, Erl or Gef do not affect fluorescence properties of Ub^{G76V}-GFP in absence of Htt-mCh. Ub^{G76V}-GFP reporter HEK293 cells were treated with DMSO (Ctrl), 50 μ M Dro, 20 μ M Flu, 20 μ M Erl or 20 μ M Gef for 20 h. GFP fluorescence intensity was analysed by FACS.

In summary, the anti-dopaminergic drugs fluphenazine and droperidol and the EGFR inhibitors gefitinib and erlotinib had a remarkable effect on the PN, in particular in the presence of aggregating Q97 disease protein. The anti-dopaminergic drugs may improve cellular proteostasis by induction of the HSR.

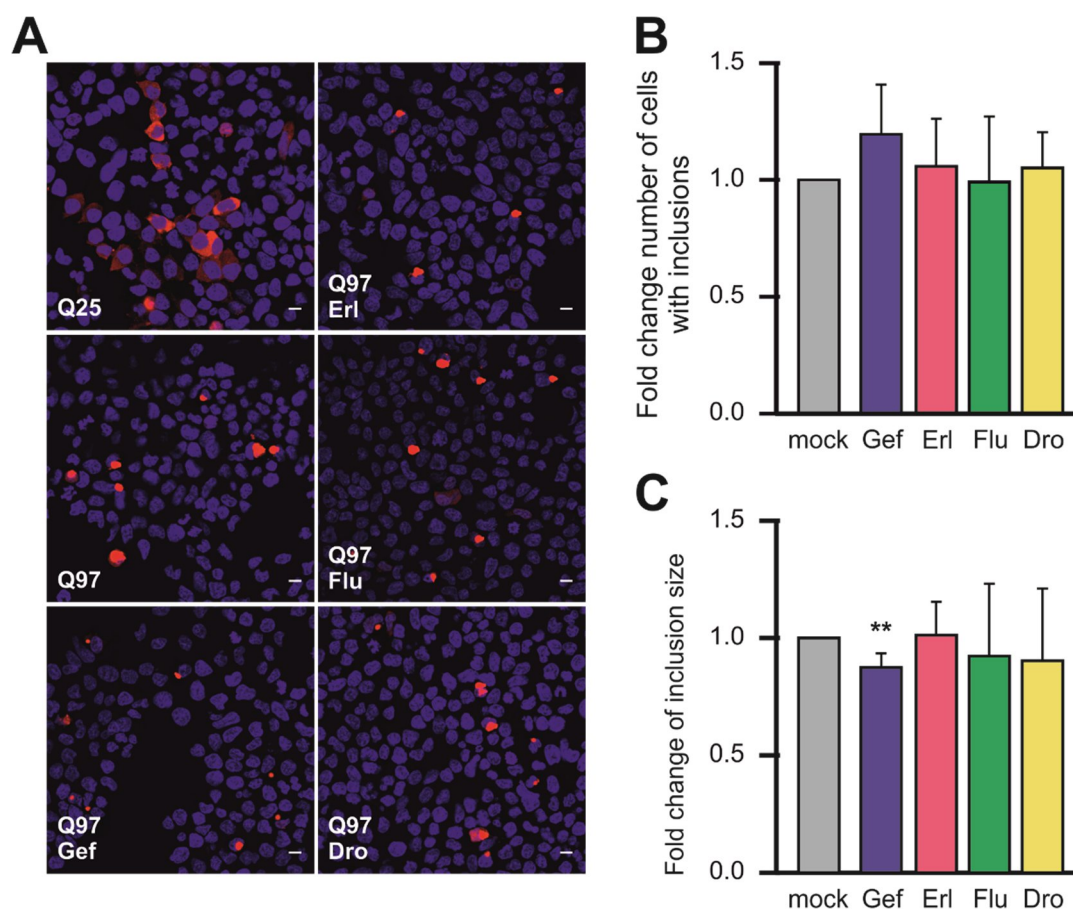


Figure 35. Gefitinib reduces the size of Q97 inclusions. (A) HEK293 cells were transfected with Q97 and 48 h later treated with 20 μ M Gef, 20 μ M Erl, 20 μ M Flu or 50 μ M Dro. Representative images of four independent experiments are shown. Scale bars represent 10 μ m. (B) Inclusions were analysed by fluorescence microscopy and quantified using the ImageJ software. The mean fold change of the number of cells with inclusions from four independent experiments counting more than 100 cells each was calculated. Error bars represent SD. (C) The mean fold change of inclusion size from four independent experiments counting more than 100 cells each was calculated. Error bars represent SD and p values are based on the Student's t-test (unpaired t-test). ** $p \leq 0.01$.

Discussion

The data presented in this thesis demonstrate that the capacity of the ERQC to maintain aggregation-prone β -proteins in a more soluble state and to limit their toxicity exceeds that of the cytosolic PN. In contrast to an α -helical protein, which passes through the secretory pathway, β -proteins are not secreted but are retained in the ER (Figure 36). Yet, unlike a classic terminally misfolded protein species, such as CPY*, ER- β 23 is not efficiently degraded but instead accumulates in the ER to high concentrations and interferes with the ERAD pathway (Figure 36). ER- β 23 appears to be targeted for ERAD as it interacts with ERAD factors, which are involved in substrate recognition and in linking substrates to the dislocon. However, ER- β 23 fails to be efficiently retro-translocated. This non-productive engagement of ERAD factors interferes with the degradation of ERAD substrates. Thus, retention of ER- β 23 comes at the price of a disturbance of the ER PN by ERAD inhibition and by adverse effects on the UPR.

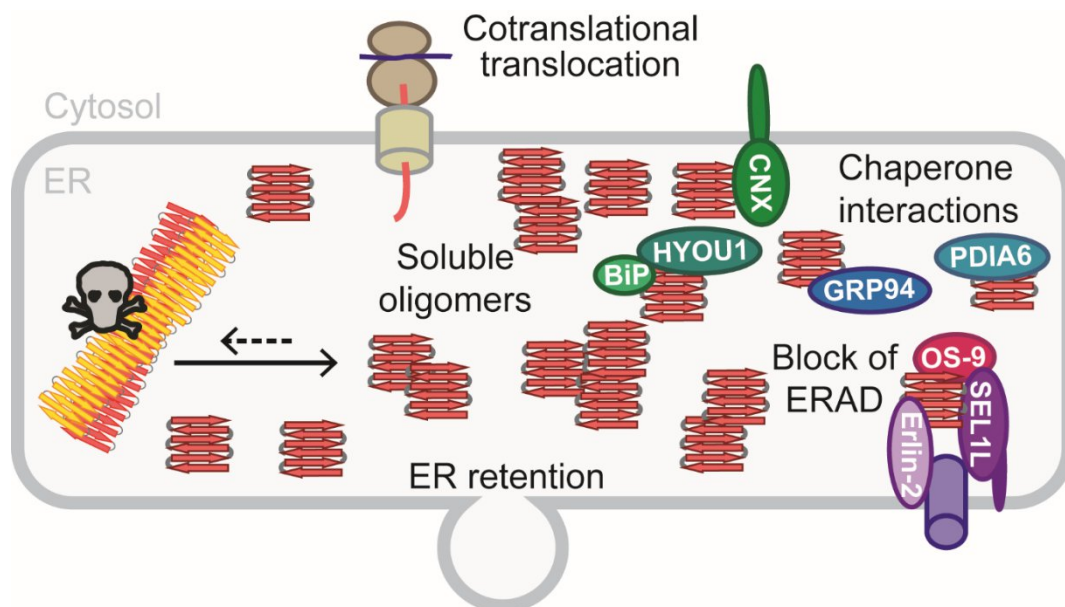


Figure 36. Fate of ER-targeted β -sheet proteins. ER- β 23 is co-translationally translocated into the ER, where it is retained, accumulates to high levels, forming a network of soluble polymers and interacts with molecular chaperones. ER- β 23 interacts with factors of the early ERAD pathway but is not efficiently degraded leading to a block in ERAD.

It is striking that ER-targeting leads to such a dramatic increase in solubility and decrease in cytotoxicity of all three β -protein constructs. The increased solubility of ER-targeted β -proteins is in line with previous reports that ER-targeting prevents the aggregation of proteins with an expanded polyQ repeat (Rousseau et al., 2004). Yet, the high solubility of ER- β -proteins is somewhat surprising when taking into account that the ER makes up only a fraction of the mammalian cell volume (e.g. around 15% in hepatocytes (Weibel et al., 1969; Alberts et al., 2014)). Accordingly, the local concentration of ER- β 23 in the ER must be at least 20-times higher than the concentration of nt- β 23, which mostly localises to the cytosol and nucleus (together around 80% volume of hepatocytes (Weibel et al., 1969)). In fact, quantitative proteomic measurements suggest that ER- β 23 concentrations exceed those of the ER chaperone BiP. Since BiP reaches low millimolar concentrations in the ER (up to 5 mM) (Weitzmann et al., 2007), ER- β 23 must be present in the ER lumen at concentrations at least in the low millimolar range. Notably, purified β 23 (as well as β 4 and β 17) has previously been shown to form insoluble amyloid-like aggregates already at low micromolar concentrations (Olzscha et al., 2011). This means that ER- β 23 accumulates in the ER at concentrations that are around 1,000 times higher than its *in vitro* solubility. Such an extremely concentrated state has been described as supersaturation (Ciryam et al., 2015). The ER thus has a remarkably high capacity to maintain aggregation-prone proteins in a soluble state. The insoluble aggregates formed by cytosolic β 23 have a diameter of 1-2 μ m (Olzscha et al., 2011). Since the ER lumen is only about 50 nm wide (Shibata et al., 2010; Westrate et al., 2015), space constraints may prevent ER- β 23 from forming such large insoluble aggregates and thus be responsible for this supersaturated state. However, at slightly higher concentrations, the mCherry-tagged construct ER- β 23-mCh did form insoluble aggregates suggesting that the ER can only counterbalance the high intrinsic aggregation propensity up to a certain threshold concentration.

Retention of β -proteins in the ER may protect cells from potentially toxic species that could aggregate in other cellular compartments or in the extracellular space such as in the case of transthyretin or light chain amyloidoses (Sorgjerd et al., 2006; Blancas-Mejia and Ramirez-Alvarado, 2013). A possible mechanism for ER- β 23 retention in the ER could be the interactions with ERQC factors that do not release ER- β 23 for secretion. However, the finding that these chaperones are less abundant than ER- β 23 argues against a mechanism of retention that involves a 1:1 interaction of ER- β 23 with chaperones. Notably, ER- β 23 did not seem to accumulate at ER exit sites (ERES) and was also not found to interact with factors involved in COPII vesicle assembly. ER- β 23 may be retained in the ER lumen for stochastic reasons because of its low mobility that is due to the formation of soluble but rather immobile oligomers and higher order polymers. ER- β 23 may form a network of polymers that is relatively dynamic and soluble, but not mobile enough to diffuse into secretory vesicles. This relatively immobile network may also prevent retro-translocation of ER- β 23 via ERAD. Even though ER- β 23 interacts with ERAD substrate recognition factors and adaptors, it does not seem to interact with cytosolic ERAD factors or the proteasome and is not efficiently degraded. This suggests that ER- β 23 is retained before passing the dislocon. This may be due to polymerisation that prevents passage or due to the lack of specific features such as glycosylation patterns or other post-translational modifications that may be required. However, the mutant NRS protein, NRS^{G392E Δ NN}, seemed to interact with SEL1L without blocking ERAD, suggesting that the lack of glycosylation sites may not be responsible for ERAD inhibition.

It was previously found that Hsc70 and HSP110, cytosolic members of the HSP70 and HSP110 chaperone families, respectively, interact with nt- β 23 (Olzscha et al., 2011). The finding that members of these chaperone families, namely BiP and HYOU1, also interact with ER- β 23, suggests that these chaperones specifically recognise β -sheet proteins. Interestingly,

diseases-causing mutants of A1AT are also specifically recognised by BiP and HYOU1 as well as by the ER-specific chaperone CNX that was also found to bind ER- β 23 (Schmidt and Perlmutter, 2005). In addition, GRP94 and OS-9 have been reported to be involved in ERAD of ER-retained disease-mutants of A1AT and NRS (Christianson et al., 2008; Schipanski et al., 2014). OS-9 has been suggested to be involved in the retention of misfolded proteins in the ER lumen in addition to the delivery of ERAD substrates (Bernasconi et al., 2008; Olzmann et al., 2013).

It should be noted that the lectin protein OS-9 has also been shown to recognise non-glycosylated substrates (Bernasconi et al., 2008; Christianson et al., 2008; Hosokawa et al., 2009; Olzmann et al., 2013). OS-9 may recognise ER- β 23 via a similar substrate binding mechanism that involves recognition of β -sheet conformations and is independent of glycosylation. Similarly, the chaperone CNX has also been suggested to recognise non-glycosylated substrates in addition to its glycan-binding activity (Rajagopalan et al., 1994; Basu and Srivastava, 1999; Saito et al., 1999; Spee et al., 1999; Danilczyk and Williams, 2001; Swanton et al., 2003). It is yet unclear, however, whether OS-9 and CNX bind ER- β 23 directly or indirectly as part of larger complexes. OS-9 was shown to be in a complex with SEL1L and Hrd1 as well as the ER chaperones BiP and GRP94 (Christianson et al., 2008; Olzmann et al., 2013). Similarly to ER- β 23, the non-glycosylated A1AT mutant NHK_{QQQ} is recognised by both isoforms of OS-9 (OS-9.1 and OS-9.2) but is yet not efficiently targeted for degradation (Bernasconi et al., 2008; Hosokawa et al., 2009). However, an ER-retained glycosylation mutant of NRS was efficiently degraded and did not affect the stability of CPY* suggesting that glycosylation of this substrate is not required for ERAD.

Disease mutants of the A1AT and NRS do not induce the UPR but instead activate the ordered protein response (Graham et al., 1990; Hidvegi et al., 2005; Davies et al., 2009). ER- β 23 did not induce the XBP1 promoter but it appeared to induce the ATF6 promoter at

basal levels. However, ER- β 23 seemed to have an overall inhibitory effect on UPR induction upon treatment with the ER stress inducer Tunicamycin (Tm). Interestingly, the cytosolic nt- β 23 was previously demonstrated to block induction of the cytosolic stress response, the HSR (Olzscha et al., 2011). It remains to be determined whether similar to the NRS and A1AT mutants, ER- β 23 induces NF κ B via the ordered protein response. Furthermore, it would be interesting to test whether NRS or A1AT mutants also have an inhibitory effect on UPR induction.

The inhibition of the ERAD pathway by ER- β 23 leads to an impairment of proteostasis and may indicate a general problem associated with ER retention of aggregation-prone proteins in pathological contexts. Primarily, retention is considered a protective mechanism and in the case of ER- β 23, prevention of secretion and retro-translocation may be relatively beneficial as it protects cells from acute toxicity of this protein in the cytosol and potentially other intra- and extracellular compartments (Olzscha et al., 2011; Woerner et al., 2016). For example, retro-translocation of the aggregation-prone prion protein leads to cytotoxicity (Ma and Lindquist, 2002) and ER-targeted versions of aggregation-prone polyQ proteins have been demonstrated to aggregate in the cytosol after retro-translocation (Rousseau et al., 2004). At the same time, due to its impairment of ERAD ER- β 23 is likely to cause toxicity in the ER if cells are challenged by additional ER stress.

The results presented in Part 2 of this thesis demonstrate the potential of improving proteostasis capacity with small molecules. The anti-dopaminergic drugs Flu and Dro, as well as the EGFR inhibitors Gef and Erl improved UPS activity in the presence of the Huntington's disease model protein Q97. Notably, Flu has also been identified in a high-throughput screen for compounds that modify A1AT Z mutant accumulation in *C. elegans* (Gosai et al., 2010). More recently Flu was also shown to reduce the toxicity of ATZ in *C. elegans* and in mammals (Li et al., 2014) and was also identified in a screen for potential

inducers of autophagy (Li et al., 2016). Importantly, the HSR and autophagy are closely linked and there is evidence that the HSR can induce autophagy (Dokladny et al., 2015). Interestingly, HSR induction and improved proteostasis in the presence of Q97 was also observed with a second anti-dopaminergic drug. It remains to be determined whether there is any link between the anti-dopaminergic action of these compounds and their effects on the proteostasis network. Conversely, dopaminergic signalling was reported to improve proteostasis (Joshi et al., 2016).

The finding that the EGFR inhibitors Gef and Erl improve proteostasis is interesting in the light of reports showing that EGF signalling plays an important role in longevity of nematodes (Rajalingam and Dikic, 2011). Conversely, EGF signalling was on the one hand reported to stimulate the UPS but on the other hand suggested to inhibit molecular chaperones. However, also in the case of Gef and Erl it is yet unclear whether their mechanism of proteostasis modulation is dependent on their inhibition on EGFR.

In summary, the work presented here demonstrates that the remarkable capacity of the mammalian ER to retain aggregation-prone β -sheet proteins in a soluble state leads to a disturbance of the ERAD pathway and demonstrates the potential of targeting the proteostasis network with small molecule modulators. These findings provide novel insights into the underlying cellular mechanisms of protein aggregation that broaden our understanding of the implications in various diseases.

Acknowledgements

I would like to thank Ulrich Hartl for giving me the opportunity to carry out this exciting work in his department, for his continuous support and his scientific inspiration.

Many thanks also to Mark Hipp for mentoring and supporting me throughout my studies.

I would like to thank Roman Körner for mass spectrometry analyses and Louise Funke and Albert Ries for assisting with experimental procedures. I would also like to thank all other former and current Hartl fighters, who have been great colleagues, collaborators, mentors and friends.

Thanks to Ralf Zenke and Martin Spitaler from the MPIB Imaging Facility for assistance with confocal microscopy and flow cytometry. I would like to thank the members of my TAC committee Konstanze Winklhofer, Julia von Blume and Rüdiger Klein for sharing reagents and for fruitful discussions. I would like to thank our collaborators, Jan Johansson, Jenny Presto and Lisa Dolfe, who generated the ER-targeted versions of the β -proteins.

I am grateful to the Boehringer Ingelheim Fonds for financial, educational and social support.

Finally, I would like to thank my family and friends, especially my parents, Lis and Hugo Vincenz, for all their love and support and my husband, Neysan Donnelly, for his love and encouragement in research and in life.

References

- Acosta-Alvear, D., Zhou, Y., Blais, A., Tsikitis, M., Lents, N.H., Arias, C., Lennon, C.J., Kluger, Y., and Dynlacht, B.D. (2007). XBP1 controls diverse cell type- and condition-specific transcriptional regulatory networks. *Molecular cell* *27*, 53-66.
- Adachi, Y., Yamamoto, K., Okada, T., Yoshida, H., Harada, A., and Mori, K. (2008). ATF6 is a transcription factor specializing in the regulation of quality control proteins in the endoplasmic reticulum. *Cell Struct Funct* *33*, 75-89.
- Aebi, M., Bernasconi, R., Clerc, S., and Molinari, M. (2010). N-glycan structures: recognition and processing in the ER. *Trends Biochem Sci* *35*, 74-82.
- Alberts, B., Johnson, A., Lewis, J., Morgan, D., Raff, M., Roberts, K., and Walter, P. (2014). *Molecular Biology of the Cell*, 6th edn (Garland Sciences).
- Ali, M.M., Bagratuni, T., Davenport, E.L., Nowak, P.R., Silva-Santisteban, M.C., Hardcastle, A., McAndrews, C., Rowlands, M.G., Morgan, G.J., Aherne, W., *et al.* (2011). Structure of the Ire1 autophosphorylation complex and implications for the unfolded protein response. *EMBO J* *30*, 894-905.
- Altier, C., Garcia-Caballero, A., Simms, B., You, H., Chen, L., Walcher, J., Tedford, H.W., Hermosilla, T., and Zamponi, G.W. (2011). The Cavbeta subunit prevents RFP2-mediated ubiquitination and proteasomal degradation of L-type channels. *Nat Neurosci* *14*, 173-180.
- Anfinsen, C.B. (1973). Principles that govern the folding of protein chains. *Science* *181*, 223-230.
- Anfinsen, C.B., Haber, E., Sela, M., and White, F.H., Jr. (1961). The kinetics of formation of native ribonuclease during oxidation of the reduced polypeptide chain. *Proceedings of the National Academy of Sciences of the United States of America* *47*, 1309-1314.
- Araki, K., and Nagata, K. (2011). Protein folding and quality control in the ER. *Cold Spring Harbor perspectives in biology* *3*, a007526.
- Balch, W.E., Morimoto, R.I., Dillin, A., and Kelly, J.W. (2008). Adapting proteostasis for disease intervention. *Science* *319*, 916-919.
- Bartlett, A.I., and Radford, S.E. (2009). An expanding arsenal of experimental methods yields an explosion of insights into protein folding mechanisms. *Nature structural & molecular biology* *16*, 582-588.
- Basu, S., and Srivastava, P.K. (1999). Calreticulin, a peptide-binding chaperone of the endoplasmic reticulum, elicits tumor- and peptide-specific immunity. *The Journal of experimental medicine* *189*, 797-802.
- Bauman, J.W., Liu, J., and Klaassen, C.D. (1993). Production of metallothionein and heat-shock proteins in response to metals. *Fundamental and applied toxicology : official journal of the Society of Toxicology* *21*, 15-22.
- Bays, N.W., Gardner, R.G., Seelig, L.P., Joazeiro, C.A., and Hampton, R.Y. (2001). Hrd1p/Der3p is a membrane-anchored ubiquitin ligase required for ER-associated degradation. *Nature cell biology* *3*, 24-29.

- Behnke, J., Feige, M.J., and Hendershot, L.M. (2015). BiP and its nucleotide exchange factors Grp170 and Sill: mechanisms of action and biological functions. *J Mol Biol* 427, 1589-1608.
- Behnke, J., and Hendershot, L.M. (2014). The large Hsp70 Grp170 binds to unfolded protein substrates in vivo with a regulation distinct from conventional Hsp70s. *The Journal of biological chemistry* 289, 2899-2907.
- Ben-Zvi, A., Miller, E.A., and Morimoto, R.I. (2009). Collapse of proteostasis represents an early molecular event in *Caenorhabditis elegans* aging. *Proc Natl Acad Sci U S A* 106, 14914-14919.
- Bernasconi, R., Galli, C., Calanca, V., Nakajima, T., and Molinari, M. (2010). Stringent requirement for HRD1, SEL1L, and OS-9/XTP3-B for disposal of ERAD-LS substrates. *The Journal of cell biology* 188, 223-235.
- Bernasconi, R., Pertel, T., Luban, J., and Molinari, M. (2008). A dual task for the Xbp1-responsive OS-9 variants in the mammalian endoplasmic reticulum: inhibiting secretion of misfolded protein conformers and enhancing their disposal. *The Journal of biological chemistry* 283, 16446-16454.
- Berndsen, C.E., and Wolberger, C. (2014). New insights into ubiquitin E3 ligase mechanism. *Nat Struct Mol Biol* 21, 301-307.
- Bernier, V., Lagace, M., Lonergan, M., Arthus, M.F., Bichet, D.G., and Bouvier, M. (2004). Functional rescue of the constitutively internalized V2 vasopressin receptor mutant R137H by the pharmacological chaperone action of SR49059. *Mol Endocrinol* 18, 2074-2084.
- Bertelsen, E.B., Chang, L., Gestwicki, J.E., and Zuiderweg, E.R. (2009). Solution conformation of wild-type *E. coli* Hsp70 (DnaK) chaperone complexed with ADP and substrate. *Proc Natl Acad Sci U S A* 106, 8471-8476.
- Bertolotti, A., Wang, X., Novoa, I., Jungreis, R., Schlessinger, K., Cho, J.H., West, A.B., and Ron, D. (2001). Increased sensitivity to dextran sodium sulfate colitis in IRE1beta-deficient mice. *J Clin Invest* 107, 585-593.
- Bhamidipati, A., Denic, V., Quan, E.M., and Weissman, J.S. (2005). Exploration of the topological requirements of ERAD identifies Yos9p as a lectin sensor of misfolded glycoproteins in the ER lumen. *Molecular cell* 19, 741-751.
- Bi, M., Naczki, C., Koritzinsky, M., Fels, D., Blais, J., Hu, N., Harding, H., Novoa, I., Varia, M., Raleigh, J., *et al.* (2005). ER stress-regulated translation increases tolerance to extreme hypoxia and promotes tumor growth. *EMBO J* 24, 3470-3481.
- Blais, J.D., Addison, C.L., Edge, R., Falls, T., Zhao, H., Wary, K., Koumenis, C., Harding, H.P., Ron, D., Holcik, M., *et al.* (2006). Perk-dependent translational regulation promotes tumor cell adaptation and angiogenesis in response to hypoxic stress. *Mol Cell Biol* 26, 9517-9532.
- Blancas-Mejia, L.M., and Ramirez-Alvarado, M. (2013). Systemic amyloidoses. *Annual review of biochemistry* 82, 745-774.

- Blom, D., Hirsch, C., Stern, P., Tortorella, D., and Ploegh, H.L. (2004). A glycosylated type I membrane protein becomes cytosolic when peptide: N-glycanase is compromised. *EMBO J* *23*, 650-658.
- Blond-Elguindi, S., Fourie, A.M., Sambrook, J.F., and Gething, M.J. (1993). Peptide-dependent stimulation of the ATPase activity of the molecular chaperone BiP is the result of conversion of oligomers to active monomers. *The Journal of biological chemistry* *268*, 12730-12735.
- Bouman, L., Schlierf, A., Lutz, A.K., Shan, J., Deinlein, A., Kast, J., Galehdar, Z., Palmisano, V., Patenge, N., Berg, D., *et al.* (2011). Parkin is transcriptionally regulated by ATF4: evidence for an interconnection between mitochondrial stress and ER stress. *Cell Death Differ* *18*, 769-782.
- Brockwell, D.J., and Radford, S.E. (2007). Intermediates: ubiquitous species on folding energy landscapes? *Current opinion in structural biology* *17*, 30-37.
- Brodsky, J.L., Werner, E.D., Dubas, M.E., Goeckeler, J.L., Kruse, K.B., and McCracken, A.A. (1999). The requirement for molecular chaperones during endoplasmic reticulum-associated protein degradation demonstrates that protein export and import are mechanistically distinct. *The Journal of biological chemistry* *274*, 3453-3460.
- Bryngelson, J.D., Onuchic, J.N., Socci, N.D., and Wolynes, P.G. (1995). Funnels, pathways, and the energy landscape of protein folding: a synthesis. *Proteins* *21*, 167-195.
- Buchberger, A., Bukau, B., and Sommer, T. (2010). Protein quality control in the cytosol and the endoplasmic reticulum: brothers in arms. *Molecular cell* *40*, 238-252.
- Burrows, J.A., Willis, L.K., and Perlmutter, D.H. (2000). Chemical chaperones mediate increased secretion of mutant alpha 1-antitrypsin (alpha 1-AT) Z: A potential pharmacological strategy for prevention of liver injury and emphysema in alpha 1-AT deficiency. *Proceedings of the National Academy of Sciences of the United States of America* *97*, 1796-1801.
- Buschhorn, B.A., Kostova, Z., Medicherla, B., and Wolf, D.H. (2004). A genome-wide screen identifies Yos9p as essential for ER-associated degradation of glycoproteins. *FEBS letters* *577*, 422-426.
- Calfon, M., Zeng, H., Urano, F., Till, J.H., Hubbard, S.R., Harding, H.P., Clark, S.G., and Ron, D. (2002). IRE1 couples endoplasmic reticulum load to secretory capacity by processing the XBP-1 mRNA. *Nature* *415*, 92-96.
- Carlino, A., Toledo, H., Skaleris, D., DeLisio, R., Weissbach, H., and Brot, N. (1992). Interactions of liver Grp78 and Escherichia coli recombinant Grp78 with ATP: multiple species and disaggregation. *Proc Natl Acad Sci U S A* *89*, 2081-2085.
- Carlsson, L., and Lazarides, E. (1983). ADP-ribosylation of the Mr 83,000 stress-inducible and glucose-regulated protein in avian and mammalian cells: modulation by heat shock and glucose starvation. *Proc Natl Acad Sci U S A* *80*, 4664-4668.
- Carvalho, P., Stanley, A.M., and Rapoport, T.A. (2010). Retrotranslocation of a misfolded luminal ER protein by the ubiquitin-ligase Hrd1p. *Cell* *143*, 579-591.

- Chen, X., Easton, D., Oh, H.J., Lee-Yoon, D.S., Liu, X., and Subjeck, J. (1996). The 170 kDa glucose regulated stress protein is a large HSP70-, HSP110-like protein of the endoplasmic reticulum. *FEBS Lett* 380, 68-72.
- Chen, X., Shen, J., and Prywes, R. (2002). The luminal domain of ATF6 senses endoplasmic reticulum (ER) stress and causes translocation of ATF6 from the ER to the Golgi. *The Journal of biological chemistry* 277, 13045-13052.
- Cheng, S.H., Gregory, R.J., Marshall, J., Paul, S., Souza, D.W., White, G.A., O'Riordan, C.R., and Smith, A.E. (1990). Defective intracellular transport and processing of CFTR is the molecular basis of most cystic fibrosis. *Cell* 63, 827-834.
- Chiti, F., and Dobson, C.M. (2006). Protein misfolding, functional amyloid, and human disease. *Annual review of biochemistry* 75, 333-366.
- Christianson, J.C., Olzmann, J.A., Shaler, T.A., Sowa, M.E., Bennett, E.J., Richter, C.M., Tyler, R.E., Greenblatt, E.J., Harper, J.W., and Kopito, R.R. (2012). Defining human ERAD networks through an integrative mapping strategy. *Nature cell biology* 14, 93-105.
- Christianson, J.C., Shaler, T.A., Tyler, R.E., and Kopito, R.R. (2008). OS-9 and GRP94 deliver mutant alpha1-antitrypsin to the Hrd1-SEL1L ubiquitin ligase complex for ERAD. *Nature cell biology* 10, 272-282.
- Chung, K.T., Shen, Y., and Hendershot, L.M. (2002). BAP, a Mammalian BiP-associated Protein, Is a Nucleotide Exchange Factor That Regulates the ATPase Activity of BiP. *Journal of Biological Chemistry* 277, 47557-47563.
- Ciryam, P., Kundra, R., Morimoto, R.I., Dobson, C.M., and Vendruscolo, M. (2015). Supersaturation is a major driving force for protein aggregation in neurodegenerative diseases. *Trends Pharmacol Sci* 36, 72-77.
- Ciryam, P., Tartaglia, G.G., Morimoto, R.I., Dobson, C.M., and Vendruscolo, M. (2013). Widespread aggregation and neurodegenerative diseases are associated with supersaturated proteins. *Cell reports* 5, 781-790.
- Clark, P.L. (2004). Protein folding in the cell: reshaping the folding funnel. *Trends in biochemical sciences* 29, 527-534.
- Cormier, J.H., Tamura, T., Sunryd, J.C., and Hebert, D.N. (2009). EDEM1 recognition and delivery of misfolded proteins to the SEL1L-containing ERAD complex. *Molecular cell* 34, 627-633.
- Cox, J.S., and Walter, P. (1996). A novel mechanism for regulating activity of a transcription factor that controls the unfolded protein response. *Cell* 87, 391-404.
- Craven, R.A., Tyson, J.R., and Stirling, C.J. (1997). A novel subfamily of Hsp70s in the endoplasmic reticulum. *Trends Cell Biol* 7, 277-282.
- Cullinan, S.B., Zhang, D., Hannink, M., Arvisais, E., Kaufman, R.J., and Diehl, J.A. (2003). Nrf2 is a direct PERK substrate and effector of PERK-dependent cell survival. *Mol Cell Biol* 23, 7198-7209.

- D'Alessio, C., Caramelo, J.J., and Parodi, A.J. (2010). UDP-Glc:glycoprotein glucosyltransferase-glucosidase II, the ying-yang of the ER quality control. *Seminars in Cell & Developmental Biology* 21, 491-499.
- Daggett, V., and Fersht, A.R. (2003). Is there a unifying mechanism for protein folding? *Trends in biochemical sciences* 28, 18-25.
- Danilczyk, U.G., and Williams, D.B. (2001). The lectin chaperone calnexin utilizes polypeptide-based interactions to associate with many of its substrates in vivo. *J Biol Chem* 276, 25532-25540.
- Davies, M.J., Miranda, E., Roussel, B.D., Kaufman, R.J., Marciniak, S.J., and Lomas, D.A. (2009). Neuroserpin polymers activate NF-kappaB by a calcium signaling pathway that is independent of the unfolded protein response. *The Journal of biological chemistry* 284, 18202-18209.
- Davis, R.L., Shrimpton, A.E., Carrell, R.W., Lomas, D.A., Gerhard, L., Baumann, B., Lawrence, D.A., Yepes, M., Kim, T.S., Ghetti, B., *et al.* (2002). Association between conformational mutations in neuroserpin and onset and severity of dementia. *Lancet* 359, 2242-2247.
- Deng, J., Lu, P.D., Zhang, Y., Scheuner, D., Kaufman, R.J., Sonenberg, N., Harding, H.P., and Ron, D. (2004). Translational repression mediates activation of nuclear factor kappa B by phosphorylated translation initiation factor 2. *Molecular and cellular biology* 24, 10161-10168.
- Denzel, M.S., Storm, N.J., Gutschmidt, A., Baddi, R., Hinze, Y., Jarosch, E., Sommer, T., Hoppe, T., and Antebi, A. (2014). Hexosamine pathway metabolites enhance protein quality control and prolong life. *Cell* 156, 1167-1178.
- Dierks, T., Volkmer, J., Schlenstedt, G., Jung, C., Sandholzer, U., Zachmann, K., Schlotterhose, P., Neifer, K., Schmidt, B., and Zimmermann, R. (1996). A microsomal ATP-binding protein involved in efficient protein transport into the mammalian endoplasmic reticulum. *EMBO J* 15, 6931-6942.
- Dill, K.A., Bromberg, S., Yue, K., Fiebig, K.M., Yee, D.P., Thomas, P.D., and Chan, H.S. (1995). Principles of protein folding--a perspective from simple exact models. *Protein science : a publication of the Protein Society* 4, 561-602.
- Dill, K.A., and Chan, H.S. (1997). From Levinthal to pathways to funnels. *Nature structural biology* 4, 10-19.
- Dobson, C.M., Šali, A., and Karplus, M. (1998). Protein folding: a perspective from theory and experiment. *Angewandte Chemie International Edition* 37, 868-893.
- Dokladny, K., Myers, O.B., and Moseley, P.L. (2015). Heat shock response and autophagy--cooperation and control. *Autophagy* 11, 200-213.
- Dolfe, L., Winblad, B., Johansson, J., and Presto, J. (2015). BRICHOS binds to a designed amyloid forming beta-protein and reduces proteasomal inhibition and aggresome formation. *The Biochemical journal*.

- Dong, M., Bridges, J.P., Apsley, K., Xu, Y., and Weaver, T.E. (2008). ERdj4 and ERdj5 are required for endoplasmic reticulum-associated protein degradation of misfolded surfactant protein C. *Mol Biol Cell* *19*, 2620-2630.
- Donnelly, N., Gorman, A.M., Gupta, S., and Samali, A. (2013). The eIF2alpha kinases: their structures and functions. *Cellular and molecular life sciences : CMLS* *70*, 3493-3511.
- Douglas, P.M., and Dillin, A. (2010). Protein homeostasis and aging in neurodegeneration. *The Journal of cell biology* *190*, 719-729.
- Dragovic, Z., Broadley, S.A., Shomura, Y., Bracher, A., and Hartl, F.U. (2006). Molecular chaperones of the Hsp110 family act as nucleotide exchange factors of Hsp70s. *The EMBO journal* *25*, 2519-2528.
- Easton, D.P., Kaneko, Y., and Subject, J.R. (2000). The hsp110 and Grp1 70 stress proteins: newly recognized relatives of the Hsp70s. *Cell Stress Chaperones* *5*, 276-290.
- Eichner, T., and Radford, S.E. (2011). A diversity of assembly mechanisms of a generic amyloid fold. *Molecular cell* *43*, 8-18.
- Eletto, D., Eletto, D., Dersh, D., Gidalevitz, T., and Argon, Y. (2014). Protein disulfide isomerase A6 controls the decay of IRE1alpha signaling via disulfide-dependent association. *Molecular cell* *53*, 562-576.
- Ellgaard, L., and Helenius, A. (2003). Quality control in the endoplasmic reticulum. *Nature Reviews Molecular Cell Biology* *4*, 181-191.
- Ellis, R.J. (2001). Macromolecular crowding: obvious but underappreciated. *Trends in biochemical sciences* *26*, 597-604.
- Etchells, S.A., and Hartl, F.U. (2004). The dynamic tunnel. *Nature structural & molecular biology* *11*, 391-392.
- Fang, S., Ferrone, M., Yang, C., Jensen, J.P., Tiwari, S., and Weissman, A.M. (2001). The tumor autocrine motility factor receptor, gp78, is a ubiquitin protein ligase implicated in degradation from the endoplasmic reticulum. *Proc Natl Acad Sci U S A* *98*, 14422-14427.
- Fiebigler, E., Story, C., Ploegh, H.L., and Tortorella, D. (2002). Visualization of the ER-to-cytosol dislocation reaction of a type I membrane protein. *EMBO J* *21*, 1041-1053.
- Finger, A., Knop, M., and Wolf, D.H. (1993). Analysis of two mutated vacuolar proteins reveals a degradation pathway in the endoplasmic reticulum or a related compartment of yeast. *European journal of biochemistry / FEBS* *218*, 565-574.
- Fitton, H.L., Pike, R.N., Carrell, R.W., and Chang, W.S. (1997). Mechanisms of antithrombin polymerisation and heparin activation probed by the insertion of synthetic reactive loop peptides. *Biol Chem* *378*, 1059-1063.
- Freiden, P.J., Gaut, J.R., and Hendershot, L.M. (1992). Interconversion of three differentially modified and assembled forms of BiP. *EMBO J* *11*, 63-70.
- Gaddam, D., Stevens, N., and Hollien, J. (2013). Comparison of mRNA localization and regulation during endoplasmic reticulum stress in *Drosophila* cells. *Mol Biol Cell* *24*, 14-20.

- Gale, M., Jr., Blakely, C.M., Hopkins, D.A., Melville, M.W., Wambach, M., Romano, P.R., and Katze, M.G. (1998). Regulation of interferon-induced protein kinase PKR: modulation of P58IPK inhibitory function by a novel protein, P52rIPK. *Mol Cell Biol* 18, 859-871.
- Gauss, R., Jarosch, E., Sommer, T., and Hirsch, C. (2006). A complex of Yos9p and the HRD ligase integrates endoplasmic reticulum quality control into the degradation machinery. *Nature cell biology* 8, 849-854.
- Gaut, J.R., and Hendershot, L.M. (1993). Mutations within the nucleotide binding site of immunoglobulin-binding protein inhibit ATPase activity and interfere with release of immunoglobulin heavy chain. *The Journal of biological chemistry* 268, 7248-7255.
- Geiger, R., Andrichke, D., Friebe, S., Herzog, F., Luisoni, S., Heger, T., and Helenius, A. (2011). BAP31 and BiP are essential for dislocation of SV40 from the endoplasmic reticulum to the cytosol. *Nature cell biology* 13, 1305-1314.
- Genereux, J.C., Qu, S., Zhou, M., Ryno, L.M., Wang, S., Shoulders, M.D., Kaufman, R.J., Lasmezas, C.I., Kelly, J.W., and Wiseman, R.L. (2015). Unfolded protein response-induced ERdj3 secretion links ER stress to extracellular proteostasis. *EMBO J* 34, 4-19.
- Ghaemmaghami, S., Huh, W.K., Bower, K., Howson, R.W., Belle, A., Dephoure, N., O'Shea, E.K., and Weissman, J.S. (2003). Global analysis of protein expression in yeast. *Nature* 425, 737-741.
- Gonzalez, D.S., Karaveg, K., Vandersall-Nairn, A.S., Lal, A., and Moremen, K.W. (1999). Identification, expression, and characterization of a cDNA encoding human endoplasmic reticulum mannosidase I, the enzyme that catalyzes the first mannose trimming step in mammalian Asn-linked oligosaccharide biosynthesis. *The Journal of biological chemistry* 274, 21375-21386.
- Gooptu, B., Hazes, B., Chang, W.S., Dafforn, T.R., Carrell, R.W., Read, R.J., and Lomas, D.A. (2000). Inactive conformation of the serpin alpha(1)-antichymotrypsin indicates two-stage insertion of the reactive loop: implications for inhibitory function and conformational disease. *Proc Natl Acad Sci U S A* 97, 67-72.
- Gosai, S.J., Kwak, J.H., Luke, C.J., Long, O.S., King, D.E., Kovatch, K.J., Johnston, P.A., Shun, T.Y., Lazo, J.S., Perlmutter, D.H., *et al.* (2010). Automated high-content live animal drug screening using *C. elegans* expressing the aggregation prone serpin alpha1-antitrypsin Z. *PloS one* 5, e15460.
- Graham, K.S., Le, A., and Sifers, R.N. (1990). Accumulation of the insoluble PiZ variant of human alpha 1-antitrypsin within the hepatic endoplasmic reticulum does not elevate the steady-state level of grp78/BiP. *The Journal of biological chemistry* 265, 20463-20468.
- Grinna, L.S., and Robbins, P.W. (1979). Glycoprotein biosynthesis. Rat liver microsomal glucosidases which process oligosaccharides. *Journal of Biological Chemistry* 254, 8814-8818.
- Guo, F., Lin, E.A., Liu, P., Lin, J., and Liu, C. (2010). XBP1U inhibits the XBP1S-mediated upregulation of the iNOS gene expression in mammalian ER stress response. *Cell Signal* 22, 1818-1828.

- Gupta, R.S., and Golding, G.B. (1993). Evolution of HSP70 gene and its implications regarding relationships between archaeobacteria, eubacteria, and eukaryotes. *J Mol Evol* 37, 573-582.
- Gupta, S., Deepti, A., Deegan, S., Lisbona, F., Hetz, C., and Samali, A. (2010). HSP72 protects cells from ER stress-induced apoptosis via enhancement of IRE1alpha-XBP1 signaling through a physical interaction. *PLoS Biol* 8, e1000410.
- Haass, C., and Selkoe, D.J. (2007). Soluble protein oligomers in neurodegeneration: lessons from the Alzheimer's amyloid beta-peptide. *Nat Rev Mol Cell Biol* 8, 101-112.
- Hammond, C., Braakman, I., and Helenius, A. (1994). Role of N-linked oligosaccharide recognition, glucose trimming, and calnexin in glycoprotein folding and quality control. *Proc Natl Acad Sci U S A* 91, 913-917.
- Han, D., Lerner, A.G., Vande Walle, L., Upton, J.P., Xu, W., Hagen, A., Backes, B.J., Oakes, S.A., and Papa, F.R. (2009). IRE1alpha kinase activation modes control alternate endoribonuclease outputs to determine divergent cell fates. *Cell* 138, 562-575.
- Harding, H.P., Novoa, I., Zhang, Y., Zeng, H., Wek, R., Schapira, M., and Ron, D. (2000). Regulated translation initiation controls stress-induced gene expression in mammalian cells. *Molecular cell* 6, 1099-1108.
- Harding, H.P., Zhang, Y., Zeng, H., Novoa, I., Lu, P.D., Calfon, M., Sadri, N., Yun, C., Popko, B., Paules, R., *et al.* (2003). An integrated stress response regulates amino acid metabolism and resistance to oxidative stress. *Molecular cell* 11, 619-633.
- Hartl, F.U. (1996). Molecular chaperones in cellular protein folding. *Nature* 381, 571-579.
- Hartl, F.U., and Hayer-Hartl, M. (2009). Converging concepts of protein folding in vitro and in vivo. *Nature structural & molecular biology* 16, 574-581.
- Hassink, G., Kikkert, M., van Voorden, S., Lee, S.J., Spaapen, R., van Laar, T., Coleman, C.S., Bartee, E., Fruh, K., Chau, V., *et al.* (2005). TEB4 is a C4HC3 RING finger-containing ubiquitin ligase of the endoplasmic reticulum. *Biochem J* 388, 647-655.
- Healy, S.J., Gorman, A.M., Mousavi-Shafaei, P., Gupta, S., and Samali, A. (2009). Targeting the endoplasmic reticulum-stress response as an anticancer strategy. *Eur J Pharmacol* 625, 234-246.
- Hebert, D.N., Foellmer, B., and Helenius, A. (1995). Glucose trimming and reglucosylation determine glycoprotein association with calnexin in the endoplasmic reticulum. *Cell* 81, 425-433.
- Hebert, D.N., Garman, S.C., and Molinari, M. (2005). The glycan code of the endoplasmic reticulum: asparagine-linked carbohydrates as protein maturation and quality-control tags. *Trends in Cell Biology* 15, 364-370.
- Hebert, D.N., and Molinari, M. (2007). In and out of the ER: protein folding, quality control, degradation, and related human diseases. *Physiol Rev* 87, 1377-1408.

- Hendershot, L., Wei, J., Gaut, J., Melnick, J., Aviel, S., and Argon, Y. (1996). Inhibition of immunoglobulin folding and secretion by dominant negative BiP ATPase mutants. *Proc Natl Acad Sci U S A* *93*, 5269-5274.
- Hendershot, L.M. (2004). The ER chaperone BiP is a master regulator of ER function. *Mount Sinai Journal of Medicine* *71*, 289-297.
- Hendershot, L.M., Wei, J.Y., Gaut, J.R., Lawson, B., Freiden, P.J., and Murti, K.G. (1995). In vivo expression of mammalian BiP ATPase mutants causes disruption of the endoplasmic reticulum. *Mol Biol Cell* *6*, 283-296.
- Henis-Korenblit, S., Zhang, P., Hansen, M., McCormick, M., Lee, S.J., Cary, M., and Kenyon, C. (2010). Insulin/IGF-1 signaling mutants reprogram ER stress response regulators to promote longevity. *Proceedings of the National Academy of Sciences of the United States of America* *107*, 9730-9735.
- Hidvegi, T., Ewing, M., Hale, P., Dippold, C., Beckett, C., Kemp, C., Maurice, N., Mukherjee, A., Goldbach, C., Watkins, S., *et al.* (2010). An autophagy-enhancing drug promotes degradation of mutant alpha1-antitrypsin Z and reduces hepatic fibrosis. *Science* *329*, 229-232.
- Hidvegi, T., Schmidt, B.Z., Hale, P., and Perlmutter, D.H. (2005). Accumulation of mutant alpha1-antitrypsin Z in the endoplasmic reticulum activates caspases-4 and -12, NFkappaB, and BAP31 but not the unfolded protein response. *The Journal of biological chemistry* *280*, 39002-39015.
- Hinnebusch, A.G. (2014). The scanning mechanism of eukaryotic translation initiation. *Annual review of biochemistry* *83*, 779-812.
- Hipp, M.S., Park, S.H., and Hartl, F.U. (2014). Proteostasis impairment in protein-misfolding and -aggregation diseases. *Trends in cell biology* *24*, 506-514.
- Hipp, M.S., Patel, C.N., Bersuker, K., Riley, B.E., Kaiser, S.E., Shaler, T.A., Brandeis, M., and Kopito, R.R. (2012). Indirect inhibition of 26S proteasome activity in a cellular model of Huntington's disease. *The Journal of cell biology* *196*, 573-587.
- Hollien, J., Lin, J.H., Li, H., Stevens, N., Walter, P., and Weissman, J.S. (2009). Regulated Ire1-dependent decay of messenger RNAs in mammalian cells. *The Journal of cell biology* *186*, 323-331.
- Hosokawa, N., Kamiya, Y., Kamiya, D., Kato, K., and Nagata, K. (2009). Human OS-9, a lectin required for glycoprotein endoplasmic reticulum-associated degradation, recognizes mannose-trimmed N-glycans. *The Journal of biological chemistry* *284*, 17061-17068.
- Hosokawa, N., Tremblay, L.O., Sleno, B., Kamiya, Y., Wada, I., Nagata, K., Kato, K., and Herscovics, A. (2010). EDEM1 accelerates the trimming of alpha1,2-linked mannose on the C branch of N-glycans. *Glycobiology* *20*, 567-575.
- Hosokawa, N., and Wada, I. (2016). Association of the SEL1L protein transmembrane domain with HRD1 ubiquitin ligase regulates ERAD-L. *FEBS J* *283*, 157-172.
- Hosokawa, N., Wada, I., Nagasawa, K., Moriyama, T., Okawa, K., and Nagata, K. (2008). Human XTP3-B forms an endoplasmic reticulum quality control scaffold with the HRD1-

- SEL1L ubiquitin ligase complex and BiP. *The Journal of biological chemistry* 283, 20914-20924.
- Hosokawa, N., You, Z., Tremblay, L.O., Nagata, K., and Herscovics, A. (2007). Stimulation of ERAD of misfolded null Hong Kong alpha1-antitrypsin by Golgi alpha1,2-mannosidases. *Biochem Biophys Res Commun* 362, 626-632.
- Howes, J., Shimizu, Y., Feige, M.J., and Hendershot, L.M. (2012). C-terminal mutations destabilize SIL1/BAP and can cause Marinesco-Sjogren syndrome. *The Journal of biological chemistry* 287, 8552-8560.
- Hussain, S.G., and Ramaiah, K.V. (2007). Reduced eIF2alpha phosphorylation and increased proapoptotic proteins in aging. *Biochem Biophys Res Commun* 355, 365-370.
- Hussain, T., and Lokhandwala, M.F. (2003). Renal dopamine receptors and hypertension. *Exp Biol Med (Maywood)* 228, 134-142.
- Hwang, C., Sinskey, A.J., and Lodish, H.F. (1992). Oxidized redox state of glutathione in the endoplasmic reticulum. *Science* 257, 1496-1502.
- Ihara, Y., Cohen-Doyle, M.F., Saito, Y., and Williams, D.B. (1999). Calnexin discriminates between protein conformational states and functions as a molecular chaperone in vitro. *Molecular cell* 4, 331-341.
- Iida, Y., Fujimori, T., Okawa, K., Nagata, K., Wada, I., and Hosokawa, N. (2011). SEL1L protein critically determines the stability of the HRD1-SEL1L endoplasmic reticulum-associated degradation (ERAD) complex to optimize the degradation kinetics of ERAD substrates. *The Journal of biological chemistry* 286, 16929-16939.
- Ikeda, J., Kaneda, S., Kuwabara, K., Ogawa, S., Kobayashi, T., Matsumoto, M., Yura, T., and Yanagi, H. (1997). Cloning and expression of cDNA encoding the human 150 kDa oxygen-regulated protein, ORP150. *Biochem Biophys Res Commun* 230, 94-99.
- Immormino, R.M., Dollins, D.E., Shaffer, P.L., Soldano, K.L., Walker, M.A., and Gewirth, D.T. (2004). Ligand-induced conformational shift in the N-terminal domain of GRP94, an Hsp90 chaperone. *The Journal of biological chemistry* 279, 46162-46171.
- Irving, J.A., Ekeowa, U.I., Belorgey, D., Haq, I., Gooptu, B., Miranda, E., Perez, J., Roussel, B.D., Ordonez, A., Dalton, L.E., *et al.* (2011). The serpinopathies studying serpin polymerization in vivo. *Methods Enzymol* 501, 421-466.
- Jahn, T.R., and Radford, S.E. (2005). The Yin and Yang of protein folding. *The FEBS journal* 272, 5962-5970.
- Jensen, T.J., Loo, M.A., Pind, S., Williams, D.B., Goldberg, A.L., and Riordan, J.R. (1995). Multiple proteolytic systems, including the proteasome, contribute to CFTR processing. *Cell* 83, 129-135.
- Johnson, A.E., and van Waes, M.A. (1999). The translocon: A dynamic gateway at the ER membrane. *Annual Review of Cell and Developmental Biology* 15, 799-842.
- Jonas, M.C., Pehar, M., and Puglielli, L. (2010). AT-1 is the ER membrane acetyl-CoA transporter and is essential for cell viability. *J Cell Sci* 123, 3378-3388.

- Joshi, K.K., Matlack, T.L., and Rongo, C. (2016). Dopamine signaling promotes the xenobiotic stress response and protein homeostasis. *The EMBO journal*.
- Kamimoto, T., Shoji, S., Hidvegi, T., Mizushima, N., Umebayashi, K., Perlmutter, D.H., and Yoshimori, T. (2006). Intracellular inclusions containing mutant alpha1-antitrypsin Z are propagated in the absence of autophagic activity. *The Journal of biological chemistry* *281*, 4467-4476.
- Kampinga, H.H., and Craig, E.A. (2010). The HSP70 chaperone machinery: J proteins as drivers of functional specificity. *Nat Rev Mol Cell Biol* *11*, 579-592.
- Kampinga, H.H., Hageman, J., Vos, M.J., Kubota, H., Tanguay, R.M., Bruford, E.A., Cheetham, M.E., Chen, B., and Hightower, L.E. (2009). Guidelines for the nomenclature of the human heat shock proteins. *Cell Stress Chaperones* *14*, 105-111.
- Kaneko, M., Niinuma, Y., and Nomura, Y. (2003). Activation signal of nuclear factor-kappa B in response to endoplasmic reticulum stress is transduced via IRE1 and tumor necrosis factor receptor-associated factor 2. *Biol Pharm Bull* *26*, 931-935.
- Kao, G., Nordenson, C., Still, M., Ronnlund, A., Tuck, S., and Naredi, P. (2007). ASNA-1 positively regulates insulin secretion in *C. elegans* and mammalian cells. *Cell* *128*, 577-587.
- Kassenbrock, C.K., and Kelly, R.B. (1989). Interaction of heavy chain binding protein (BiP/GRP78) with adenine nucleotides. *EMBO J* *8*, 1461-1467.
- Kawahara, T., Yanagi, H., Yura, T., and Mori, K. (1997). Endoplasmic reticulum stress-induced mRNA splicing permits synthesis of transcription factor Hac1p/Ern4p that activates the unfolded protein response. *Mol Biol Cell* *8*, 1845-1862.
- Kerem, E. (2005). Pharmacological induction of CFTR function in patients with cystic fibrosis: mutation-specific therapy. *Pediatr Pulmonol* *40*, 183-196.
- Kikkert, M., Doolman, R., Dai, M., Avner, R., Hassink, G., van Voorden, S., Thanedar, S., Roitelman, J., Chau, V., and Wiertz, E. (2004). Human HRD1 is an E3 ubiquitin ligase involved in degradation of proteins from the endoplasmic reticulum. *The Journal of biological chemistry* *279*, 3525-3534.
- Kim, Y.E., Hipp, M.S., Bracher, A., Hayer-Hartl, M., and Hartl, F.U. (2013). Molecular chaperone functions in protein folding and proteostasis. *Annual review of biochemistry* *82*, 323-355.
- Kingston, R.E., Schuetz, T.J., and Larin, Z. (1987). Heat-inducible human factor that binds to a human hsp70 promoter. *Molecular and cellular biology* *7*, 1530-1534.
- Klausner, R.D., Donaldson, J.G., and Lippincott-Schwartz, J. (1992). Brefeldin A: insights into the control of membrane traffic and organelle structure. *The Journal of cell biology* *116*, 1071-1080.
- Klemm, E.J., Spooner, E., and Ploegh, H.L. (2011). Dual role of ancient ubiquitous protein 1 (AUP1) in lipid droplet accumulation and endoplasmic reticulum (ER) protein quality control. *The Journal of biological chemistry* *286*, 37602-37614.

- Knowles, T.P., Vendruscolo, M., and Dobson, C.M. (2014). The amyloid state and its association with protein misfolding diseases. *Nat Rev Mol Cell Biol* *15*, 384-396.
- Ko, M.H., and Puglielli, L. (2009). Two endoplasmic reticulum (ER)/ER Golgi intermediate compartment-based lysine acetyltransferases post-translationally regulate BACE1 levels. *The Journal of biological chemistry* *284*, 2482-2492.
- Kowalski, J.M., Parekh, R.N., Mao, J., and Wittrup, K.D. (1998). Protein folding stability can determine the efficiency of escape from endoplasmic reticulum quality control. *The Journal of biological chemistry* *273*, 19453-19458.
- Lamb, H.K., Mee, C., Xu, W., Liu, L., Blond, S., Cooper, A., Charles, I.G., and Hawkins, A.R. (2006). The affinity of a major Ca²⁺ binding site on GRP78 is differentially enhanced by ADP and ATP. *The Journal of biological chemistry* *281*, 8796-8805.
- Laufen, T., Mayer, M.P., Beisel, C., Klostermeier, D., Mogk, A., Reinstein, J., and Bukau, B. (1999). Mechanism of regulation of hsp70 chaperones by DnaJ cochaperones. *Proc Natl Acad Sci U S A* *96*, 5452-5457.
- Lawless, M.W., Greene, C.M., Mulgrew, A., Taggart, C.C., O'Neill, S.J., and McElvaney, N.G. (2004). Activation of endoplasmic reticulum-specific stress responses associated with the conformational disease Z alpha 1-antitrypsin deficiency. *J Immunol* *172*, 5722-5726.
- Lederkremer, G.Z. (2009). Glycoprotein folding, quality control and ER-associated degradation. *Current opinion in structural biology* *19*, 515-523.
- Lee, A.H., Iwakoshi, N.N., and Glimcher, L.H. (2003). XBP-1 regulates a subset of endoplasmic reticulum resident chaperone genes in the unfolded protein response. *Mol Cell Biol* *23*, 7448-7459.
- Lee, A.H., Scapa, E.F., Cohen, D.E., and Glimcher, L.H. (2008a). Regulation of hepatic lipogenesis by the transcription factor XBP1. *Science* *320*, 1492-1496.
- Lee, K.P., Dey, M., Neculai, D., Cao, C., Dever, T.E., and Sicheri, F. (2008b). Structure of the dual enzyme Ire1 reveals the basis for catalysis and regulation in nonconventional RNA splicing. *Cell* *132*, 89-100.
- Lerner, M., Corcoran, M., Cepeda, D., Nielsen, M.L., Zubarev, R., Ponten, F., Uhlen, M., Hober, S., Grander, D., and Sangfelt, O. (2007). The RBCC gene RFP2 (Leu5) encodes a novel transmembrane E3 ubiquitin ligase involved in ERAD. *Mol Biol Cell* *18*, 1670-1682.
- Li, J., Pak, S.C., O'Reilly, L.P., Benson, J.A., Wang, Y., Hidvegi, T., Hale, P., Dippold, C., Ewing, M., Silverman, G.A., *et al.* (2014). Fluphenazine reduces proteotoxicity in *C. elegans* and mammalian models of alpha-1-antitrypsin deficiency. *PloS one* *9*, e87260.
- Li, Y., McGreal, S., Zhao, J., Huang, R., Zhou, Y., Zhong, H., Xia, M., and Ding, W.X. (2016). A cell-based quantitative high-throughput image screening identified novel autophagy modulators. *Pharmacol Res* *110*, 35-49.
- Lilley, B.N., Gilbert, J.M., Ploegh, H.L., and Benjamin, T.L. (2006). Murine polyomavirus requires the endoplasmic reticulum protein Derlin-2 to initiate infection. *J Virol* *80*, 8739-8744.

- Lilley, B.N., and Ploegh, H.L. (2004). A membrane protein required for dislocation of misfolded proteins from the ER. *Nature* 429, 834-840.
- Lin, H.Y., Masso-Welch, P., Di, Y.P., Cai, J.W., Shen, J.W., and Subject, J.R. (1993). The 170-kDa glucose-regulated stress protein is an endoplasmic reticulum protein that binds immunoglobulin. *Mol Biol Cell* 4, 1109-1119.
- Lisbona, F., Rojas-Rivera, D., Thielen, P., Zamorano, S., Todd, D., Martinon, F., Glavic, A., Kress, C., Lin, J.H., Walter, P., *et al.* (2009). BAX inhibitor-1 is a negative regulator of the ER stress sensor IRE1alpha. *Molecular cell* 33, 679-691.
- Liu, B., Yang, Y., Qiu, Z., Staron, M., Hong, F., Li, Y., Wu, S., Li, Y., Hao, B., Bona, R., *et al.* (2010). Folding of Toll-like receptors by the HSP90 paralogue gp96 requires a substrate-specific cochaperone. *Nature communications* 1, 79.
- Liu, K.Y., Shyu, Y.C., Barbaro, B.A., Lin, Y.T., Chern, Y., Thompson, L.M., James Shen, C.K., and Marsh, J.L. (2015). Disruption of the nuclear membrane by perinuclear inclusions of mutant huntingtin causes cell-cycle re-entry and striatal cell death in mouse and cell models of Huntington's disease. *Hum Mol Genet* 24, 1602-1616.
- Loureiro, J., Lilley, B.N., Spooner, E., Noriega, V., Tortorella, D., and Ploegh, H.L. (2006). Signal peptide peptidase is required for dislocation from the endoplasmic reticulum. *Nature* 441, 894-897.
- Lu, J., and Deutsch, C. (2005). Folding zones inside the ribosomal exit tunnel. *Nature structural & molecular biology* 12, 1123-1129.
- Lu, J.P., Wang, Y., Sliter, D.A., Pearce, M.M., and Wojcikiewicz, R.J. (2011). RNF170 protein, an endoplasmic reticulum membrane ubiquitin ligase, mediates inositol 1,4,5-trisphosphate receptor ubiquitination and degradation. *The Journal of biological chemistry* 286, 24426-24433.
- Lu, Y., Liang, F.X., and Wang, X. (2014). A synthetic biology approach identifies the mammalian UPR RNA ligase RtcB. *Molecular cell* 55, 758-770.
- Lyman, S.K., and Schekman, R. (1997). Binding of secretory precursor polypeptides to a translocon subcomplex is regulated by BiP. *Cell* 88, 85-96.
- Ma, J., and Lindquist, S. (2002). Conversion of PrP to a self-perpetuating PrPSc-like conformation in the cytosol. *Science* 298, 1785-1788.
- Maemondo, M., Inoue, A., Kobayashi, K., Sugawara, S., Oizumi, S., Isobe, H., Gemma, A., Harada, M., Yoshizawa, H., Kinoshita, I., *et al.* (2010). Gefitinib or chemotherapy for non-small-cell lung cancer with mutated EGFR. *N Engl J Med* 362, 2380-2388.
- Marcu, M.G., Doyle, M., Bertolotti, A., Ron, D., Hendershot, L., and Neckers, L. (2002). Heat shock protein 90 modulates the unfolded protein response by stabilizing IRE1alpha. *Mol Cell Biol* 22, 8506-8513.
- Martino, M.B., Jones, L., Brighton, B., Ehre, C., Abdulah, L., Davis, C.W., Ron, D., O'Neal, W.K., and Ribeiro, C.M. (2013). The ER stress transducer IRE1beta is required for airway epithelial mucin production. *Mucosal immunology* 6, 639-654.

- Maruyama, Y., Yamada, M., Takahashi, K., and Yamada, M. (2008). Ubiquitin ligase Kf-1 is involved in the endoplasmic reticulum-associated degradation pathway. *Biochem Biophys Res Commun* 374, 737-741.
- Marzec, M., Eletto, D., and Argon, Y. (2012). GRP94: An HSP90-like protein specialized for protein folding and quality control in the endoplasmic reticulum. *Biochim Biophys Acta* 1823, 774-787.
- Mattoo, R.U., Sharma, S.K., Priya, S., Finka, A., and Goloubinoff, P. (2013). Hsp110 is a bona fide chaperone using ATP to unfold stable misfolded polypeptides and reciprocally collaborate with Hsp70 to solubilize protein aggregates. *The Journal of biological chemistry* 288, 21399-21411.
- Mayer, M., Reinstein, J., and Buchner, J. (2003). Modulation of the ATPase cycle of BiP by peptides and proteins. *J Mol Biol* 330, 137-144.
- McDuffee, A.T., Senisterra, G., Huntley, S., Lepock, J.R., Sekhar, K.R., Meredith, M.J., Borrelli, M.J., Morrow, J.D., and Freeman, M.L. (1997). Proteins containing non-native disulfide bonds generated by oxidative stress can act as signals for the induction of the heat shock response. *Journal of cellular physiology* 171, 143-151.
- Meunier, L., Usherwood, Y.K., Chung, K.T., and Hendershot, L.M. (2002). A subset of chaperones and folding enzymes form multiprotein complexes in endoplasmic reticulum to bind nascent proteins. *Mol Biol Cell* 13, 4456-4469.
- Miranda, E., Romisch, K., and Lomas, D.A. (2004). Mutants of neuroserpin that cause dementia accumulate as polymers within the endoplasmic reticulum. *The Journal of biological chemistry* 279, 28283-28291.
- Molinari, M. (2007). N-glycan structure dictates extension of protein folding or onset of disposal. *Nat Chem Biol* 3, 313-320.
- Molinari, M., and Helenius, A. (2000). Chaperone selection during glycoprotein translocation into the endoplasmic reticulum. *Science* 288, 331-333.
- Mueller, B., Klemm, E.J., Spooner, E., Claessen, J.H., and Ploegh, H.L. (2008). SEL1L nucleates a protein complex required for dislocation of misfolded glycoproteins. *Proc Natl Acad Sci U S A* 105, 12325-12330.
- Mueller, B., Lilley, B.N., and Ploegh, H.L. (2006). SEL1L, the homologue of yeast Hrd3p, is involved in protein dislocation from the mammalian ER. *The Journal of cell biology* 175, 261-270.
- Muller, L., de Escauriaza, M.D., Lajoie, P., Theis, M., Jung, M., Muller, A., Burgard, C., Greiner, M., Snapp, E.L., Dudek, J., *et al.* (2010). Evolutionary gain of function for the ER membrane protein Sec62 from yeast to humans. *Mol Biol Cell* 21, 691-703.
- Nadav, E., Shmueli, A., Barr, H., Gonen, H., Ciechanover, A., and Reiss, Y. (2003). A novel mammalian endoplasmic reticulum ubiquitin ligase homologous to the yeast Hrd1. *Biochem Biophys Res Commun* 303, 91-97.

- Naidoo, N., Ferber, M., Master, M., Zhu, Y., and Pack, A.I. (2008). Aging impairs the unfolded protein response to sleep deprivation and leads to proapoptotic signaling. *J Neurosci* 28, 6539-6548.
- Netzer, W.J., and Hartl, F.U. (1997). Recombination of protein domains facilitated by co-translational folding in eukaryotes. *Nature* 388, 343-349.
- Neutzner, A., Neutzner, M., Benischke, A.S., Ryu, S.W., Frank, S., Youle, R.J., and Karbowski, M. (2011). A systematic search for endoplasmic reticulum (ER) membrane-associated RING finger proteins identifies Nixin/ZNRF4 as a regulator of calnexin stability and ER homeostasis. *The Journal of biological chemistry* 286, 8633-8643.
- Nichols, W.C., Seligsohn, U., Zivelin, A., Terry, V.H., Hertel, C.E., Wheatley, M.A., Moussalli, M.J., Hauri, H.P., Ciavarella, N., Kaufman, R.J., *et al.* (1998). Mutations in the ER-Golgi intermediate compartment protein ERGIC-53 cause combined deficiency of coagulation factors V and VIII. *Cell* 93, 61-70.
- Nishitoh, H., Matsuzawa, A., Tobiume, K., Saegusa, K., Takeda, K., Inoue, K., Hori, S., Kakizuka, A., and Ichijo, H. (2002). ASK1 is essential for endoplasmic reticulum stress-induced neuronal cell death triggered by expanded polyglutamine repeats. *Genes Dev* 16, 1345-1355.
- Nishitoh, H., Saitoh, M., Mochida, Y., Takeda, K., Nakano, H., Rothe, M., Miyazono, K., and Ichijo, H. (1998). ASK1 is essential for JNK/SAPK activation by TRAF2. *Molecular cell* 2, 389-395.
- Nuss, J.E., Choksi, K.B., DeFord, J.H., and Papaconstantinou, J. (2008). Decreased enzyme activities of chaperones PDI and BiP in aged mouse livers. *Biochem Biophys Res Commun* 365, 355-361.
- O'Brien, R.J., and Wong, P.C. (2011). Amyloid precursor protein processing and Alzheimer's disease. *Annual review of neuroscience* 34, 185-204.
- Oda, Y., Okada, T., Yoshida, H., Kaufman, R.J., Nagata, K., and Mori, K. (2006). Derlin-2 and Derlin-3 are regulated by the mammalian unfolded protein response and are required for ER-associated degradation. *The Journal of cell biology* 172, 383-393.
- Okuda-Shimizu, Y., and Hendershot, L.M. (2007). Characterization of an ERAD pathway for nonglycosylated BiP substrates, which require Herp. *Molecular cell* 28, 544-554.
- Okumiya, T., Ishii, S., Takenaka, T., Kase, R., Kamei, S., Sakuraba, H., and Suzuki, Y. (1995). Galactose stabilizes various missense mutants of alpha-galactosidase in Fabry disease. *Biochem Biophys Res Commun* 214, 1219-1224.
- Olivari, S., Cali, T., Salo, K.E., Paganetti, P., Ruddock, L.W., and Molinari, M. (2006). EDEM1 regulates ER-associated degradation by accelerating de-mannosylation of folding-defective polypeptides and by inhibiting their covalent aggregation. *Biochem Biophys Res Commun* 349, 1278-1284.
- Olzmann, J.A., and Kopito, R.R. (2011). Lipid droplet formation is dispensable for endoplasmic reticulum-associated degradation. *The Journal of biological chemistry* 286, 27872-27874.

- Olzmann, J.A., Kopito, R.R., and Christianson, J.C. (2013). The mammalian endoplasmic reticulum-associated degradation system. *Cold Spring Harbor perspectives in biology* 5.
- Olzscha, H., Schermann, S.M., Woerner, A.C., Pinkert, S., Hecht, M.H., Tartaglia, G.G., Vendruscolo, M., Hayer-Hartl, M., Hartl, F.U., and Vabulas, R.M. (2011). Amyloid-like aggregates sequester numerous metastable proteins with essential cellular functions. *Cell* 144, 67-78.
- Ong, S.E., and Mann, M. (2006). A practical recipe for stable isotope labeling by amino acids in cell culture (SILAC). *Nature protocols* 1, 2650-2660.
- Ordonez, A., Snapp, E.L., Tan, L., Miranda, E., Marciniak, S.J., and Lomas, D.A. (2013). Endoplasmic reticulum polymers impair luminal protein mobility and sensitize to cellular stress in alpha1-antitrypsin deficiency. *Hepatology* 57, 2049-2060.
- Otero, J.H., Lizak, B., and Hendershot, L.M. (2010). Life and death of a BiP substrate. *Semin Cell Dev Biol* 21, 472-478.
- Ou, W.J., Bergeron, J.J., Li, Y., Kang, C.Y., and Thomas, D.Y. (1995). Conformational changes induced in the endoplasmic reticulum luminal domain of calnexin by Mg-ATP and Ca²⁺. *J Biol Chem* 270, 18051-18059.
- Park, S.H., Kukushkin, Y., Gupta, R., Chen, T., Konagai, A., Hipp, M.S., Hayer-Hartl, M., and Hartl, F.U. (2013). PolyQ proteins interfere with nuclear degradation of cytosolic proteins by sequestering the Sis1p chaperone. *Cell* 154, 134-145.
- Parker, C.S., and Topol, J. (1984). A Drosophila RNA polymerase II transcription factor binds to the regulatory site of an hsp 70 gene. *Cell* 37, 273-283.
- Paton, A.W., Beddoe, T., Thorpe, C.M., Whisstock, J.C., Wilce, M.C., Rossjohn, J., Talbot, U.M., and Paton, J.C. (2006). AB5 subtilase cytotoxin inactivates the endoplasmic reticulum chaperone BiP. *Nature* 443, 548-552.
- Paz Gavilan, M., Vela, J., Castano, A., Ramos, B., del Rio, J.C., Vitorica, J., and Ruano, D. (2006). Cellular environment facilitates protein accumulation in aged rat hippocampus. *Neurobiol Aging* 27, 973-982.
- Pehar, M., and Puglielli, L. (2013). Lysine acetylation in the lumen of the ER: a novel and essential function under the control of the UPR. *Biochim Biophys Acta* 1833, 686-697.
- Perlmutter, D.H. (2011). Alpha-1-antitrypsin deficiency: importance of proteasomal and autophagic degradative pathways in disposal of liver disease-associated protein aggregates. *Annu Rev Med* 62, 333-345.
- Plempner, R.K., Bohmler, S., Bordallo, J., Sommer, T., and Wolf, D.H. (1997). Mutant analysis links the translocon and BiP to retrograde protein transport for ER degradation. *Nature* 388, 891-895.
- Ploegh, H.L. (2007). A lipid-based model for the creation of an escape hatch from the endoplasmic reticulum. *Nature* 448, 435-438.
- Plumb, R., Zhang, Z.R., Appathurai, S., and Mariappan, M. (2015). A functional link between the co-translational protein translocation pathway and the UPR. *eLife* 4.

- Powers, E.T., Morimoto, R.I., Dillin, A., Kelly, J.W., and Balch, W.E. (2009). Biological and chemical approaches to diseases of proteostasis deficiency. *Annual review of biochemistry* 78, 959-991.
- Puthalakath, H., O'Reilly, L.A., Gunn, P., Lee, L., Kelly, P.N., Huntington, N.D., Hughes, P.D., Michalak, E.M., McKimm-Breschkin, J., Motoyama, N., *et al.* (2007). ER stress triggers apoptosis by activating BH3-only protein Bim. *Cell* 129, 1337-1349.
- Rabek, J.P., Boylston, W.H., 3rd, and Papaconstantinou, J. (2003). Carbonylation of ER chaperone proteins in aged mouse liver. *Biochem Biophys Res Commun* 305, 566-572.
- Rajagopalan, S., Xu, Y., and Brenner, M.B. (1994). Retention of unassembled components of integral membrane proteins by calnexin. *Science* 263, 387-390.
- Rajalingam, K., and Dikic, I. (2011). Healthy ageing through regulated proteostasis. *The EMBO journal* 30, 2983-2985.
- Rampelt, H., Kirstein-Miles, J., Nillegoda, N.B., Chi, K., Scholz, S.R., Morimoto, R.I., and Bukau, B. (2012). Metazoan Hsp70 machines use Hsp110 to power protein disaggregation. *EMBO J* 31, 4221-4235.
- Richter, K., Haslbeck, M., and Buchner, J. (2010). The heat shock response: life on the verge of death. *Molecular cell* 40, 253-266.
- Ritossa, F. (1962). A new puffing pattern induced by temperature shock and DNP in *Drosophila*. *Experientia* 18, 571-573.
- Rodriguez-Lopez, J., Martinez-Centeno, C., Padmanaban, A., Guillen, G., Olivares, J.E., Stefano, G., Lledias, F., Ramos, F., Ghabrial, S.A., Brandizzi, F., *et al.* (2014). Nodulin 22, a novel small heat-shock protein of the endoplasmic reticulum, is linked to the unfolded protein response in common bean. *Mol Plant Microbe Interact* 27, 18-29.
- Rousseau, E., Dehay, B., Ben-Haiem, L., Trottier, Y., Morange, M., and Bertolotti, A. (2004). Targeting expression of expanded polyglutamine proteins to the endoplasmic reticulum or mitochondria prevents their aggregation. *Proceedings of the National Academy of Sciences of the United States of America* 101, 9648-9653.
- Ruiz-Canada, C., Kelleher, D.J., and Gilmore, R. (2009). Cotranslational and Posttranslational N-Glycosylation of Polypeptides by Distinct Mammalian OST Isoforms. *Cell* 136, 272-283.
- Rutkevich, L.A., and Williams, D.B. (2011). Participation of lectin chaperones and thiol oxidoreductases in protein folding within the endoplasmic reticulum. *Current Opinion in Cell Biology* 23, 157-166.
- Saeed, M., Suzuki, R., Watanabe, N., Masaki, T., Tomonaga, M., Muhammad, A., Kato, T., Matsuura, Y., Watanabe, H., Wakita, T., *et al.* (2011). Role of the endoplasmic reticulum-associated degradation (ERAD) pathway in degradation of hepatitis C virus envelope proteins and production of virus particles. *The Journal of biological chemistry* 286, 37264-37273.
- Saito, Y., Ihara, Y., Leach, M.R., Cohen-Doyle, M.F., and Williams, D.B. (1999). Calreticulin functions in vitro as a molecular chaperone for both glycosylated and non-glycosylated proteins. *EMBO J* 18, 6718-6729.

- Saraogi, I., and Shan, S.O. (2011). Molecular Mechanism of Co-translational Protein Targeting by the Signal Recognition Particle. *Traffic* 12, 535-542.
- Sato, T., Sako, Y., Sho, M., Momohara, M., Suico, M.A., Shuto, T., Nishitoh, H., Okiyoneda, T., Kokame, K., Kaneko, M., *et al.* (2012). STT3B-dependent posttranslational N-glycosylation as a surveillance system for secretory protein. *Molecular cell* 47, 99-110.
- Schipanski, A., Oberhauser, F., Neumann, M., Lange, S., Szalay, B., Krasemann, S., van Leeuwen, F.W., Galliciotti, G., and Glatzel, M. (2014). The lectin OS-9 delivers mutant neuroserpin to endoplasmic reticulum associated degradation in familial encephalopathy with neuroserpin inclusion bodies. *Neurobiology of aging* 35, 2394-2403.
- Schmidt, B.Z., and Perlmutter, D.H. (2005). Grp78, Grp94, and Grp170 interact with alpha1-antitrypsin mutants that are retained in the endoplasmic reticulum. *American journal of physiology Gastrointestinal and liver physiology* 289, G444-455.
- Schwanhausser, B., Busse, D., Li, N., Dittmar, G., Schuchhardt, J., Wolf, J., Chen, W., and Selbach, M. (2011). Global quantification of mammalian gene expression control. *Nature* 473, 337-342.
- Scott, D.C., and Schekman, R. (2008). Role of Sec61p in the ER-associated degradation of short-lived transmembrane proteins. *The Journal of cell biology* 181, 1095-1105.
- Sekijima, Y., Wiseman, R.L., Matteson, J., Hammarstrom, P., Miller, S.R., Sawkar, A.R., Balch, W.E., and Kelly, J.W. (2005). The biological and chemical basis for tissue-selective amyloid disease. *Cell* 121, 73-85.
- Senderek, J., Krieger, M., Stendel, C., Bergmann, C., Moser, M., Breitbach-Faller, N., Rudnik-Schoneborn, S., Blaschek, A., Wolf, N.I., Harting, I., *et al.* (2005). Mutations in SIL1 cause Marinesco-Sjogren syndrome, a cerebellar ataxia with cataract and myopathy. *Nat Genet* 37, 1312-1314.
- Shibata, Y., Shemesh, T., Prinz, W.A., Palazzo, A.F., Kozlov, M.M., and Rapoport, T.A. (2010). Mechanisms determining the morphology of the peripheral ER. *Cell* 143, 774-788.
- Shibatani, T., David, L.L., McCormack, A.L., Frueh, K., and Skach, W.R. (2005). Proteomic analysis of mammalian oligosaccharyltransferase reveals multiple subcomplexes that contain sec61, TRAP, and two potential new subunits. *Biochemistry* 44, 5982-5992.
- Shoulders, M.D., Ryno, L.M., Genereux, J.C., Moresco, J.J., Tu, P.G., Wu, C., Yates, J.R., 3rd, Su, A.I., Kelly, J.W., and Wiseman, R.L. (2013). Stress-independent activation of XBP1s and/or ATF6 reveals three functionally diverse ER proteostasis environments. *Cell reports* 3, 1279-1292.
- Sivasothy, P., Dafforn, T.R., Gettins, P.G., and Lomas, D.A. (2000). Pathogenic alpha 1-antitrypsin polymers are formed by reactive loop-beta-sheet A linkage. *The Journal of biological chemistry* 275, 33663-33668.
- Smith, M.J., and Koch, G.L. (1989). Multiple zones in the sequence of calreticulin (CRP55, calregulin, HACBP), a major calcium binding ER/SR protein. *EMBO J* 8, 3581-3586.
- Solda, T., Galli, C., Kaufman, R.J., and Molinari, M. (2007). Substrate-specific requirements for UGT1-dependent release from calnexin. *Molecular cell* 27, 238-249.

- Soldano, K.L., Jivan, A., Nicchitta, C.V., and Gewirth, D.T. (2003). Structure of the N-terminal domain of GRP94. Basis for ligand specificity and regulation. *The Journal of biological chemistry* 278, 48330-48338.
- Sonenberg, N., and Hinnebusch, A.G. (2009). Regulation of translation initiation in eukaryotes: mechanisms and biological targets. *Cell* 136, 731-745.
- Sorgjerd, K., Ghafouri, B., Jonsson, B.H., Kelly, J.W., Blond, S.Y., and Hammarstrom, P. (2006). Retention of misfolded mutant transthyretin by the chaperone BiP/GRP78 mitigates amyloidogenesis. *J Mol Biol* 356, 469-482.
- Soto, C. (2003). Unfolding the role of protein misfolding in neurodegenerative diseases. *Nat Rev Neurosci* 4, 49-60.
- Spee, P., Subjeck, J., and Neefjes, J. (1999). Identification of novel peptide binding proteins in the endoplasmic reticulum: ERp72, calnexin, and grp170. *Biochemistry* 38, 10559-10566.
- Stagg, H.R., Thomas, M., van den Boomen, D., Wiertz, E.J., Drabkin, H.A., Gemmill, R.M., and Lehner, P.J. (2009). The TRC8 E3 ligase ubiquitinates MHC class I molecules before dislocation from the ER. *The Journal of cell biology* 186, 685-692.
- Starck, S.R., Tsai, J.C., Chen, K., Shodiya, M., Wang, L., Yahiro, K., Martins-Green, M., Shastri, N., and Walter, P. (2016). Translation from the 5' untranslated region shapes the integrated stress response. *Science* 351, aad3867.
- Stefanovic, S., and Hegde, R.S. (2007). Identification of a targeting factor for posttranslational membrane protein insertion into the ER. *Cell* 128, 1147-1159.
- Sun, S., Shi, G., Han, X., Francisco, A.B., Ji, Y., Mendonca, N., Liu, X., Locasale, J.W., Simpson, K.W., Duhamel, G.E., *et al.* (2014). Sel1L is indispensable for mammalian endoplasmic reticulum-associated degradation, endoplasmic reticulum homeostasis, and survival. *Proceedings of the National Academy of Sciences of the United States of America* 111, E582-591.
- Swanton, E., High, S., and Woodman, P. (2003). Role of calnexin in the glycan-independent quality control of proteolipid protein. *EMBO J* 22, 2948-2958.
- Taipale, M., Jarosz, D.F., and Lindquist, S. (2010). HSP90 at the hub of protein homeostasis: emerging mechanistic insights. *Nat Rev Mol Cell Biol* 11, 515-528.
- Takatsuki, A., and Tamura, G. (1971). Effect of tunicamycin on the synthesis of macromolecules in cultures of chick embryo fibroblasts infected with Newcastle disease virus. *J Antibiot (Tokyo)* 24, 785-794.
- Taylor, R.C. (2016). Aging and the UPR(ER). *Brain Res.*
- Taylor, R.C., and Dillin, A. (2013). XBP-1 is a cell-nonautonomous regulator of stress resistance and longevity. *Cell* 153, 1435-1447.
- Teckman, J.H., and Perlmutter, D.H. (2000). Retention of mutant alpha(1)-antitrypsin Z in endoplasmic reticulum is associated with an autophagic response. *Am J Physiol Gastrointest Liver Physiol* 279, G961-974.

- Tirosh, B., Furman, M.H., Tortorella, D., and Ploegh, H.L. (2003). Protein unfolding is not a prerequisite for endoplasmic reticulum-to-cytosol dislocation. *The Journal of biological chemistry* *278*, 6664-6672.
- Tremblay, L.O., and Herscovics, A. (1999). Cloning and expression of a specific human alpha 1,2-mannosidase that trims Man₉GlcNAc₂ to Man₈GlcNAc₂ isomer B during N-glycan biosynthesis. *Glycobiology* *9*, 1073-1078.
- Tyanova, S., Mann, M., and Cox, J. (2014). MaxQuant for in-depth analysis of large SILAC datasets. *Methods in molecular biology* *1188*, 351-364.
- Ueno, T., Linder, S., Na, C.L., Rice, W.R., Johansson, J., and Weaver, T.E. (2004). Processing of pulmonary surfactant protein B by napsin and cathepsin H. *J Biol Chem* *279*, 16178-16184.
- Urano, F., Wang, X., Bertolotti, A., Zhang, Y., Chung, P., Harding, H.P., and Ron, D. (2000). Coupling of stress in the ER to activation of JNK protein kinases by transmembrane protein kinase IRE1. *Science* *287*, 664-666.
- Ushioda, R., Hoseki, J., Araki, K., Jansen, G., Thomas, D.Y., and Nagata, K. (2008). ERdj5 is required as a disulfide reductase for degradation of misfolded proteins in the ER. *Science* *321*, 569-572.
- Vabulas, R.M., Raychaudhuri, S., Hayer-Hartl, M., and Hartl, F.U. (2010). Protein folding in the cytoplasm and the heat shock response. *Cold Spring Harbor perspectives in biology* *2*, a004390.
- Van, P.N., Peter, F., and Soling, H.D. (1989). Four intracisternal calcium-binding glycoproteins from rat liver microsomes with high affinity for calcium. No indication for calsequestrin-like proteins in inositol 1,4,5-trisphosphate-sensitive calcium sequestering rat liver vesicles. *The Journal of biological chemistry* *264*, 17494-17501.
- Vincenz, L., and Hartl, F.U. (2014). Sugarcoating ER Stress. *Cell* *156*, 1125-1127.
- Vincenz, L., Jager, R., O'Dwyer, M., and Samali, A. (2013). Endoplasmic reticulum stress and the unfolded protein response: targeting the Achilles heel of multiple myeloma. *Mol Cancer Ther* *12*, 831-843.
- Vishnu, N., Jadoon Khan, M., Karsten, F., Groschner, L.N., Waldeck-Weiermair, M., Rost, R., Hallstrom, S., Imamura, H., Graier, W.F., and Malli, R. (2014). ATP increases within the lumen of the endoplasmic reticulum upon intracellular Ca²⁺ release. *Mol Biol Cell* *25*, 368-379.
- Wada, I., Rindress, D., Cameron, P.H., Ou, W.J., Doherty, J.J., 2nd, Louvard, D., Bell, A.W., Dignard, D., Thomas, D.Y., and Bergeron, J.J. (1991). SSR alpha and associated calnexin are major calcium binding proteins of the endoplasmic reticulum membrane. *J Biol Chem* *266*, 19599-19610.
- Walter, P., and Ron, D. (2011). The unfolded protein response: from stress pathway to homeostatic regulation. *Science* *334*, 1081-1086.

- Walther, D.M., Kasturi, P., Zheng, M., Pinkert, S., Vecchi, G., Ciryam, P., Morimoto, R.I., Dobson, C.M., Vendruscolo, M., Mann, M., *et al.* (2015). Widespread Proteome Remodeling and Aggregation in Aging *C. elegans*. *Cell* *161*, 919-932.
- Wang, X.Z., Harding, H.P., Zhang, Y., Jolicoeur, E.M., Kuroda, M., and Ron, D. (1998). Cloning of mammalian Ire1 reveals diversity in the ER stress responses. *EMBO J* *17*, 5708-5717.
- Wang, Z.V., Deng, Y., Gao, N., Pedrozo, Z., Li, D.L., Morales, C.R., Criollo, A., Luo, X., Tan, W., Jiang, N., *et al.* (2014). Spliced X-box binding protein 1 couples the unfolded protein response to hexosamine biosynthetic pathway. *Cell* *156*, 1179-1192.
- Ward, C.L., Omura, S., and Kopito, R.R. (1995). Degradation of CFTR by the ubiquitin-proteasome pathway. *Cell* *83*, 121-127.
- Ware, F.E., Vassilakos, A., Peterson, P.A., Jackson, M.R., Lehrman, M.A., and Williams, D.B. (1995). The molecular chaperone calnexin binds Glc1Man9GlcNAc2 oligosaccharide as an initial step in recognizing unfolded glycoproteins. *J Biol Chem* *270*, 4697-4704.
- Wei, Y., Liu, T., Sazinsky, S.L., Moffet, D.A., Pelczer, I., and Hecht, M.H. (2003). Stably folded de novo proteins from a designed combinatorial library. *Protein science : a publication of the Protein Society* *12*, 92-102.
- Weibel, E.R., Staubli, W., Gnagi, H.R., and Hess, F.A. (1969). Correlated morphometric and biochemical studies on the liver cell. I. Morphometric model, stereologic methods, and normal morphometric data for rat liver. *The Journal of cell biology* *42*, 68-91.
- Weitzmann, A., Baldes, C., Dudek, J., and Zimmermann, R. (2007). The heat shock protein 70 molecular chaperone network in the pancreatic endoplasmic reticulum - a quantitative approach. *FEBS J* *274*, 5175-5187.
- Welch, W.J., Garrels, J.I., Thomas, G.P., Lin, J.J., and Feramisco, J.R. (1983). Biochemical characterization of the mammalian stress proteins and identification of two stress proteins as glucose- and Ca²⁺-ionophore-regulated proteins. *The Journal of biological chemistry* *258*, 7102-7111.
- West, M.W., Wang, W., Patterson, J., Mancias, J.D., Beasley, J.R., and Hecht, M.H. (1999). De novo amyloid proteins from designed combinatorial libraries. *Proceedings of the National Academy of Sciences of the United States of America* *96*, 11211-11216.
- Westrate, L.M., Lee, J.E., Prinz, W.A., and Voeltz, G.K. (2015). Form follows function: the importance of endoplasmic reticulum shape. *Annual review of biochemistry* *84*, 791-811.
- Williams, D.B. (2006). Beyond lectins: the calnexin/calreticulin chaperone system of the endoplasmic reticulum. *Journal of Cell Science* *119*, 615-623.
- Wisniewski, J.R., Zielinska, D.F., and Mann, M. (2011). Comparison of ultrafiltration units for proteomic and N-glycoproteomic analysis by the filter-aided sample preparation method. *Anal Biochem* *410*, 307-309.
- Woerner, A.C., Frottin, F., Hornburg, D., Feng, L.R., Meissner, F., Patra, M., Tatzelt, J., Mann, M., Winklhofer, K.F., Hartl, F.U., *et al.* (2016). Cytoplasmic protein aggregates interfere with nucleocytoplasmic transport of protein and RNA. *Science* *351*, 173-176.

- Xiong, H., Buckwalter, B.L., Shieh, H.M., and Hecht, M.H. (1995). Periodicity of polar and nonpolar amino acids is the major determinant of secondary structure in self-assembling oligomeric peptides. *Proceedings of the National Academy of Sciences of the United States of America* *92*, 6349-6353.
- Yamamoto, K., Yoshida, H., Kokame, K., Kaufman, R.J., and Mori, K. (2004). Differential contributions of ATF6 and XBP1 to the activation of endoplasmic reticulum stress-responsive cis-acting elements ERSE, UPRE and ERSE-II. *J Biochem* *136*, 343-350.
- Yamasaki, M., Li, W., Johnson, D.J., and Huntington, J.A. (2008). Crystal structure of a stable dimer reveals the molecular basis of serpin polymerization. *Nature* *455*, 1255-1258.
- Yan, W., Frank, C.L., Korth, M.J., Sopher, B.L., Novoa, I., Ron, D., and Katze, M.G. (2002). Control of PERK eIF2alpha kinase activity by the endoplasmic reticulum stress-induced molecular chaperone P58IPK. *Proc Natl Acad Sci U S A* *99*, 15920-15925.
- Yanagitani, K., Imagawa, Y., Iwawaki, T., Hosoda, A., Saito, M., Kimata, Y., and Kohno, K. (2009). Cotranslational targeting of XBP1 protein to the membrane promotes cytoplasmic splicing of its own mRNA. *Molecular cell* *34*, 191-200.
- Ye, Y., Shibata, Y., Yun, C., Ron, D., and Rapoport, T.A. (2004). A membrane protein complex mediates retro-translocation from the ER lumen into the cytosol. *Nature* *429*, 841-847.
- Yoshida, H., Matsui, T., Hosokawa, N., Kaufman, R.J., Nagata, K., and Mori, K. (2003). A time-dependent phase shift in the mammalian unfolded protein response. *Dev Cell* *4*, 265-271.
- Yoshida, H., Matsui, T., Yamamoto, A., Okada, T., and Mori, K. (2001). XBP1 mRNA is induced by ATF6 and spliced by IRE1 in response to ER stress to produce a highly active transcription factor. *Cell* *107*, 881-891.
- Yoshida, H., Oku, M., Suzuki, M., and Mori, K. (2006). pXBP1(U) encoded in XBP1 pre-mRNA negatively regulates unfolded protein response activator pXBP1(S) in mammalian ER stress response. *The Journal of cell biology* *172*, 565-575.
- Younger, J.M., Chen, L., Ren, H.Y., Rosser, M.F., Turnbull, E.L., Fan, C.Y., Patterson, C., and Cyr, D.M. (2006). Sequential quality-control checkpoints triage misfolded cystic fibrosis transmembrane conductance regulator. *Cell* *126*, 571-582.
- Zhang, K., Donnelly, C.J., Haeusler, A.R., Grima, J.C., Machamer, J.B., Steinwald, P., Daley, E.L., Miller, S.J., Cunningham, K.M., Vidensky, S., *et al.* (2015). The C9orf72 repeat expansion disrupts nucleocytoplasmic transport. *Nature* *525*, 56-61.
- Zhao, Y., Tian, T., Huang, T., Nakajima, S., Saito, Y., Takahashi, S., Yao, J., Paton, A.W., Paton, J.C., and Kitamura, M. (2011). Subtilase cytotoxin activates MAP kinases through PERK and IRE1 branches of the unfolded protein response. *Toxicol Sci* *120*, 79-86.
- Zuehlke, A., and Johnson, J.L. (2010). Hsp90 and co-chaperones twist the functions of diverse client proteins. *Biopolymers* *93*, 211-217.

Appendices

Supplementary table 1. Amino acid sequences of model proteins.

Name	Amino acid sequence
CPY*-mCh	MGWSCILFLVATATGAHSQVQLQVDLEMISLQRPGLGDKDVLQAAAEKFGLDLDDLHLLKELDSNVLDAWAQIE HLYPNQVMSLETSTKPKFPEAIKTKKDWDFVVKNDAIENYQLRVNKKIDPKILGIDPNVTQYTGYLDEVEDKHF FFWTFESRNDPAKDPVILWLNGGPGCSSLTGLFFELGPSSIGPDLKPIGNPYSWNSNATVIFLDQPVNVGFSYS GSSGVSNTVAAGKDVYNFLELFFDQFPEYVNGQDFHIARESYAGHYIPVFASEILSHKDRNFNLTSVLIGNLT DPLTQYNYEPMACGEGGEPVLPSEECSAMEDSLERCLGLIESCYDSQSVWSCVPATICYCNAQLAPYQRT GRNVYDIRKDCEGGNLCYPTLQDIDDYLNQDYVKEAVGAEVDHYESCNFDIRNRFAGDWMKPYHTAVTDLL NQDLPILVYAGDKDFICNWLGNKAWTDVLPWKYDEEFASQKVRNWTASITDEVAGEVKSYPKHTYLRVFNNGH MVPFDV/PENALSMVNEWHGGFSLEF M VSKGEEDNMAIIKEFMRFKVMHEGSVNGHEFEIEGEGEGRPYEGT QTAKLKVTKGGPLPFAWDILSPQFMYGSKAYVKHPADIPDYLLKLSFPEGFKWERVMNFEDGGVVTVDSSLDQ DGEFIYKVKLRGTFNPSDGPVMQKKTMGWEASSERMYPEDGALKGEIKQRLKLDGGGHYDAEVKTTYKAKKP VQLPGAYNVNIKLDITSHNEDYTIVEQYERAEGRHSTGGMDELYKAAAEQKLISEEDLNGAAAEKDEL
ER-α	MAESHLLQWLLLLPTLCGPGTACEQKLISEEDLGMYGKLNLDLLEDLQEVLNKLNHKNWHGGKDNLHDVDNHLQ NVIEDIHDFMQGGGSGGKLQEMMKEFQQVLDLNNHLQGGKHTVHHIEQNIKEIFHHLEELVHR
ER-β4	MAESHLLQWLLLLPTLCGPGTACEQKLISEEDLGMQISM DYQLEIEGNDNKVELQLNDSGGEVKLQIRGPGGR VHFNVHSSGSNLEVNFNNDGGEVQFHMH
ER-β17	MAESHLLQWLLLLPTLCGPGTACEQKLISEEDLGMQISM DYQLEIEGNDNKVELQLNDSGGEVKLQIRGPGGR VHFNVHSSGSNLEVNFNNDGGEVQFHMH
ER-β23	MAESHLLQWLLLLPTLCGPGTACEQKLISEEDLGMQISM DYQLEIEGNDNKVELQLNDSGGEVKLQIRGPGGR VHFNVHSSGSNLEVNFNNDGGEVQFHMH
ER-α-mCh	MAESHLLQWLLLLPTLCGPGTACEQKLISEEDLGMYGKLNLDLLEDLQEVLNKLNHKNWHGGKDNLHDVDNHLQ NVIEDIHDFMQGGGSGGKLQEMMKEFQQVLDLNNHLQGGKHTVHHIEQNIKEIFHHLEELVHRGPVAT M VSK GEEDNMAIIKEFMRFKVMHEGSVNGHEFEIEGEGEGRPYEGTQTAKLKVTKGGPLPFAWDILSPQFMYGSKAY VKHPADIPDYLLKLSFPEGFKWERVMNFEDGGVVTVDSSLDQDGEFIYKVKLRGTFNPSDGPVMQKKTMGWE ASSERMYPEDGALKGEIKQRLKLDGGGHYDAEVKTTYKAKKPVQLPGAYNVNIKLDITSHNEDYTIVEQYERA EGRHSTGGMDELYK
ER-β23-mCh	MAESHLLQWLLLLPTLCGPGTAA ⁺ EQKLISEEDLGMQISM DYQLEIEGNDNKVELQLNDSGGEVKLQIRGPGGR VHFNVHSSGSNLEVNFNNDGGEVQFHMH M VSKGEEDNMAIIKEFMRFKVMHEGSVNGHEFEIEGEGEGR PYEGTQTAKLKVTKGGPLPFAWDILSPQFMYGSKAYVKHPADIPDYLLKLSFPEGFKWERVMNFEDGGVVTVD SSLDQDGEFIYKVKLRGTFNPSDGPVMQKKTMGWEASSERMYPEDGALKGEIKQRLKLDGGGHYDAEVKTTY KAKKPVQLPGAYNVNIKLDITSHNEDYTIVEQYERAEGRHSTGGMDELYK
ER-mCh	MAESHLLQWLLLLPTLCGPGTAAEQKLISEEDL M VSKGEEDNMAIIKEFMRFKVMHEGSVNGHEFEIEGEGE GRPYEGTQTAKLKVTKGGPLPFAWDILSPQFMYGSKAYVKHPADIPDYLLKLSFPEGFKWERVMNFEDGGVVT VDSSLDQDGEFIYKVKLRGTFNPSDGPVMQKKTMGWEASSERMYPEDGALKGEIKQRLKLDGGGHYDAEVKTT YKAKKPVQLPGAYNVNIKLDITSHNEDYTIVEQYERAEGRHSTGGMDELYK KDEL
Q25	MATLEKLMKAFESLKSFQQPPPPPPPPPPQ LPPPPPPPPPPGPAVAEPLHRPGSL VSKGEEDNMAIIKEFMRFKVMHEGSVNGHEFEIEGEGEGRPYEGTQT AKLKVTKGGPLPFAWDILSPQFMYGSKAYVKHPADIPDYLLKLSFPEGFKWERVMNFEDGGVVTVDSSLDQD GEFIYKVKLRGTFNPSDGPVMQKKTMGWEASSERMYPEDGALKGEIKQRLKLDGGGHYDAEVKTTYKAKKP VQLPGAYNVNIKLDITSHNEDYTIVEQYERAEGRHSTGGMDELYKLRPPSGRSRIDS RGPFEQKLISEEDLN MHTGH HHHHH
Q97	MATLEKLMKAFESLKSFQQPPPPPPPPPPQ LPPPPPPPPPPGPAVAEPLHRPGSL VSKGEEDNMAIIKEFMRFKVMHEGSVNGHEFEIEGEGE GRPYEGTQTAKLKVTKGGPLPFAWDILSPQFMYGSKAYVKHPADIPDYLLKLSFPEGFKWERVMNFEDGGVVT VDSSLDQDGEFIYKVKLRGTFNPSDGPVMQKKTMGWEASSERMYPEDGALKGEIKQRLKLDGGGHYDAEVK TTYKAKKPVQLPGAYNVNIKLDITSHNEDYTIVEQYERAEGRHSTGGMDELYKLRPPSGRSRIDS RGPFEQKL ISEEDLN MHTGH HHHHHHH
nt-α	MCEQKLISEEDLGMYGKLNLDLLEDLQEVLNKLNHKNWHGGKDNLHDVDNHLQNVIEDIHDFMQGGGSGGKLQ EMMKEFQQVLDLNNHLQGGKHTVHHIEQNIKEIFHHLEELVHR
nt-β4	MCEQKLISEEDLGMQISM DYQLEIEGNDNKVELQLNDSGGEVKLQIRGPGGRVHFNVHSSGSNLEVNFNNDGG EVQFHMH
nt-β17	MCEQKLISEEDLGMQISM DYQLEIEGNDNKVELQLNDSGGEVKLQIRGPGGRVHFNVHSSGSNLEVNFNNDGG EVQFHMH
nt-β23	MCEQKLISEEDLGMQISM DYQLEIEGNDNKVELQLNDSGGEVKLQIRGPGGRVHFNVHSSGSNLEVNFNNDGG EVQFHMH

Supplementary table 1. Amino acid sequences of model proteins. Signal sequences are presented in green, Myc-tags in purple, the sequence of α -helical proteins in blue, β -proteins in red and mCherry is highlighted in red.

Supplementary table 2. List of ER- β 23 interactors

Description	Protein IDs	Gene names	MW (kDa)	Ratio H/L (IP)	Ratio H/L (Total)	GO cellular compartments
Protein sel-1 homolog 1 (SEL1L)	Q9UBV2	SEL1L	88.75	8.72	1.07	ER membrane
Lysosome-associated membrane glycoprotein 1	P11279	LAMP1	44.88	7.86	0.95	late endosome; lysosome
Protein OS-9	Q13438	OS9	75.56	6.57	*	ER lumen; ER ubiquitin ligase complex
PR domain zinc finger protein 10	Q9NQV6	PRDM10	137.42	6.51	*	nucleus
Zinc finger protein 335	Q9H4Z2	ZNF335	129.61	6.50	0.97	nucleus
Nuclear pore membrane glycoprotein 210	Q8TEM1	NUP210	205.11	6.10	0.78	ER;nuclear envelope;nuclear pore complex;ER membrane
HCLS1-associated protein X-1	O00165	HAX1	32.42	5.76	0.91	actin cytoskeleton;cytoplasmic vesicle;ER;mitochondria;sarcoplasmic reticulum
Tetratricopeptide repeat protein 13	Q8NBP0	TTC13	96.81	5.46	*	
Tetratricopeptide repeat protein 17	Q96AE7	TTC17	129.56	5.02	*	
52 kDa repressor of the inhibitor of the protein kinase	O43422	PRKRIR	87.70	4.90	0.97	nucleus
Ensconsin	Q14244	MAP7	84.05	4.75	0.76	cytoplasm;microtubule; perinuclear region of cytoplasm
Nodal modulator 1/2/3	Q5JPE7	NOMO1/2/3	139.44	4.71	0.89	ER membrane
Zinc finger protein 579	Q8NAF0	ZNF579	60.51	4.40	0.70	nucleus
Hypoxia up-regulated protein 1 (HYOU1/GRP170)	Q9Y4L1	HYOU1	111.33	4.32	1.16	ER lumen
MAP7 domain-containing protein 1	Q3KQU3	MAP7D1	92.82	4.27	0.76	cytoplasm;cytoskeletal part;spindle

Transcription intermediary factor 1-beta	Q13263	TRIM28	88.55	4.26	0.96	euchromatin;heterochromatin;nuclear chromatin
Hypermethylated in cancer 2 protein	Q96JB3	HIC2	66.16	4.20	*	adherens junction;anchoring junction;cell junction;nucleus;PM
Protein kinase C-binding protein 1	Q9ULU4	ZMYND8	131.58	4.10	*	nucleus
Neuralized-like protein 4	Q96JN8	NEURL4	166.90	3.94	*	centriole;intracellular non-microtubule organizing center part
Centrosomal protein of 170 kDa	Q5SW79	CEP170	175.29	3.80	1.04	centriole;centrosome;cytoskeletal;microtubule organizing center;spindle
Single-stranded DNA-binding protein, mitochondrial	Q04837	SSBP1	17.26	3.79	1.04	mitochondria
Uncharacterized protein KIAA0889	O94964-2	KIAA0889/SOGA1	183.86	3.73	*	extracell. space
Cullin-7	F5H0L1	CUL7	199.75	3.70	*	cytosol;Golgi apparatus;nuclear ubiquitin ligase complex part
Coiled-coil domain-containing protein 8	Q9H0W5	CCDC8	59.37	3.66	0.95	PM
Protein disulfide-isomerase A6 (PDIA6)	Q15084	PDIA6	53.90	3.64	1.04	ER lumen;ER-Golgi intermediate compartment;ER membrane
Kinesin light chain 4	Q9NSK0	KLC4	70.55	3.58	0.97	cytoplasm;cytoskeletal part;microtubule
Myeloid leukemia factor 2	Q15773	MLF2	28.15	3.46	0.78	cytoplasm;nucleus
Cytochrome c oxidase subunit 2	P00403	MT-CO2	25.57	3.46	1.00	mitochondrial inner membrane
E3 ubiquitin-protein ligase HERC2	O95714	HERC2	527.22	3.43	1.05	centriole; cytoplasm; mitochondrial inner membrane
Zinc finger protein 687	Q8N1G0	ZNF687	129.53	3.43	*	nucleolus part
Mitochondrial import inner membrane translocase subunit Tim13	Q9Y5L4	TIMM13	10.50	3.38	0.80	macromolecular complex; mitochondrial inner intermembrane

Erlin-2	O94905	ERLIN2	37.84	3.26	0.98	ER membrane; PM
NADH dehydrogenase [ubiquinone] 1 alpha subcomplex subunit 13	E7ENQ6	NDUFA13	30.10	3.26	0.99	mitochondrial membrane; respiratory chain complex I; nuclear
Chromobox protein homolog 6	O95503	CBX6	43.90	3.24	*	heterochromatin; macromolecular complex; nuclear; PcG protein complex
Zinc finger and BTB domain-containing protein 24	O43167	ZBTB24	78.28	3.15	*	nucleus
Obscurin-like protein 1	O75147	OBSL1	206.94	3.10	*	cell-cell junction; Golgi apparatus; intercalated disc; perinuclear region of cytoplasm
Kinesin-1 heavy chain	P33176	KIF5B	109.68	2.96	0.98	cytosol; microtubule associated complex
Zinc finger protein 462	Q96JM2	ZNF462	291.11	2.96	*	nucleus
Kinesin light chain 1	E7EVH7	KLC1	83.69	2.92	*	cytosol; microtubule
Zinc finger protein 592	Q92610	ZNF592	137.53	2.86	*	nucleus
Zinc finger protein 316	A6NFI3	ZNF316	108.44	2.82	*	nucleus
Liprin-beta-1	Q86W92	PPFIBP1	114.02	2.77	*	PM
Kinesin light chain 2	Q9H0B6	KLC2	68.93	2.73	0.95	cell projection; ciliary rootlet; cytoskeletal; kinesin I complex
UDP-glucose: glycoprotein glucosyltransferase 2	Q9NYU1	UGGT2	174.73	2.72	*	ER lumen; ER-Golgi intermediate compartment
Endoplasmic/GRP94	P14625	HSP90B1	92.47	2.70	1.10	ER lumen; ER membrane
Mitochondrial import inner membrane translocase subunit Tim8 B	G3XAN8	TIMM8B	11.16	2.59	0.90	protein transporter complex; mitochondrial inner membrane
Zinc finger protein 574	Q6ZN55	ZNF574	108.57	2.57	*	nucleus

Calnexin (CNX)	P27824	CANX	67.57	2.56	0.95	ER lumen;ER membrane;ribonucleoprotein complex
Caseinolytic peptidase B protein homolog	Q9H078	CLPB	75.45	2.56	0.90	mitochondria
Telomere-associated protein RIF1	Q5UIP0	RIF1	274.46	2.50	0.57	chromosome, telomeric region;cytoplasm;pronucleus;spindle
Low molecular weight phosphotyrosine protein phosphatase	P24666	ACP1	18.04	2.49	0.91	cytoplasm;nucleus;PM part
Polycomb complex protein BMI-1	P35226	BMI1	36.95	2.47	0.98	cytoplasm;heterochromatin; nucleolus
Centrosomal protein of 97 kDa	Q8IW35	CEP97	96.98	2.47	1.13	centrosome;cytoplasm; cytoskeletal part
Coiled-coil-helix-coiled-coil-helix domain-containing protein 3	F8WAR4	CHCHD3	27.74	2.46	1.06	mitochondrial inner membrane;nucleus
Peroxidase homolog	Q92626	PXDN	165.27	2.44	1.24	ER;extracell. space;proteinaceous extracellular matrix
Chromatin assembly factor 1 subunit B	Q13112	CHAF1B	61.49	2.42	0.90	chromatin assembly complex;cytoplasm
Collagen alpha-1(XIV) chain	Q05707	COL14A1	193.51	2.42	*	anchoring collagen;ER lumen;extracell. matrix
Binding immunoglobulin protein (BiP/GRP78)	P11021	HSPA5	72.33	2.41	1.30	ER chaperone complex;ER lumen;ER-Golgi intermediate compartment;ER membrane
ATP-dependent DNA helicase Q4	O94761	RECQL4	133.08	2.40	*	cytoplasm;nucleus
HLA class I histocompatibility antigen	P10321; P01889; P30460; P01893	HLA-C;HLA-B;HLA-H	44.32	2.33	0.85	endosome;ER to Golgi transport;ER membrane;extracell.;Golgi; transport vesicle
Protein SCO2 homolog, mitochondrial	O43819	SCO2	29.81	2.33	0.89	mitochondrial inner membrane
E3 SUMO-protein ligase CBX4	O00257	CBX4	61.37	2.32	*	Golgi;nuclear speck
Voltage-dependent anion-selective channel protein 1	P21796	VDAC1	30.77	2.30	1.13	mitochondrial membrane

Zinc finger and BTB domain-containing protein 7A	O95365	ZBTB7A	61.44	2.29	1.06	nucleus
Formin-like protein 3	Q8IVF7	FMNL3	117.21	2.27	*	cytoplasm
Polyhomeotic-like protein 2	Q8IXK0	PHC2	90.81	2.24	1.06	nuclear part
Dolichyl-diphosphooligosaccharide-protein glycosyltransferase 48 kDa subunit	P39656	DDOST	50.80	2.19	0.96	ER macromolecular complex; ER membrane
E3 SUMO-protein ligase RanBP2; Putative peptidyl-prolyl cis-trans isomerase	P49792	RANBP2	358.20	2.17	1.09	cytosol; nuclear inclusion body
E3 ubiquitin-protein ligase RING2	Q99496	RNF2	37.66	2.17	1.02	heterochromatin
Neutral alpha-glucosidase AB	Q14697	GANAB	106.87	2.16	0.95	ER lumen; Golgi
Zinc finger protein 483	Q8TF39	ZNF483	85.10	2.15	0.78	nucleus
Chromatin assembly factor 1 subunit A	Q13111	CHAF1A	106.92	2.13	0.89	chromatin remodeling complex; cytosol
Dynamin-like 120 kDa protein	E5KLJ5	OPA1	117.74	2.11	0.92	mitochondrial crista; mitochondrial intermembrane space
Histone chaperone ASF1A	Q9Y294	ASF1A	22.97	2.10	0.82	nucleus
Ran GTPase-activating protein 1	P46060	RANGAP1	63.54	2.10	1.02	chromosomal; cytoskeletal; cytosol; nuclear pore membrane; pore complex; spindle pole
Zinc finger protein 770	Q6IQ21	ZNF770	80.01	2.07	*	nucleus
Zinc finger protein 295	Q9ULJ3	ZNF295	118.87	2.05	*	nucleus
Voltage-dependent anion-selective channel protein 3	F5H740	VDAC3	30.76	2.04	1.14	mitochondrial outer membrane
Procollagen galactosyltransferase 1	Q8NBJ5	GLT25D1	71.64	1.96	0.87	ER lumen

Histone chaperone ASF1B	Q9NVP2	ASF1B	22.43	1.89	0.88	chromatin;nucleus
Nuclear envelope pore membrane protein POM 121	Q96HA1	POM121	127.72	1.75	*	ER envelope;nuclear envelope;nuclear pore complex;ER membrane
Crossover junction endonuclease MUS81	Q96NY9	MUS81	61.17	1.74	*	nucleolus
Ubiquitin carboxyl- terminal hydrolase isozyme L5	Q5LJA9	UCHL5	41.69	1.32	0.99	chromosomal part; cytoplasm; cytosol

Supplementary table 2. List of ER- β 23 interactors. Interactors are sorted according to their enrichment in ER- β 23 IPs (H/L ratio corresponding to ER- β 23/pcDNA) from high to low values. The H/L ratio represents the combined ratio calculated by MaxQuant (version 1.3.0.5) from three independent SILAC MS experiments. Listed are proteins that are enriched ≥ 2 -fold in at least two out of three independent experiments. The localisations of interactors were annotated using Perseus (1.5.2.12) (annotation of Gene Ontology Cellular Compartments). ER-localised chaperones and ERAD factors are highlighted in pale blue. *No ratio could be calculated by MaxQuant because measurements were below threshold.

Supplementary table 3. Compartmental enrichment of ER- β 23 interactors

Category value	Total size	Selection size	Category size	Inter-section size	Enrichment factor	p value	Benj. Hoch. FDR
PRC1 complex	3317	83	9	4	17.76	4.08E-05	5.34E-03
endoplasmic reticulum lumen	3317	83	27	10	14.80	3.20E-10	2.93E-07
kinesin complex	3317	83	12	4	13.32	1.49E-04	1.52E-02
PcG protein complex	3317	83	22	5	9.08	1.53E-04	1.40E-02
endoplasmic reticulum part	3317	83	140	17	4.85	2.63E-08	1.20E-05
intracellular organelle lumen	3317	83	84	10	4.76	2.88E-05	5.29E-03
organelle lumen	3317	83	89	10	4.49	4.74E-05	5.43E-03
mitochondrial membrane	3317	83	84	9	4.28	1.64E-04	1.37E-02
membrane-enclosed lumen	3317	83	104	11	4.23	3.42E-05	5.23E-03
organelle membrane	3317	83	353	22	2.49	2.20E-05	6.73E-03

Supplementary table 3. Compartmental enrichment values of ER- β 23 interactors. Gene Ontology Cellular Component (GOCC) annotations (category value) of proteins identified by MS were assigned using Perseus (1.5.2.12). The enrichment of these category annotations among the set of ER- β 23 interactors (83 proteins) was calculated over the background of GOCC category annotations of all proteins identified (3317 proteins) using the Fisher exact test. Enrichment factors of significantly enriched cellular components (cut-off Benjamini-Hochberg $FDR \leq 0.02$) are listed.

Supplementary table 4. Abundances of ER- β 23 interactors in IP eluates

Description	Gene names	Abundance in eluate (% of all interactors)	GO cellular compartments
Transcription intermediary factor 1-beta	TRIM28	29.82	euchromatin;heterochromatin ;nuclear chromatin
Binding immunoglobulin protein (BiP/GRP78)	HSPA5	20.60	ER chaperone complex;ER lumen;ER-Golgi intermediate compartment;ER membrane
MAP7 domain-containing protein 1	MAP7D1	6.65	cytoplasm;cytoskeletal part;spindle
Single-stranded DNA-binding protein, mitochondrial	SSBP1	4.85	Mitochondria
Centrosomal protein of 170 kDa	CEP170	3.66	centriole;centrosome; cytoskeletal;microtubule organizing center;spindle
Kinesin-1 heavy chain	KIF5B	3.45	cytosol;microtubule associated complex
Enscosin	MAP7	3.44	cytoplasm;microtubule; perinuclear region of cytoplasm
E3 ubiquitin-protein ligase RING2	RNF2	2.32	heterochromatin
HCLS1-associated protein X-1	HAX1	1.42	actin cytoskeleton;cytoplasmic vesicle;ER;mitochondria; sarcoplasmic reticulum
Mitochondrial import inner membrane translocase subunit Tim13	TIMM13	1.24	macromolecular complex;mitochondrial inner intermembrane
Histone chaperone ASF1A	ASF1A	1.24	Nucleus
Protein sel-1 homolog 1 (SEL1L)	SEL1L	1.11	ER membrane
Mitochondrial import inner membrane translocase subunit Tim8 B	TIMM8B	1.11	protein transporter complex;mitochondrial inner membrane
Hypermethylated in cancer 2 protein	HIC2	1.09	adherens junction;anchoring junction;cell junction;nucleus;PM
Endoplasmic/GRP94	HSP90B1	1.06	ER lumen;ER membrane

Chromatin assembly factor 1 subunit A	CHAF1A	0.97	chromatin remodeling complex;cytosol
Telomere-associated protein RIF1	RIF1	0.95	chromosome, telomeric region;cytoplasm;pronucleus; spindle
Chromatin assembly factor 1 subunit B	CHAF1B	0.94	chromatin assembly complex;cytoplasm
Polycomb complex protein BMI-1	BMI1	0.93	cytoplasm;heterochromatin; nucleolus
Neuralized-like protein 4	NEURL4	0.77	centriole;intracellular non-microtubule organizing center part
Cytochrome c oxidase subunit 2	MT-CO2	0.75	mitochondrial inner membrane
Erlin-2	ERLIN2	0.64	ER membrane;PM
Coiled-coil domain-containing protein 8	CCDC8	0.62	PM
E3 ubiquitin-protein ligase HERC2	HERC2	0.61	centriole;cytoplasm; mitochondrial inner membrane
Protein kinase C-binding protein 1	ZMYND8	0.56	Nucleus
Caseinolytic peptidase B protein homolog	CLPB	0.53	mitochondria
PR domain zinc finger protein 10	PRDM10	0.48	Nucleus
Myeloid leukemia factor 2	MLF2	0.45	cytoplasm;nucleus
52 kDa repressor of the inhibitor of the protein kinase	PRKRIR	0.45	Nucleus
Lysosome-associated membrane glycoprotein 1	LAMP1	0.40	late endosome; lysosome
Kinesin light chain 2	KLC2	0.37	cell projection;ciliary rootlet;cytoskeletal;kinesin I complex
Histone chaperone ASF1B	ASF1B	0.37	chromatin;nucleus

Zinc finger protein 579	ZNF579	0.36	Nucleus
Polyhomeotic-like protein 2	PHC2	0.36	nuclear part
ATP-dependent DNA helicase Q4	RECQL4	0.35	cytoplasm;nucleus
Nuclear pore membrane glycoprotein 210	NUP210	0.31	ER;nuclear envelope;nuclear pore complex;ER membrane
Coiled-coil-helix-coiled-coil-helix domain-containing protein 3	CHCHD3	0.30	mitochondrial inner membrane;nucleus
Protein disulfide-isomerase A6 (PDIA6)	PDIA6	0.26	ER lumen;ER-Golgi intermediate compartment;ER membrane
Calnexin (CNX)	CANX	0.23	ER lumen;ER membrane;ribonucleoprotein complex
Zinc finger protein 574	ZNF574	0.21	Nucleus
Uncharacterized protein KIAA0889	KIAA0889 ;SOGA1	0.21	extracell. space
Zinc finger and BTB domain-containing protein 7A	ZBTB7A	0.19	Nucleus
NADH dehydrogenase [ubiquinone] 1 alpha subcomplex subunit 13	NDUFA13	0.19	mitochondrial membrane;respiratory chain complex I;nuclear
Voltage-dependent anion-selective channel protein 1	VDAC1	0.18	mitochondrial membrane
Cullin-7	CUL7	0.17	cytosol;Golgi apparatus;nuclear ubiquitin ligase complex part
Zinc finger protein 687	ZNF687	0.17	nucleolus part
Protein OS-9	OS9	0.16	ER lumen; ER ubiquitin ligase complex
Ubiquitin carboxyl-terminal hydrolase isozyme L5	UCHL5	0.15	chromosomal part;cytoplasm;cytosol
Peroxidasin homolog	PXDN	0.15	ER;extracell. space;proteinaceous extracellular matrix

Tetratricopeptide repeat protein 13	TTC13	0.14	
HLA class I histocompatibility antigen	HLA-C;HLA-B;HLA-H	0.14	endosome;ER to Golgi transport;ER membrane;extracell.;Golgi; transport vesicle
Low molecular weight phosphotyrosine protein phosphatase	ACP1	0.13	cytoplasm;nucleus;PM part
Nuclear envelope pore membrane protein POM 121	POM121	0.13	ER envelope;nuclear envelope;nuclear pore complex;ER membrane
Zinc finger protein 592	ZNF592	0.12	Nucleus
Zinc finger protein 295	ZNF295	0.11	Nucleus
Voltage-dependent anion-selective channel protein 3	VDAC3	0.11	mitochondrial outer membrane
Obscurin-like protein 1	OBSL1	0.10	cell-cell junction;Golgi apparatus;intercalated disc;perinuclear region of cytoplasm
Zinc finger protein 316	ZNF316	0.10	Nucleus
Nodal modulator 1/2/3	NOMO2;NOMO3;NOMO1	0.09	ER membrane
Tetratricopeptide repeat protein 17	TTC17	0.09	
Kinesin light chain 1	KLC1	0.08	cytosol;microtubule
Kinesin light chain 4	KLC4	0.07	cytoplasm;cytoskeletal part;microtubule
Formin-like protein 3	FMNL3	0.07	Cytoplasm
Neutral alpha-glucosidase AB	GANAB	0.07	ER lumen;Golgi
Protein SCO2 homolog, mitochondrial	SCO2	0.07	mitochondrial inner membrane
Hypoxia up-regulated protein 1 (HYOU1/GRP170)	HYOU1	0.07	ER lumen

Dolichyl-diphosphooligosaccharide-protein glycosyltransferase 48 kDa subunit	DDOST	0.06	ER macromolecular complex;ER membrane
Chromobox protein homolog 6	CBX6	0.06	heterochromatin; macromolecular complex; nuclear;PcG protein complex
Centrosomal protein of 97 kDa	CEP97	0.05	centrosome;cytoplasm; cytoskeletal part
Zinc finger protein 483	ZNF483	0.04	Nucleus
UDP-glucose:glycoprotein glucosyltransferase 2	UGGT2	0.04	ER lumen;ER-Golgi intermediate compartment
Zinc finger protein 462	ZNF462	0.04	Nucleus
Ran GTPase-activating protein 1	RANGAP 1	0.04	chromosomal;cytoskeletal; cytosol;nuclear pore membrane;pore complex;spindle pole
Procollagen galactosyltransferase 1	GLT25D1	0.04	ER lumen
E3 SUMO-protein ligase RanBP2;Putative peptidyl-prolyl cis-trans isomerase	RANBP2	0.03	cytosol;nuclear inclusion body
Liprin-beta-1	PPFIBP1	0.03	PM
Zinc finger and BTB domain-containing protein 24	ZBTB24	0.02	Nucleus
Dynamin-like 120 kDa protein	OPA1	0.02	mitochondrial crista;mitochondrial intermembrane space
Zinc finger protein 770	ZNF770	0.01	Nucleus
E3 SUMO-protein ligase CBX4	CBX4	0.00	Golgi;nuclear speck
Collagen alpha-1(XIV) chain	COL14A1	0.00	anchoring collagen;ER lumen;extracell. matrix
Crossover junction endonuclease MUS81	MUS81	0.00	Nucleolus
Zinc finger protein 335	ZNF335	0.00	Nucleus

Supplementary table 4. Relative abundance of ER- β 23 interactors in the ER- β 23 IP eluate. ER- β 23 interactors are sorted according to their relative abundances in the ER- β 23 IP eluates. Relative abundance values were calculated from IBAQ values of heavy-labelled samples after subtraction of IBAQs from light-labelled samples (pcDNA control eluates) and are expressed as % of total (sum of abundance values of all interactors). Localisations were annotated using Perseus (1.5.2.12) (GOCC). ER-localised chaperones and ERAD factors are highlighted in pale yellow.

Supplementary table 5. Cellular abundance values of ER chaperones and ERAD factors.

Description	Gene names	Mol. weight (kDa)	Median ppm
ER- β 23-mCh		36.01	4540.30
BiP	HSPA5	72.33	3635.15
GRP94	HSP90B1	92.47	1118.01
PDIA6	PDIA6	48.12	651.62
Calnex	CANX	67.57	235.71
GRP170	HYOU1	111.33	300.18
Erlin-2	ERLIN2	37.84	229.98
SEL1L	SEL1L	88.754	4.91
OS-9	OS9	75.561	4.78

Supplementary table 5. Cellular abundance values of ER chaperones and ERAD factors.

Abundance (ppm) of ER- β 23-interacting ERQC factors was calculated from IBAQ values of proteins identified by label-free MS in ER- β 23-mCh-expressing HEK293T cells. Medians of three independent experiments are listed.

Supplementary table 6. SILAC H/L ratios of UPR transcriptional targets in total proteome

Protein names	Gene names	Mol. weight (kDa)	Combined ratio H/L in total proteome	UPR transcription factor
Alpha-1,3/1,6-mannosyltransferase ALG2	ALG2	47.09	1.12	XBP1
Asparagine synthetase [glutamine-hydrolyzing];Asparagine synthetase	ASNS	64.37	1.00	ATF4
Calreticulin	CALR	48.14	1.01	ATF6
Calnexin	CANX	67.57	0.95	XBP1
Coatomer subunit alpha;Xenin;Proxenin	COPA	138.34	1.01	XBP1
Coatomer subunit beta	COPB1	107.14	0.99	XBP1
Coatomer subunit beta	COPB2	102.49	1.01	XBP1
Coatomer subunit epsilon	COPE	34.48	1.02	XBP1
Coatomer subunit gamma-1	COPG1; COPG	97.72	1.02	XBP1
Coproporphyrinogen-III oxidase, mitochondrial	CPOX	50.15	0.88	ATF4
NADH-cytochrome b5 reductase 3;NADH-cytochrome b5 reductase 3 membrane-bound form;NADH-cytochrome b5 reductase 3 soluble form	CYB5R3	38.23	0.91	ATF4
Dolichyl-diphosphooligosaccharide--protein glycosyltransferase 48 kDa subunit	DDOST	50.80	0.96	XBP1
Derlin-1	DERL1	28.80	0.90	XBP1
Derlin-2	DERL2	27.57	0.72	ATF6 and XBP1 cooperatively
DnaJ homolog subfamily B member 11 (ERDJ3)	DNAJB1 1	40.51	1.07	ATF6 and XBP1
DnaJ homolog subfamily C member 1 (ERDJ1)	DNAJC1	63.88	0.82	
DnaJ homolog subfamily C member 10 (ERDJ5)	DNAJC1 0	91.08	1.00	XBP1
ER degradation-enhancing alpha-mannosidase-like 3	EDEM3	104.66	1.18	XBP1
ERO1-like protein alpha	ERO1L	54.39	0.92	ATF6
ERO1-like protein alpha	ERO1L	54.39	0.92	ATF4
Growth factor receptor-bound protein 10	GRB10	67.23	0.75	ATF4
Homocysteine-responsive endoplasmic reticulum-resident ubiquitin-like domain member 1 protein	HERPUD 1	43.72	0.90	ATF6
Heme oxygenase 1	HMOX1	32.82	1.01	ATF4
Endoplasmic	HSP90B 1	92.47	1.10	ATF6
78 kDa glucose-regulated protein	HSPA5	72.33	1.30	ATF6

Hypoxia up-regulated protein 1	HYOU1	111.33	1.16	ATF6 and XBP1 cooperatively
ER lumen protein retaining receptor 1	KDEL1	24.54	0.96	
Galectin-3	LGALS3	26.15	0.71	ATF4
Lon protease homolog, mitochondrial;Lon protease homolog	LONP1	106.49	0.95	ATF4
Protein OS-9	OS9	75.56	0.71	ATF6
Oligosaccharyltransferase complex subunit OSTC	OSTC	16.83	0.83	XBP1
Protein disulfide-isomerase A3 (ERp57)	PDIA3	56.78	1.05	XBP1
Protein disulfide-isomerase A4	PDIA4	72.93	1.12	ATF6
Protein disulfide-isomerase A5	PDIA5	59.59	0.98	XBP1
Protein disulfide-isomerase A6	PDIA6	53.90	1.04	ATF6 and XBP1
Dolichyl-diphosphooligosaccharide--protein glycosyltransferase subunit 1	RPN1	68.57	0.95	XBP1
Dolichyl-diphosphooligosaccharide--protein glycosyltransferase subunit 2	RPN2	69.28	0.92	XBP1
Signal peptidase complex catalytic subunit SEC11C	SEC11C	21.54	1.10	ATF6 and XBP1 cooperatively
Protein SEC13 homolog	SEC13	35.54	1.10	ATF6 and XBP1 cooperatively
Protein transport protein Sec23A	SEC23A	86.16	1.01	XBP1
Protein transport protein Sec23B	SEC23B	86.48	1.03	XBP1
Protein transport protein Sec24A	SEC24A	119.75	1.01	XBP1
Protein transport protein Sec24B	SEC24B	140.42	0.90	
Protein transport protein Sec24C	SEC24C	118.32	0.95	XBP1
Protein transport protein Sec24D	SEC24D	113.08	1.00	XBP1
Protein transport protein Sec31A	SEC31A	136.22	1.01	XBP1
Protein transport protein Sec61 subunit alpha isoform 1	SEC61A1	52.95	0.95	XBP1
Protein transport protein Sec61 subunit beta	SEC61B	9.97	1.02	XBP1
Protein transport protein Sec61 subunit gamma	SEC61G	7.74	0.85	XBP1
Translocation protein SEC62	SEC62	45.86	0.93	XBP1
Translocation protein SEC63 homolog	SEC63	88.00	0.94	XBP1
Protein sel-1 homolog 1	SEL1L	88.75	1.07	ATF6
Nucleotide exchange factor SIL1	SIL1	52.75	0.91	
Signal peptidase complex subunit 2	SPCS2	25.00	1.00	XBP1
Signal peptidase complex subunit 3	SPCS3	20.31	1.03	XBP1
Signal recognition particle 19 kDa protein	SRP19	16.16	1.01	XBP1

Signal recognition particle 54 kDa protein	SRP54	55.70	1.02	XBP1
Signal recognition particle 68 kDa protein	SRP68	70.73	1.04	XBP1
Signal recognition particle receptor subunit alpha	SRPR	69.81	0.99	XBP1
Signal recognition particle receptor subunit beta	SRPRB	29.70	0.95	XBP1
Translocon-associated protein subunit alpha	SSR1	33.89	0.99	XBP1
Translocon-associated protein subunit gamma	SSR3	22.61	0.96	XBP1
Translocon-associated protein subunit delta	SSR4	19.00	0.94	XBP1
Dolichyl-diphosphooligosaccharide--protein glycosyltransferase subunit STT3A	STT3A	80.53	0.99	XBP1
Dolichyl-diphosphooligosaccharide--protein glycosyltransferase subunit STT3B	STT3B	93.67	0.86	XBP1
UDP-glucose:glycoprotein glucosyltransferase 1	UGGT1	177.19	1.06	ATF6 and XBP1
Transitional endoplasmic reticulum ATPase	VCP	89.32	1.01	ATF6 and XBP1

Supplementary table 6. SILAC H/L ratios (ER- β 23 over control) of UPR targets in the total proteome (input lysates). UPR-inducible proteins are sorted alphabetically. The H/L ratio represents the combined ratio calculated by MaxQuant (version 1.3.0.5) from three independent SILAC MS experiments. The UPR transcription factors responsible for induction of each gene were annotated based on findings by (Shoulders et al., 2013) (ATF6 and XBP1) and (Harding et al., 2003) (ATF4).

Abbreviations

A1AT	α 1-antitrypsin
A β	Amyloid β protein
ACN	Acetonitrile
AD	Alzheimer's disease
APP	Amyloid precursor protein
APS	Ammonium Persulfate
ATCC	American Type Culture Collection
ATF6	Activating transcription factor 6
BCA	Bicinchoninic acid
BFA	Brefeldin A
BiP	Binding immunoglobulin protein/glucose-regulated protein 78 (GRP78)
BRUB	Britton & Robinson Buffer
BSA	Bovine serum albumin
CAPS	3-(Cyclohexylamino)-1-propanesulfonic acid
CFTR	Cystic fibrosis transmembrane conductance regulator
CHX	Cycloheximide
CNX	Calnexin
CPY	Carboxypeptidase Y
CRT	Calreticulin
CTRL	Control
DAPI	4',6-diamidino-2-phenylindole
DMEM	Dulbecco's Modified Eagle's medium
DMF	Dimethylformamide
DMSO	Dimethylsulphoxide
DNA	Deoxyribonucleic acid
dNTP	Deoxynucleotide

DTT	1,4-Dithiothreitol
dsRNA	Double-stranded RNA
EDTA	Ethylenediaminetetraacetic acid
EGFR	Epidermal growth factor receptor
eIF2 α	Eukaryotic initiation factor 2 α
EOR	ER overload response
ER	Endoplasmic reticulum
ERAD	Endoplasmic reticulum-associated degradation
ERES	ER exit sites
ERQC	Endoplasmic reticulum quality control
FACS	Fluorescence-activated cell sorting
FASP	Filter-aided sample preparation
FBS	Foetal bovine serum
FENIB	Familial encephalopathy with neuroserpin inclusion bodies
FDA	Food and Drug Administration
FLIP	Fluorescence loss in photobleaching
FWHM	Full width at half maximum
GCN2	General control nonderepressible 2
GFP	Green fluorescent protein
Glc	Glucose
GlcNAc	N-acetylglucosamine
GRP	Glucose-regulated protein
H	Heavy labelled
HBP	Hexosamine biosynthetic pathway
HD	Huntingtin's disease
HEK293T	Human embryonic kidney cells 293T
HPLC	High-performance liquid chromatography

HRI	Heme-regulated inhibitor kinase
HSF1	Heat shock factor 1
HSP	Heat shock protein
HSR	Heat shock response
IB	Inclusion body
IRE1	Inositol requiring enzyme 1
IRES	Internal ribosome entry site
ISR	Integrated stress response
JNK	c-Jun N-terminal kinase
KEAP1	Kelch-like ECH-associated protein 1
L	Light labelled
LB	Lysogeny broth
M	Medium labelled
mAB	Monoclonal antibody
Man	Mannose
MAP	Mitogen-activated protein
mCh	mCherry
MEM	Modified Eagle's medium
MES	2-(N-Morpholino)ethanesulfonic acid
MM	Multiple myeloma
MOPS	3-(N-Morpholino)propanesulfonic acid
MRH	Mannose-6-phosphate receptor homology
MS	Mass spectrometry
MSS	Marinesco-Sjögren syndrome
MTT	3-(4,5-Dimethylthiazol-2-yl)-2,5-diphenyltetrazoliumbromide
NEF	Nucleotide exchange factor
NRF2	Nuclear factor-erythroid 2-related factor 2

NRS	Neuroserpin
NT	Non-targeted
OD	Optical density
OPR	Ordered protein response
OST	Oligosaccharyltransferase
PAGE	Polyacrylamide gel electrophoresis
pAB	Polyclonal antibody
PBS	Phosphate-buffered saline
PD	Parkinson's disease
PDI	Protein disulphide isomerase
PERK	PKR-like ER kinase
PIC	Pre-initiation complex
PKR	Protein kinase R
PLL	Poly-L-Lysine
PNGase F	Peptide:N-Glycosidase F
PVDF	Polyvinylidene difluoride
RIDD	Regulated IRE1-dependent decay of mRNA
RIPA	Radioimmunoprecipitation assay
RNA	Ribonucleic acid
RNC	Ribosome/nascent chain complex
RQC	Ribosome quality control complex
RT	Room temperature
SAX	Strong anion-exchange
SD	Standard deviation
SDS	Sodium dodecyl sulfate
SILAC	Stable isotope labelling by amino acids in cell culture
SR	Signal-recognition particle receptor

SRP	Signal-recognition particle
TA	Tail-anchored
TCA	Trichloric acid
TEMED	N,N,N',N'-Tetramethyl-ethane-1,2-diamine
TFA	Trifluoroacetic acid
TfB	Transformation buffer
Tm	Tunicamycin
UGGT	UDP-glucose/glycoprotein glucosyl transferase
uORFs	Upstream open reading frames
UPR	Unfolded protein response
UPS	Ubiquitin proteasome system
WT	Wild type
XBP1	X-box binding protein 1
XBP1s	Spliced X-box binding protein 1